Thermography for soil salinity assessment

Konstantin Ivushkin

Thesis committee

Promotor
Prof. Dr A.K. Bregt
Professor of Geo-Information Science
Wageningen University & Research

Co-promotors
Prof. Dr A.S. Pulatov
Professor of Environmental Protection and Rational Utilization of Natural Resources
EcoGIS center, Tashkent Institute of Irrigation and Agricultural Mechanization Engineers, Uzbekistan

Dr H.M. Bartholomeus
Assistant professor, Laboratory of Geo-Information Science and Remote Sensing
Wageningen University & Research

Other members
Prof. Dr S.E.A.T.M. van der Zee, Wageningen University & Research
Dr A.J.W. de Wit, Wageningen University & Research
Dr E.A. Addink, Utrecht University, the Netherlands
Dr E. Scudiero, UC Riverside, USDA-ARS, U.S. Salinity Laboratory, USA

This research was conducted under the auspices of the C.T. de Wit Graduate School of Production Ecology & Resource Conservation (PE&RC)

Thermography for soil salinity assessment

Konstantin Ivushkin

Thesis
submitted in fulfilment of the requirements for the degree of doctor
at Wageningen University
by the authority of the Rector Magnificus,
Prof. Dr A.P.J. Mol,
in the presence of the
Thesis Committee appointed by the Academic Board
to be defended in public
on Wednesday 27 March 2019
at 4 p.m. in the Aula.

Konstantin Ivushkin
Thermography for soil salinity assessment, 136 pages

PhD thesis, Wageningen University, Wageningen, the Netherlands (2019)
With references, with summary in English and Russian

ISBN: 978-94-6343-590-1
DOI: 10.18174/470312

Table of content

Chapter 1

Introduction

The constant increase of human population put more and more pressure on agricultural production systems (FAO, 2018a). Agriculture in last several decades adopted more intensive practices for productivity increase on the already cultivated lands. Moreover, new lands have been included in cultivation. This increased pressure on lands and cultivation of new lands by wrong agricultural practices lead to many environmental problems. Likely outcomes on the negative side are a continuing rise in groundwater nitrate levels from poor fertilizer management, further land and yield losses through salinization, and growing air and water pollution from livestock (FAO, 2003). One of these problems, namely soil salinization, is the focus if this thesis.

Soil salinization is a process during which concentration of water-soluble salts is increasing to the levels that negatively influence plant growth and development. It can happen as a consequence of natural processes, like weathering of a parent material (primary salinization), but on cultivated areas more often this is a consequence of human activity (secondary salinization). One of the examples of such an activity is a massive expansion of irrigated cotton growing areas in the Soviet Central Asia in the 1950s. The turning point was the Golodnaya (Hunger) steppe irrigation project which was the first one in a row of large scale irrigation projects (Ghassemi et al., 1995). The implementation of this and following irrigation projects had several problems which after decades of development lead to soil salinization. Water use has been inefficient and excessive, climatic and hydrogeological conditions of the area were not taken into account to the necessary degree, drainage problems and mistakes in water management allowed highly saline return flows to be discharged to the rivers (Ghassemi et al., 1995). Nowadays the area of this irrigation project and those that followed are suffering severe soil salinization and, therefore, decreased productivity.

1.1 Salt stress in plants

Decreased productivity is a result of the plant responses to salt stress. Salt stress is very similar to drought stress, but not completely. Plant response to salt stress consists of two phases (Figure 1.1): osmotic phase (very similar to drought stress), and ion toxicity phase (specific for each ion) (Munns, 1993).

Salt in soil solution inhibits plant growth for two reasons. First, it reduces the plant's ability to take up water, and this leads to slower growth. This is the osmotic or water-deficit effect of salinity. Second, it may enter the transpiration stream and eventually injure cells in the transpiring leaves, further reducing growth. This is the salt-specific or ion-excess effect of salinity (Munns, 2005). In general, ion toxicity effects (Figure 1.1) show greater variation between species than osmotic effects (Munns, 2002).

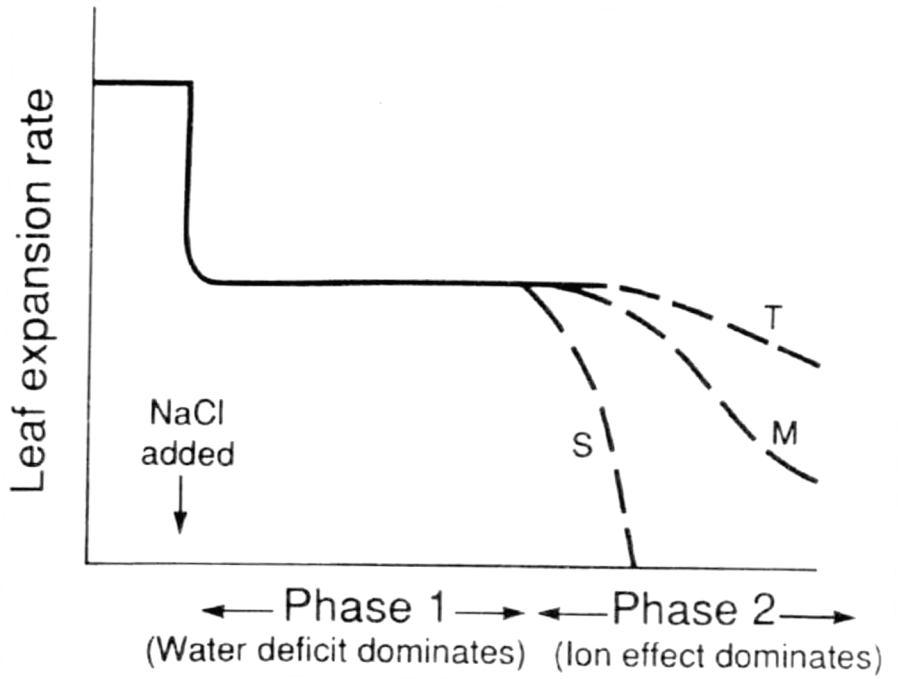

Figure 1.1. Illustration of the two phase growth response to salt for three varieties of a given species that differ in salt tolerance: sensitive (S), moderately tolerant (M) and tolerant (T). From Munns (1993).

All this together leads to many negative effects (Figure 1.2), one of which is photosynthetic inhibition. Total photosynthesis decreases due to inhibited leaf development and expansion, as well as early leaf abscission, and as salt stress is prolonged, ion toxicity, membrane disruption, and complete stomatal closure become the prime factors responsible for photosynthetic inhibition (Farooq et al., 2015). When photosynthesis is expressed on a unit chlorophyll basis, rather than a leaf area basis, a reduction due to salinity can usually be measured. In any case, the reduction in leaf area due to salinity means that photosynthesis per plant is always reduced (Munns and Tester, 2008). Salinity leads to chlorophyll degradation (Don et al., 2010) and decrease in pigment content, including chlorophyll a and b (Manaa et al., 2011).

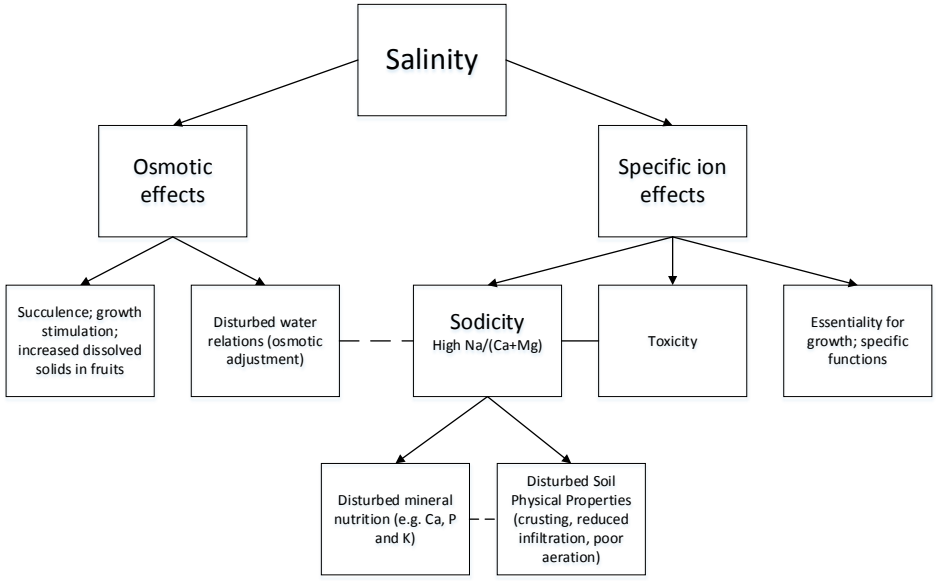

Figure 1.2. Effects of salinity on plants (From Läuchli and Grattan (2012)).

Changes in plant morphology in response to salinity also can be observed. Leaves from salt-treated plants have a higher weight/area ratio, which means that their transpiration efficiency is higher (more carbon fixed per water lost), a feature that is common in plants adapted to dry and to saline soil (Shabala and Munns, 2012).

Curiously, shoot growth is more sensitive than root growth, a phenomenon that also occurs in drying soils and for which there is yet no mechanistic explanation. The benefit is that a reduction in leaf area development relative to root growth would decrease the water use by the plant, thus allowing it to conserve soil moisture and prevent an escalation in the salt concentration in the soil (Shabala and Munns, 2012). But in an experiment of Gama et al. (2009) on common bean there was a marked reduction in root/shoot ratios. Some reports showed that root biomass increased with salinity in some species (Hester et al., 2001), indicating that roots grows faster to adjust to water deficit. But their data agreed that the root dry weight was considerably decreased as salinity intensified. Root-to-shoot ratio was able to differentiate population salt tolerance; under salinity stress the most salt tolerant populations of the same species displayed smaller root-to-shoot ratios than the least salt-tolerant populations (Hester et al., 2001). So morphological changes depend on plant species and salt concentration in growing media.

1.2 Canopy temperature change in response to soil salinity

Besides the effects mentioned above, the stress response in crops due to soil salinity is evident in decreased stomatal conductance (Álvarez and Sánchez-Blanco, 2014; Biber, 2006; Hussain et al., 2012; James et al., 2002; Munns and Tester, 2008; Rahnama et al., 2010). As a result of stomatal closure, significant changes in canopy temperature can be observed. Multiple controlled laboratory and greenhouse studies have examined changes in canopy temperature in response to soil salinity at the plant level. The crops studied were euonymus (Gómez-Bellot et al., 2015), *Syngonium podophyllum* and *Philodendron erubescens* (Urrestarazu, 2013), grapevine (Grant et al., 2007), barley (Peñuelas et al., 1997), wheat (Hackl et al., 2012), sorghum (Kluitenberg and Biggar, 1992) and cotton (Howell et al., 1984). All these studies concluded that temperature change can be used as an indicator of salinity stress in plants. Observed differences in canopy temperature varied from

less than one degree (Urrestarazu, 2013) to 1–3°C (Hackl et al., 2012; Kluitenberg and Biggar, 1992) and even 8°C (Peñuelas et al., 1997).

1.3 Extent of the problem

Soil salinity is a globally widespread problem. About a third of all agricultural lands are increasingly saline, encompassing more than 100 countries and spanning all types of climates. While statistics vary on the extent of salt-affected lands, estimates suggest that close to 1 billion hectares worldwide are salinized (Squires and Glenn, 2004; Szabolcs, 1989). Soil salinization is spreading at a rate of up to 2 million hectares per year, offsetting a significant proportion of crop production (Abbas et al., 2013).

Having such a big spatial extent, soil salinization is more and more often monitored and assessed by remote sensing methods. The extensive overview of broad range of methods and sensor types used for this is given in Metternicht and Zinck (2009). Here I will mention the most important groups of the approaches used.

1.4 Remote sensing in soil salinity assessment[1]

The methods applied in remote sensing of soil salinity can be divided in two big groups. The first group, which might be called direct estimation, uses the reflectance of the soil when it is free of vegetation to assess salinity. The second group, termed indirect estimation, uses vegetation reflectance as an indicator of soil salinity; salinity stress is thus inferred via the spectral response of vegetation and crop cover. For both approaches, multiple techniques and methods exist, though most use salinity indices, calculated for bare soil or vegetated areas.

[1] This section is partially based on the extracts from Ivushkin, K., Bartholomeus, H., Bregt, A.K., Pulatov, A., 2017. Satellite Thermography for Soil Salinity Assessment of Cropped Areas in Uzbekistan. Land Degradation & Development 28, 870-877. 10.1002/ldr.2670

Numerous indices exist and have been applied with a various degrees of success in arid and semi-arid areas across the world (Abbas et al., 2013; Al-Khaier, 2003; Allbed et al., 2014a; Douaoui et al., 2006; Hamzeh et al., 2013). Few studies have gone on to test these indices in a variety of regions and for different soil types than those for which they were developed. Those doing so have found much lower correlations and predictive power than reported for the initial applications (Allbed et al., 2014a; Douaoui et al., 2006).

A larger body of research has explored the sensitivity of spectral data to soil salinity and proposed classification techniques based on sensitivity data. These studies – based both on laboratory and field spectrometry of soils and on aerial and satellite imagery analysis – have shown good performance for bare soil areas. As a result, some sensitive spectral features and spectral bands have been defined. Most mentioned among these are the near-infrared (NIR) and short wave infrared (SWIR) bands of Landsat and other multispectral satellites (Setia et al., 2013b; Sidike et al., 2014; Yu et al., 2010) and the narrower absorption features of the same (NIR and SWIR) spectral region (Bannari et al., 2007; Farifteh et al., 2008; Howari, 2003; Mashimbye et al., 2012; Melendez-Pastor et al., 2010; Wang et al., 2012). Some authors have proposed use of visible spectra in addition to infrared (IR) (Noroozi et al., 2012; Setia et al., 2013b; Zhang et al., 2012). Karavanova et al. (2001) noted that dry saline soils have increased overall reflectance compared to unaffected soils. Similar findings were mentioned by Abbas et al. (2013) and Howari (2003), and this is considered useful in soil salinity delineation. Almost all currently available spectral bands have been evaluated for soil salinity analysis.

A number of researchers have investigated the use of vegetation as an indirect indicator for soil salinity (Akramova, 2008; Dehni and Lounis, 2012; Ding et al., 2011; Elhaddad and Garcia, 2009; Fernández-Buces et al., 2006; Scudiero et al., 2015; Wang et al., 2013). Salinity undermines plant growth and diminishes yields, and these effects can be detected by remote sensing. In general, reduced reflectance in the NIR band compared to the Red band is indicative of vegetation health and as such could provide an indirect measure of salinity levels. As any indirect indicator, however, use of vegetation data for soil salinity assessments introduces additional

inaccuracies. For example, a reduced normalized difference vegetation index (NDVI) can be caused by many factors, including limited water availability and poor management. It is also difficult to find vegetation indices that can be accurately correlated with salinity levels for specific soils and vegetation species. A diversity of approaches have been used, including averaging vegetation index values per field (Akramova, 2008) and decision tree classification (Ding et al., 2011). None, however, has proven universally applicable, with performance tested in different areas.

1.5 Problem statement and research questions

Widespread distribution and severity of soil salinity problem requires up to date and spatially explicit information on the extent of the problem. This information is required on the scales from local to global. Traditionally, soil salinity assessment has been done by analysing soil samples, either by defining total dissolved solids content or by measuring electrical conductivity of soil saturated paste (ECe). Though these methods are accurate and reliable, their high cost and spatial non-continuity are serious drawbacks.

Though remote sensing approaches are used, they still have drawbacks that make them not universally applicable. Therefore, it made us looking into the question of developing an approach that will be more universal.

To base it on direct estimation, using the soil reflectance itself, seemed to be less promising. The main reason of this is the wide range of soil spectral responses influenced by many other factors except soil salinity. That would require the approach calibration on many occasions to suit it for each soil type and probably for many other soil properties. Moreover, the direct estimation will characterise salt content only on the surface, but not in the root layer, which is of highest interest for agriculture.

The indirect assessment by using vegetation signal as a proxy has higher potential, especially on cultivated areas. There the variety of species grown is limited,

therefore tailoring the methods to different areas will require less time. Moreover, the plants' responses to many stressors are similar among majority of plants, and soil salinity is not an exception here. Among these responses I considered canopy temperature change having a potential to constitute a base for the development of a more universal remote sensing approach.

Most previous studies of canopy temperature changes in response to soil salinity were done at the individual plant level. The use of satellite or aerial thermography for this purpose has not yet been investigated. Therefore, the overall objective of this thesis is to investigate the potential of thermal imagery analysis as an approach for soil salinity assessment in cropped areas at different scales.

To achieve it the next research questions have been developed:

1. Can remotely sensed canopy temperature be used as an indicator of soil salinity in cropped areas?
2. Do UAV based observations show comparable result to satellite based observations?
3. How robust is the thermography approach when applied on study areas with different crops grown in both rainfed and irrigated conditions?
4. Can a combination of soil properties maps and thermal imagery allow us to track the development of soil salinity in space and time on global scale?

1.6 Thesis outline

This thesis consists of 6 chapters. The first introductory chapter focuses on the background information and the line of reasoning that brought me to the development of the thermography approach.

Chapter 2 represents a proof of concept where the first results of application on the study area in Uzbekistan are presented. The chapter addresses research question 1 and shows the applicability of the thermography approach.

Chapter 3 describes the thermography approach validation on local (plot) scale in the Netherlands. Moreover, it discusses the specifics of UAV use and remote sensing

data integration. Therefore, this chapter addresses question 2. The auxiliary line of research described in this chapter is the specificities of application on salt tolerant crops (quinoa).

Chapter 4 is devoted to the validation of the thermography approach on regional scale and a robustness test, by applying the approach in several different locations of Australia where different crops are grown both in irrigated and rainfed conditions. This way research question 3 is addressed.

Chapter 5 describes the validation on the global scale and issues of temporal development of the soil salinization problem. Comparison with several studies describing soil salinity change presented in the chapter together with global assessment of affected lands and its change in the period from 1986 to 2016.

Chapter 6 synthesises the findings from all the chapters, puts them into a broader perspective and reflects on implications, methods and data used. Moreover, suggestions for further research are given.

The general overview of the structure is given in Figure 1.3.

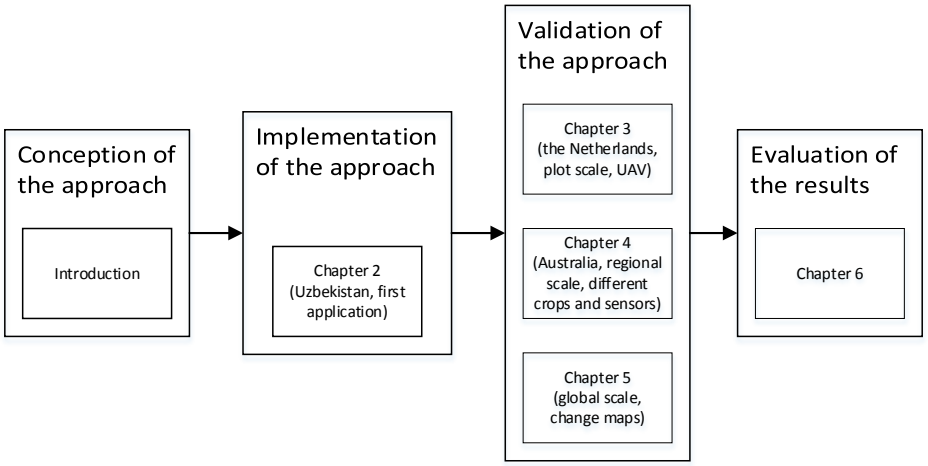

Figure 1.3. Structure of the thesis.

Chapter 2

Satellite thermography for soil salinity assessment of cropped areas in Uzbekistan

This chapter is based on:

Ivushkin, K., Bartholomeus, H., Bregt, A.K., Pulatov, A., 2017. Satellite Thermography for Soil Salinity Assessment of Cropped Areas in Uzbekistan. Land Degradation & Development 28, 870-877. 10.1002/ldr.2670.

Abstract

A change of canopy temperature can indicate stress in vegetation. Use of canopy temperature to assess salt stress in specific plant species has been well studied in laboratory and greenhouse experiments, but its potential for use in landscape-level studies using remote sensing techniques has not yet been explored. Our study investigated the application of satellite thermography to assess soil salinity of cropped areas at the landscape level. The study region was Syrdarya Province, a salt-affected, irrigated semi-arid province of Uzbekistan planted mainly to cotton and wheat. We used moderate-resolution imaging spectroradiometer (MODIS) satellite images as an indicator for canopy temperature and the provincial soil salinity map as a ground truth dataset. Using analysis of variance (ANOVA), we examined relations between the soil salinity map and canopy temperature, normalized difference vegetation index (NDVI), enhanced vegetation index (EVI), and digital elevation model (DEM). The results showed significant correlations between soil salinity and canopy temperature, but the strength of the relation varied over the year. The strongest relation was observed for cotton in September. The calculated F-values were higher for canopy temperature than for the other indicators investigated. Our results suggest that satellite thermography is a valuable landscape-level approach for detecting soil salinity in areas under agricultural crops.

2.1 Introduction

Soil salinization is a major driver of land degradation, which usually goes hand in hand with accelerated soil erosion rates, agricultural mismanagement, overgrazing, mining, and deforestation (Gómez-Acata et al., 2016; Novara et al., 2015; Seutloali and Beckedahl, 2015). Salinization of soils is a consequence of both natural processes and human interference (Hack-ten Broeke et al., 2016; Oo et al., 2015; Panagea et al., 2016; Young et al., 2015). Salinity particularly affects arid and semi-arid regions. Globally, about a third of all agricultural lands are increasingly saline, encompassing more than 100 countries and spanning all types of climates. While statistics vary on the extent of salt-affected areas, estimates suggest that close to 1 billion hectares worldwide are salinized, including 77 million hectares salinized as a result of human activity (secondary salinization) (Squires and Glenn, 2004). Soil salinization is spreading at a rate of up to 2 million hectares per year, offsetting a significant proportion of crop production (Abbas et al., 2013).

Central Asia has large expanses of salinized lands. Of this region's 7.8 million irrigated hectares, about 50% is saline, of which 29% has a moderate to high salinity level. Indeed, soil salinity is one of major factors in diminishing agricultural production in Central Asia (Shirokova et al., 2000). In Uzbekistan, 51% of irrigated land is affected by some degree of soil salinity (Bucknall et al., 2003). There are nearly 2 million hectares of highly saline areas, costing Uzbekistan some US $1 billion annually (UNDP, 2009; World Bank, 2007).

Current information on soil salinity is vital for initiating appropriate management practices and reclamation strategies. Especially valuable in this regard is data at a high spatial and temporal resolution. Conventional soil sampling and associated laboratory analyses are slow, expensive, and unsuitable for providing high temporal and spatial specificity (Zribi et al., 2011). In Uzbekistan, for example, soil mapping is executed every five years at a sampling density of at least one soil profile per 100 hectares (V.V. Dokuchaev Soil Science Institute, 1970). In view of the considerable variability of soil salinity, in both spatial and temporal terms, there is

an urgent need for improved salinity mapping of soils in cropped areas. We set out to explore the use of remote sensing for this purpose.

Remote sensing has been employed to assess soil salinity for some three decades (Metternicht and Zinck, 2009). Two groups of remote sensing techniques have been applied. The first group, called direct estimation, uses the reflectance of the soil when it is free of vegetation to assess salinity. The second group, termed indirect estimation, uses vegetation reflectance as an indicator of soil salinity; salinity stress is thus inferred via the spectral response of vegetation and crop cover. For both approaches, multiple techniques and methods exist, though most use salinity indices, calculated for bare soil or vegetated areas. Numerous such indices exist and have been applied with a various degrees of success in arid and semi-arid areas across the world (Abbas et al., 2013; Al-Khaier, 2003; Allbed et al., 2014a; Douaoui et al., 2006; Hamzeh et al., 2013). Few studies have gone on to test these indices in a variety of regions and for different soil types than those for which they were developed. Those doing so have found much lower correlations and predictive power than reported for the initial applications (Allbed et al., 2014a; Douaoui et al., 2006). A larger body of research has explored the sensitivity of spectral data to soil salinity and proposed classification techniques based on sensitivity data. These studies – based both on laboratory and field spectrometry of soils and on aerial and satellite imagery analysis – have shown good performance for bare soil areas. As a result, some sensitive spectral features and spectral bands have been defined. Most mentioned among these are the near-infrared (NIR) and short wave infrared (SWIR) bands of Landsat and other multispectral satellites (Setia et al., 2013b; Sidike et al., 2014; Yu et al., 2010) and the narrower absorption features of the same (NIR and SWIR) spectral region (Bannari et al., 2007; Farifteh et al., 2008; Howari, 2003; Mashimbye et al., 2012; Melendez-Pastor et al., 2010; Wang et al., 2012). Some authors have proposed use of visible spectra in addition to infrared (IR) (Noroozi et al., 2012; Setia et al., 2013b; Zhang et al., 2012). Karavanova et al. (2001) noted that dry saline soils have increased overall reflectance compared to unaffected soils. Similar findings were mentioned by Abbas et al. (2013) and

Howari (2003), and this is considered useful in soil salinity delineation. Almost all currently available spectral bands have been evaluated for soil salinity analysis.

A number of researchers have investigated the use of vegetation as an indirect indicator for soil salinity (Akramova, 2008; Dehni and Lounis, 2012; Ding et al., 2011; Elhaddad and Garcia, 2009; Fernández-Buces et al., 2006; Wang et al., 2013). Salinity undermines plant growth and diminishes yields, and these effects can be detected by remote sensing. In general, reduced reflectance in the NIR band compared to the Red band is indicative of vegetation health and as such could provide an indirect measure of salinity levels. As any indirect indicator, however, use of vegetation data for soil salinity assessments introduces additional inaccuracies. For example, a reduced normalized difference vegetation index (NDVI) can be caused by many factors, including limited water availability and poor management. It is also difficult to find vegetation indices that can be accurately correlated with salinity levels for specific soils and vegetation species. A diversity of approaches have been used, including averaging vegetation index values per field (Akramova, 2008) and decision tree classification (Ding et al., 2011). None, however, has proven universally applicable, with performance tested in different areas.

Our study was done in a semi-arid cropped area where losses due to soil salinity are particularly high. The stress response in crops due to soil salinity is evident in decreased chlorophyll fluorescence (Biber, 2006; Jimenez et al., 1997; Li et al., 2010; Percival, 2005; Wankhade et al., 2013) and stomatal conductance (Álvarez and Sánchez-Blanco, 2014; Biber, 2006; Hussain et al., 2012; James et al., 2002; Munns and Tester, 2008; Rahnama et al., 2010). As a result of stomatal closure, significant changes in canopy temperature can be observed. Multiple controlled laboratory and greenhouse studies have examined changes in canopy temperature in response to soil salinity at the plant level. The crops studied were euonymus (Gómez-Bellot et al., 2015), *Syngonium podophyllum* and *Philodendron erubescens* (Urrestarazu, 2013), grapevine (Grant et al., 2007), barley (Peñuelas et al., 1997), wheat (Hackl et al., 2012), sorghum (Kluitenberg and Biggar, 1992) and cotton (Howell et al., 1984). All these studies concluded that temperature change can be

used as an indicator of salinity stress in plants. Observed differences in canopy temperature varied from less than one degree (Urrestarazu, 2013) to 1–3°C (Hackl et al., 2012; Kluitenberg and Biggar, 1992) and even 8°C (Peñuelas et al., 1997).

Most previous studies of changes in canopy temperature in response to soil salinity were done at the individual plant level. To the best of our knowledge, use of satellite thermography for this purpose has not yet been investigated. In the current study we therefore investigated the potential of thermal imagery as a non-destructive and rapid method of soil salinity assessment in cropped areas at the landscape level. We furthermore compared the performance of thermal imagery with other approaches previously used, particularly NDVI, the enhanced vegetation index (EVI), and terrain properties.

2.2 Methods and materials

2.2.1 Study area

The study area is Syrdarya Province of Uzbekistan, which is a highly salt affected semi-arid region. Syrdarya Province is located at the centre of the country on a vast piedmont plain on the west bank of the Syrdarya River. On the terraces above the floodplain the water table depth is 1–2.5 m, while in the central plain it increases to 2–3 m. In depressions and hollows, water table depth is 0.5–1 m. High groundwater levels are also observed on the Syrdarya River floodplains (0.5–1 m) (Goskomgeodezkadastr, 2010). Most agricultural lands in the province are affected by various degrees of salinity: 9% is extremely saline, 60% is highly saline, and 21% has moderately saline soils (State Research Institute of Soil Science and Agrochemistry, 2005). The area has a mean annual temperature of –5°C in winter and +28°C in summer and an average annual precipitation of 180–220 mm. Crops are furrow irrigated. The main crops are cotton (*Gossypium hirsutum L.*) and winter wheat (*Triticum aestivum L.).*

2.2.2 Soil salinity map

For our core dataset we used 2005 provincial soil salinity data and maps based on Goskomgeodezkadastr (2010) and the State Research Institute of Soil Science and Agrochemistry (2005) sources. Maps from 2005 were chosen, as they were the latest with coverage of the whole study area. The maps were created in accordance with methodological guidelines for melioration of solonetz soils and accounting of salt affected soils (V.V. Dokuchaev Soil Science Institute, 1970). According to these guidelines, at least one soil profile of 2 m deep is analysed for each square kilometre of area. Salinity classification was based on the content of Cl and SO_4 ions (Table 2.1). Four soil salinity classes were distinguished: non-saline, slightly saline, moderately saline, and highly saline (Figure 2.1a). According to the maps, the slightly saline class was most abundant in the area.

Table 2.1. Classification of saline soils used in the ground truth map (V.V. Dokuchaev Soil Science Institute, 1970).

Salinity level	**Cl content (%)**	**SO_4 content (%)**
Non saline	<0.01	<0.006
Slightly saline	0.01–0.03	0.006–0.02
Moderately saline	0.03–0.10	0.02–0.06
Highly saline	0.10–0.25	0.06–0.13

2.2.3 Satellite imagery analysis

For this research we used satellite imagery captured by the moderate-resolution imaging spectroradiometer (MODIS) sensor aboard the Aqua satellite, which passes at around 13:30 local time. We selected the Aqua satellite instead of the Terra because Gómez-Bellot et al. (2015) observed the best correlation between canopy temperature and salinity treatment at midday.

First, all datasets were projected to the WGS 1984 UTM Zone 42N coordinate system and clipped to the extent of the study area. After that, we used an NDVI mask to extract the vegetated areas. Using the MOD13A2 vegetation index with an NDVI threshold of 0.3, we distinguished vegetated from non-vegetated pixels. All further analysis, both on thermal data and other remote sensing datasets, was done on the vegetated areas only (NDVI > 0.3). For elevation analysis, we used the Shuttle Radar Topography Mission digital elevation model (DEM) with 30 m resolution (accessed through EarthExplorer of the US Geological Survey). For every unit of the soil salinity map, we calculated mean values for the different parameters (surface temperature (*T*), NDVI, EVI, and elevation). Statistical analysis was performed using the SPSS Statistics software (IBM Corp, 2015). Analysis of variance (ANOVA) was our main method, with *F*-values compared to evaluate the different indicators' performance.

For cropped areas, the point of time of monitoring is important. To determine the best time for salinity monitoring we repeated our analysis at different points during the growing season. All images available for the period from April to September were analysed, and *F*-values were calculated for *T*, NDVI, and EVI.

2.3 Results

To determine the best time for soil salinity monitoring, we analysed images throughout the growing season (April–September). Figure 2.2 presents temporal profiles of NDVI and EVI. Two vegetation peaks are clearly evident, for wheat in May and for cotton in August. The difference between salinity classes is obvious, as both NDVI and EVI decrease when moving from non-saline to highly saline classes. The cotton season data is clearer and demonstrates greater differences between salinity classes. The canopy temperature time series (Figure 2.3) also shows a clear and consistent distinctions between salinity classes. The highest temperatures are observed in highly saline areas and the lowest temperatures in non-saline areas. The figure presents averaged data for the whole study area. The standard deviation of the thermal data for different periods varies from 1 to 2°C.

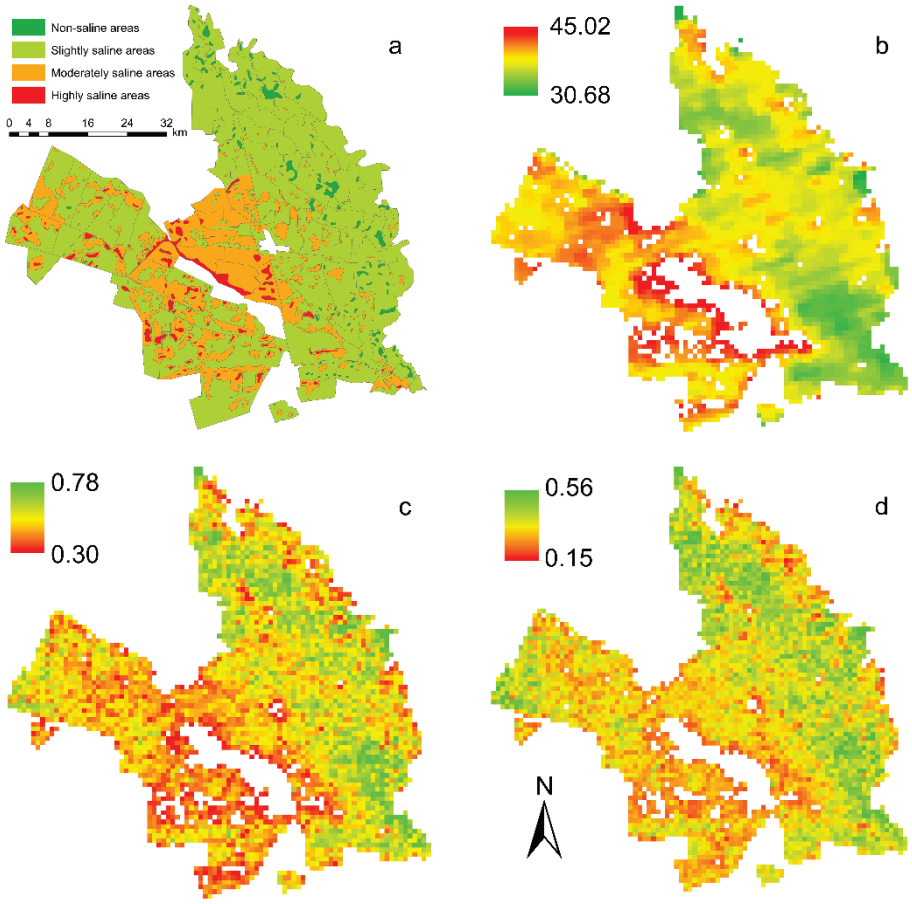

Figure 2.1 Comparison of soil salinity, canopy temperature, normalized difference vegetation index, and enhanced vegetation index maps of Syrdarya province in Uzbekistan: (a) soil salinity map in 2005; (b) canopy temperature (°C) map on 14 September 2005; (c) normalized difference vegetation index map on 13 August 2005; (d) enhanced vegetation index map on 28 July 2005.

According to the results of our ANOVA test, the best relation between the soil salinity map and thermal imagery occurs from end August to mid-September (Table 2.2). For NDVI and EVI, the strongest relation is found from end July to mid-August. In general, *F*-values are high for the whole period of maximum cotton development, which is from end July to mid-September. This indicates that cotton is influenced

most by soil salinity in this period. The *F*-values during wheat season are much lower, but still significant, meaning that wheat was less salt-affected.

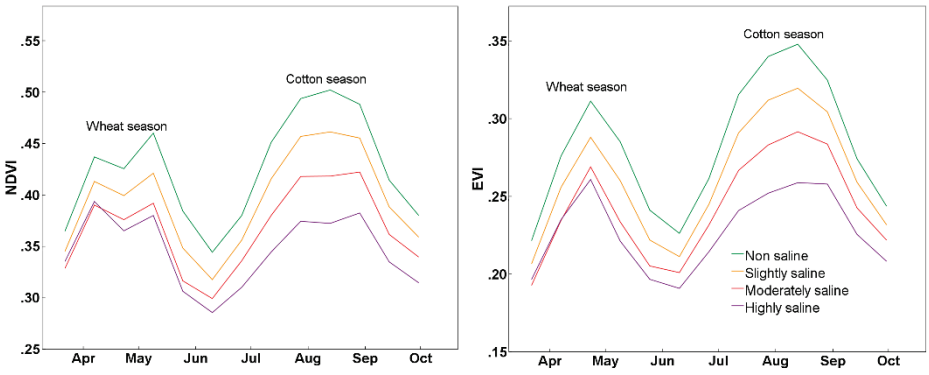

Figure 2.2 Time series of normalized difference vegetation index and enhanced vegetation index for Syrdarya province in Uzbekistan (averaged for the whole study area).

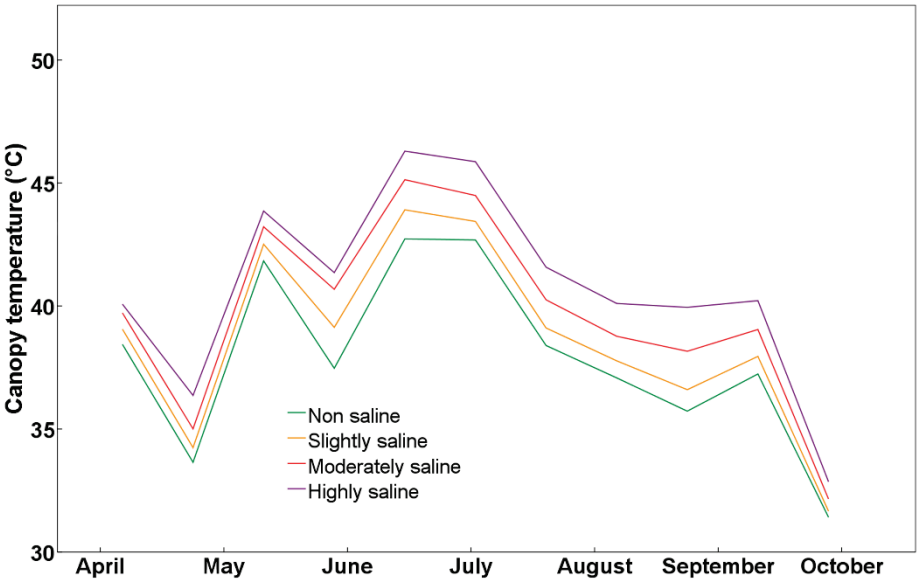

Figure 2.3 Time series of canopy temperature for Syrdarya province in Uzbekistan (averaged for the whole study area).

Table 2.2. *F*-values of ANOVA tests between soil salinity map and MODIS thermal imagery, NDVI, and EVI for Syrdarya Province in Uzbekistan (all *p*-values are less than 0.01, except for elevation data).

Date	22 Apr	10 May	28 May	12 Jun	25 Jun	11 Jul	28 Jul	13 Aug	30 Aug	14 Sep	30 Sep
Canopy *T*	18.6	27.4	16.3	29.6	36.1	25.1	37.6	30.4	39.0	41.7	20.5
NDVI	8.9	17.6	19.4	20.8	23.1	33.7	37.1	39.4	27.3	34.0	21.9
EVI	5.9	16.2	12.1	7.9	13.3	20.2	29.2	27.9	23.4	26.2	12.9
Elevation	0.3 (*p*-value = 0.87)										

Figure 2.4 presents the differences in means between the salinity classes. Higher *F*-values are indicative of larger differences between salinity classes.

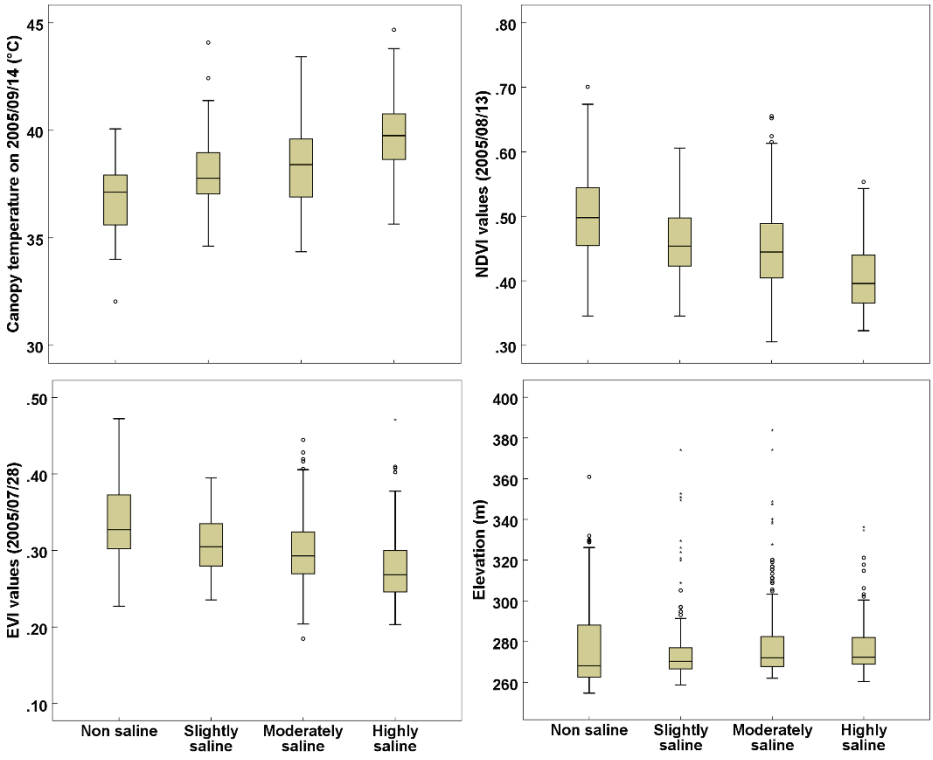

Figure 2.4 Boxplots of canopy temperature, NDVI, EVI, and elevation data versus salinity levels for Syrdarya province in Uzbekistan.

In general, data variability is high, but similar for all the evaluated variables. The classes do show overlap, but the means are significantly different. The boxplots in the figure show that mean temperatures increased with increased salinity level, in line with previous plant-level studies (Gómez-Bellot et al., 2015; Hackl et al., 2012; Howell et al., 1984). However, we found only small differences between the slight and the moderate salinity classes. Distinguishing these classes will therefore be difficult.

Differences in means were also observed in the boxplots of NDVI and EVI for the different salinity classes, but here we see a decrease in NDVI and EVI as salinity level increases, indicating that NDVI and EVI also respond to changes in soil salinity. ANOVA results for NDVI and EVI data indicate significant differences between salinity classes (p-value <0.01), but F-values are smaller than those found using thermal imagery analysis, especially in the case of the EVI. It is interesting to note that the maximum F-values for NDVI and EVI were observed in different months than for canopy temperature. For canopy temperature the strongest correlation with the salinity map occurs from end August to mid-September, while for NDVI and EVI it is from end July to mid-August.

DEM analysis results suggest that elevation is not a good predictor of soil salinity (Figure 2.4). ANOVA results (Table 2.2) show an F-value of 0.245 and a p-value of 0.865, indicating no significant relation between altitude and salinity. We also analysed derivatives of the DEM (slope and aspect) and found no significant relations for these either.

A visual comparison of the soil salinity map and the canopy temperature map revealed some similar spatial patterns (Figure 2.1a and b). The central part of the province, where the most highly saline areas are located, had higher canopy temperatures. Visual interpretation of the NDVI and EVI maps revealed a random, noisy pattern, which was less pronounced on the thermal map. This is surprising, considering the ANOVA results and boxplots. We would expect more similarity with salinity, since these vegetation indices were previously used for salinity monitoring and other studies found high correlations.

2.4 Discussion

The main goal of our research was to investigate the potential of thermal imagery as a rapid, non-destructive landscape-level method for assessing the soil salinity of areas under crops. Our results confirm that remotely sensed canopy temperature at the landscape level is significantly related to soil salinity. Statistical analysis showed significant differences between salinity classes. Differences between salinity classes were also pronounced in the thermography time series graph (Figure 2.3), despite a standard deviation of 1–2°C in the dataset. Interestingly, the ANOVA of canopy temperature was higher than that of vegetation indices, as seen in the larger *F*-values. Many previous studies have used vegetation indices, and often found strong correlations with soil salinity (Aldakheel et al., 2006; Brunner et al., 2007; Platonov et al., 2013). Several factors may explain why we found canopy temperature to perform better and show more statistically significant differences between salinity classes. First, our study area was a uniform agricultural province, the vast majority of which was covered by only one crop at a particular point in time (wheat in spring and cotton in summer). This uniformity allowed us to use MODIS data with a 1 km resolution. The coarse data resolution and large size of the study area might have masked other factors that could influence the temperature, like irrigation schedule and management differences. These features might have made of our study area amenable to aggregation over larger areas and allowed identification of patterns that might not have been visible with more detailed data. However, the coarse resolution of the MODIS data could impose limitations as well. The large pixel size might mix vegetation and soil signals, mediating temperature values. In this respect, use of Landsat data may be a worthwhile path for future research. The Landsat archive provides continuous data for most of the Earth starting from the 1970s. Moreover, Landsat data's potential for use in soil salinity monitoring has already been shown at the regional level (Judkins and Myint, 2012; Scudiero et al., 2015) and at the local level (Akramova, 2008; Hamzeh et al., 2016; Setia et al., 2013b).

We found the strongest correlation between thermal data and soil salinity from end August to mid-September. This confirms Metternicht and Zinck (2003), who found the end of a dry season to be the best time for monitoring. However, their study used optical remote sensing for bare soil rather than canopy thermography. Nevertheless, their explanation is also plausible in our case. In Syrdarya Province, leaching of salts occurs from December to February. Thus, in May, when winter wheat is fully developed and at peak biomass, the salt content in the root zone is low because of recent leaching. As a result, no strong correlation between canopy temperature and soil salinity is observed. The influence of salts is greater closer to the end of a dry season due to the capillary rise of saline groundwater. Therefore, despite the fact that cotton is considered to be more salt tolerant than wheat (Ayers and Westcot, 1985), we observed a stronger correlation between canopy temperature and salinity during cotton season. Considering cotton's relatively high salt tolerance (Ayers and Westcot, 1985), we would expect less salt-tolerant crops (e.g., rice, corn, vegetables) to show an even stronger relation between canopy temperature and soil salinity.

Our DEM analysis did not reveal any influence of topography on soil salinity, even though topography and micro relief are known to be significant factors in soil salinity distribution (Akramkhanov, 2005; Hillel and Feinerman, 2000; US Salinity Laboratory Staff, 1954). A plausible explanation for this finding is that our study area was overall relatively flat.

The methods applied in this study were simple, which favours further practical applications and dissemination of the approach to other areas. Of course, the simplicity raises issues as well, like the problem of differentiating the signals from soil and vegetation and the need to take irrigation schedule into account, as irrigation will influence temperature. These issues can also be considered potential directions for future studies. As an additional path for future research we suggest inclusion of auxiliary data in the analyses, such as data on soil types and groundwater level. Inclusion of auxiliary data could help create a soil salinity assessment method for agricultural areas that is flexible enough for application in various different arid and semi-arid regions of the world. The methods we used

here were straightforward, and the data are open and universally available. We therefore consider this research a first step towards development of a more widely applicable approach for soil salinity assessment.

2.5 Conclusions

The present study explored the potential of canopy temperature as an indicator of soil salinity at the landscape level, and compared the performance of this indicator with NDVI, EVI, and elevation. We concluded that satellite thermography data is significantly correlated to soil salinity. Our satellite thermography data clearly distinguished between salinity classes, producing *F*-values higher than those for the other indicators investigated. Moreover, visual examination of maps showed that actual salinity patterns were more similar to the canopy temperature map than to the map produced using vegetation indices. Satellite thermography thus appears to harbour substantial potential for salinity monitoring on cropped areas. However, the timing of monitoring is important. Thermal images taken in September produced the highest *F*-values, meaning they had the greatest predictive power. Nevertheless, for the whole period from end July to mid-September, *F*-values were fairly steady and showed significant relations, indicating considerable potential for use in monitoring. In our study region of Syrdarya Province, the highest *F*-values corresponded with the period of maximum crop development at the end of the dry season. Maximum *F*-values for vegetation indices were observed a bit earlier in the season, in July and August, when cotton's green biomass was close to its maximum. Therefore, the point of maximum vegetation development after the dry season can be considered the best time for application of the methods we used.

Similarly, we found promising results for use of satellite thermography to detect soil salinity on irrigated croplands for our study area in Uzbekistan. A promising path of future research might be evaluation of the general applicability of the proposed approach in terms of different crops and regions.

Chapter 3

UAV based soil salinity assessment of cropland

This chapter is based on:

Ivushkin, K., Bartholomeus, H., Bregt, A.K., Pulatov, A., Franceschini, M.H.D., Kramer, H., van Loo, E.N., Jaramillo Roman, V., Finkers, R., 2018. UAV based soil salinity assessment of cropland. Geoderma. https://doi.org/10.1016/j.geoderma.2018.09.046.

Abstract

Increased soil salinity is a significant agricultural problem that decreases yields for common agricultural crops. Its dynamics require cost and labour effective measurement techniques and widely acknowledged methods are not present yet. We investigated the potential of Unmanned Aerial Vehicle (UAV) remote sensing to measure salt stress in quinoa plants. Three different UAV sensors were used: a WIRIS thermal camera, a Rikola hyperspectral camera and a Riegl VUX-SYS Light Detection and Ranging (LiDAR) scanner. Several vegetation indices, canopy temperature and LiDAR measured plant height were derived from the remote sensing data and their relation with ground measured parameters like salt treatment, stomatal conductance and actual plant height is analysed. The results show that widely used multispectral vegetation indices are not efficient in discriminating between salt affected and control quinoa plants. The hyperspectral Physiological Reflectance Index (PRI) performed best and showed a clear distinction between salt affected and treated plants. This distinction is also visible for LiDAR measured plant height, where salt treated plants were on average 10 centimetres shorter than control plants. Canopy temperature was significantly affected, though detection of this required an additional step in analysis – Normalised difference Vegetation Index (NDVI) clustering. This step assured temperature comparison for equally vegetated pixels. Data combination of all three sensors in a multiple linear regression model increased the prediction power and for the whole dataset R2 reached 0.46, with some subgroups reaching an R2 of 0.64. We conclude that UAV borne remote sensing is useful for measuring salt stress in plants and a combination of multiple measurement techniques is advised to increase the accuracy.

3.1 Introduction

Increased soil salinity is a significant agricultural problem that decreases yields for common agricultural crops (Maas and Grattan, 1999). Moreover, soil salinity is a dynamic phenomenon which makes timely soil salinity data essential for agricultural management of affected regions. Remote sensing can provide the necessary spatial and temporal resolution, but widely acknowledged methods and techniques for soil salinity monitoring of cropland using remote sensing are not present yet. Most of them propose to use vegetation indices, Normalised Difference Vegetation Index (NDVI) being the most popular(Rahmati and Hamzehpour, 2017; Zhang et al., 2015). Other plant parameters, like remotely sensed canopy temperature (Ivushkin et al., 2017; Ivushkin et al., 2018), have been applied as a proxy for soil salinity. Bare soil remote sensing was also used, though less often (Bai et al., 2016; Nawar et al., 2014). This can be explained by the fact that upper layer of soil does not reflect actual salinity levels in root zone, which is the most important information for agriculture.

Though the above mentioned studies reported high correlations and accuracies of prediction in some situations, their application on other study areas did not show the same usability and accuracy (Allbed et al., 2014a; Douaoui et al., 2006). Moreover, widely available satellite images cannot provide high spatial resolution and temporal flexibility of data acquisition, which are important for agricultural application.

One of the solutions to overcome the issues of scale, resolution and temporal flexibility is the use of Unmanned Aerial Vehicles (UAV) as a sensor platform. UAV-based remote sensing is currently used for a wide range of applications in agriculture and soil science. These applications include but are not limited to: soil erosion monitoring (Oleire-Oltmanns et al., 2012), crop and soil mapping for precision farming (Honkavaara et al., 2013; Sona et al., 2016), quantifying field-based plant–soil feedback (van der Meij et al., 2017) and measuring physiological indicators of crops (Domingues Franceschini et al., 2017; Roosjen et al., 2018). There is an increasing amount of operational UAV service providers in agriculture

industry and many farmers start to maintain their own fleet. All this makes UAV's widely available remote sensing platforms with vast potential applications, including soil salinity monitoring.

Several studies discuss the potential of UAV-borne remote sensing for soil salinity and water deficit stresses, which often leads to a similar stress response in plants. Romero-Trigueros et al. (2017) investigated Citrus species grown under deficit irrigation with reclaimed water of increased salinity. They found that Red and Near Infrared spectral bands are significantly correlated with the chlorophyll content, stomatal conductance and net photosynthesis and concluded on the feasibility of an UAV-borne imagery to assess physiological and structural properties of Citrus under water and saline stress. Quebrajo et al. (2018) used thermal imagery from a UAV mounted camera to detect water stress in sugar beet plants. They concluded that this a reliable method to monitor the spatio-temporal variations of crop water use in sugar beet fields, but further research is required to propose optimal recommendations for a specific plant species.

These examples show that effects of salt and water stress in plants are definitely detectable by UAV remote sensing systems, but UAV's specific application for salinity stress was investigated only in one of them (Romero-Trigueros et al., 2017) and with the focus on water stress rather than salinity stress. Therefore, considering that available research on the topic is limited, we have formulated two research questions:

1. Do the UAV sensed variables significantly change in salt treated plants on plot scale?
2. Does a combination of the different variables have an added value?

To answer them we have conducted our research using UAV platforms with three significantly different sensors: thermal camera, hyperspectral camera and Light Detection and Ranging sensor (LiDAR). The research was conducted in the frame of a bigger experiment on salt tolerance of quinoa crop which has been set up on the experimental field at Wageningen University & Research, the Netherlands.

3.2 Methods and materials

3.2.1 Planting experiment set-up

The experiment was set up on the experimental farm of Wageningen University & Research located in the central part of the Netherlands. Plants for the experimental trial were sown on March 28, 2017 in a greenhouse, the plants were put outside for cold acclimation on April 21, 2017 and were planted in the field on April 24, 2017 (salt trial) and April 25, 2017 (control trial).

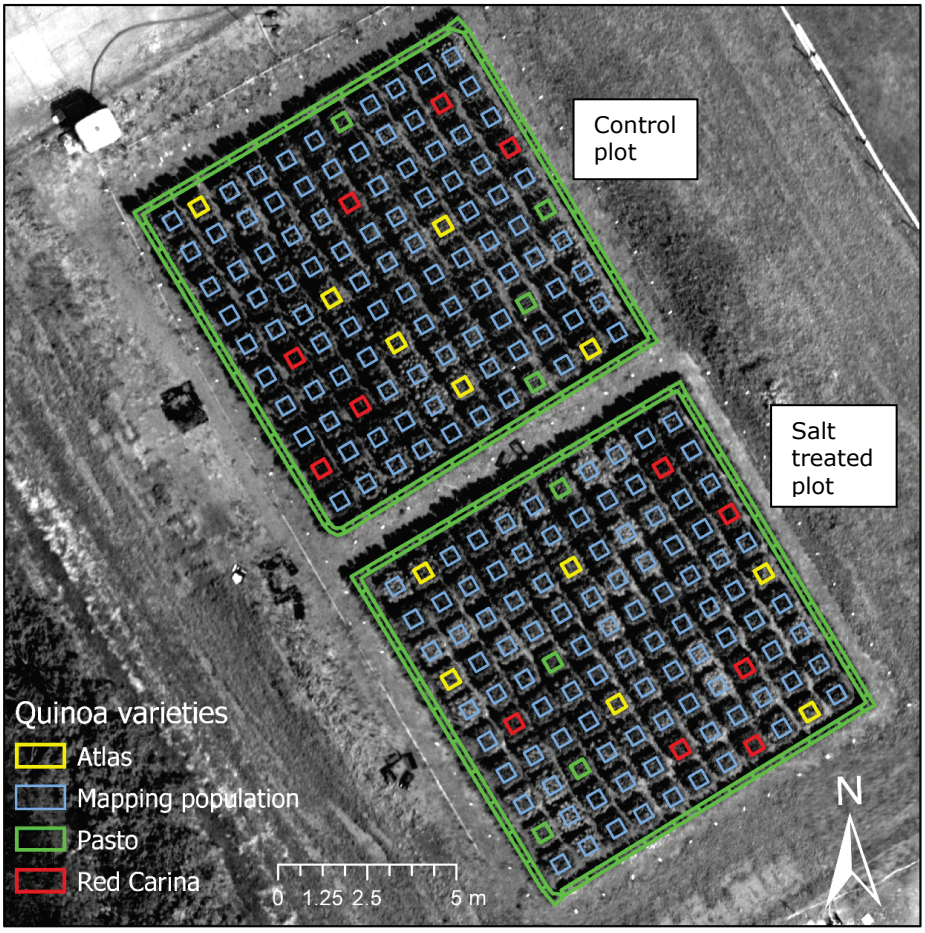

Figure 3.1 Planting experiment spatial layout. The planting units are marked by the coloured squares on an aerial photo background. Each variety is colour coded.

The two experimental plots of 13 x 13 m were planted with in total 97 different genotypes and varieties of quinoa Figure 3.1. The three varieties were Atlas, Red Carina and Pasto. The other 94 genotypes were F3-families of a cross between Atlas and Red Carina. Each plot consists of 110 planting units measuring 60x70 cm with a gap between the units of 40 cm (gross unit size = 100 x 110 cm). In the unit, the inner 60 x 70 cm was planted with 42 plants spaced at 10 x 10 cm. The southern plot is treated with salt and the northern plot is used as control plot. Around each plot of 110 planting units, an edge row of Pasto plants was planted in order to make sure the light conditions of the experimental edge rows were similar to that further away from the edge.

Salt was applied to the salt treated plot in 14 steps to create a final EC of just above 30 dS/m (equivalent to 300 mM NaCl) by adding irrigation water with NaCl, initially at 200 mM and later at 400 mM NaCl (Table 3.1). In the end natural rainfall occurred so frequently, that prior to a rainfall event an equivalent amount of salt was added equal to the amount applied with each 400 mM NaCl irrigation application. These solid applications quickly dissolved in the rainwater and infiltrated in less than 24 hours.

Table 3.1. Salt applications. From 11/5 to 30/6 each application was given in irrigation water as 5 L of solution at the mentioned concentration of NaCl.

Date	mM, concentration of NaCl solutions	g NaCl/planting unit
11/5/2017	200	58
15/5/2017	400	117
17/5/2017	400	117
24/5/2017	400	117
2/6/2017	400	117
9/6/2017	400	117
16/6/2017	400	117
30/6/2017	400	117
11/7/2017	as solid	120
14/7/2017	as solid	240
17/7/2017	as solid	240

21/7/2017	as solid	240
Total (g per planting unit)		1717
Total (g per m2)		1561

Electrical conductivity was measured at 0-10, 10-20 and 20-30 cm soil depth regularly. For each planting unit, three locations were sampled. Soil samples were weighed fresh and dried in order to see humidity of the current soil. Following this, electric conductivity meter (ProfiLine Cond 315i, Xylem Analytics, Germany) was used to measure the concentration of salts in saturated soil. Twenty grams of soil and 160 ml of water (1:8) were mixed and EC of the solution measured by EC meter. During the salt applications, soil samples were taken three days after the treatments. The EC values increased from about 2 dS/m (the same level as in the control plot at the start of the season after fertilisation) to about 40 dS/m in the layer 0-10 cm, 15 dS/m in the layer 10-20 cm and 18 dS/m in the layer 20-30 cm of soil depth (at flowering, after June 16, 2017). EC-levels were variable as they were higher just after application and lower after rainfall events, but gradually increased as mentioned. The level of 40 dS/m in the top layer exactly reflects the NaCl concentration of 400 mM used in the application. The surface soil salinity of 40 dS/m corresponds to extremely saline conditions (>16dS/m) and 10-20 cm values of up to 15 correspond to highly saline conditions (8-16 dS/m). In general, experimental setup corresponds to highly-extremely saline conditions where only tolerant species can grow.

The total irrigation plus rainfall from planting to harvest (on August 7, 2017) was 229 mm. The initial soil moisture content was about 100 mm (30 % relative water content taken over the first 30 cm soil). At harvest the relative water content was about 20-25 % (or 60-75 mm in the first 30 cm of soil). So, on average the total water use (soil evaporation and transpiration) was about 260-270 mm.

3.2.2 Field measurements of plant variables

3.2.2.1 Stomatal conductance measurements

The stomatal conductance measurements were taken on two consecutive days from two leaves per one plant in each planting unit twice a day, in the morning and the afternoon using a Decagon SC-1 porometer. The morning measurement took place from 10 to 12 o'clock and afternoon from 13 to 15 o'clock. The standard deviation between the units on control plot is 68 mmol/m^2/s and on salt treated plot 28 mmol/m^2/s. In our analysis we have used the average value of these four measurements as an estimate of the midday values to ensure best comparison with the UAV flight data which were taken at midday. The stomatal conductance map (Figure 3.2) is based on these ground measurements and is produced for visualisation and spatial analysis.

3.2.2.2 Plant height measurements

Final plant height was measured after the final harvest (on August 7, 2017) by taking the 90 % quantile of the plant height (so from the 42 plants the longest four plants were excluded, so the length of the 5th longest plant was taken). Plant height was measured from the base of the plant to the top of the head on the main stem using regular ruler.

3.2.2.3 Biomass and grain measurements

After the final harvest, the plants were split into stem (plus some remaining leaves, but most were dead and/or fallen off) and head. The head was dried at 35°C until the weight was stable (about 4 days) prior to separating grain and residual head in order to obtain viable seeds for follow-up experiments. The weight of residual head and grain were determined after being dried at 35°C and from these dried materials subsamples were taken to determine dry weights after 24h drying at 105°C. Stem weights were also determined after drying at 105°C. The total biomass (dry weight) is the sum of the dry grain weight, the dry residual head weight and the stem dry weight.

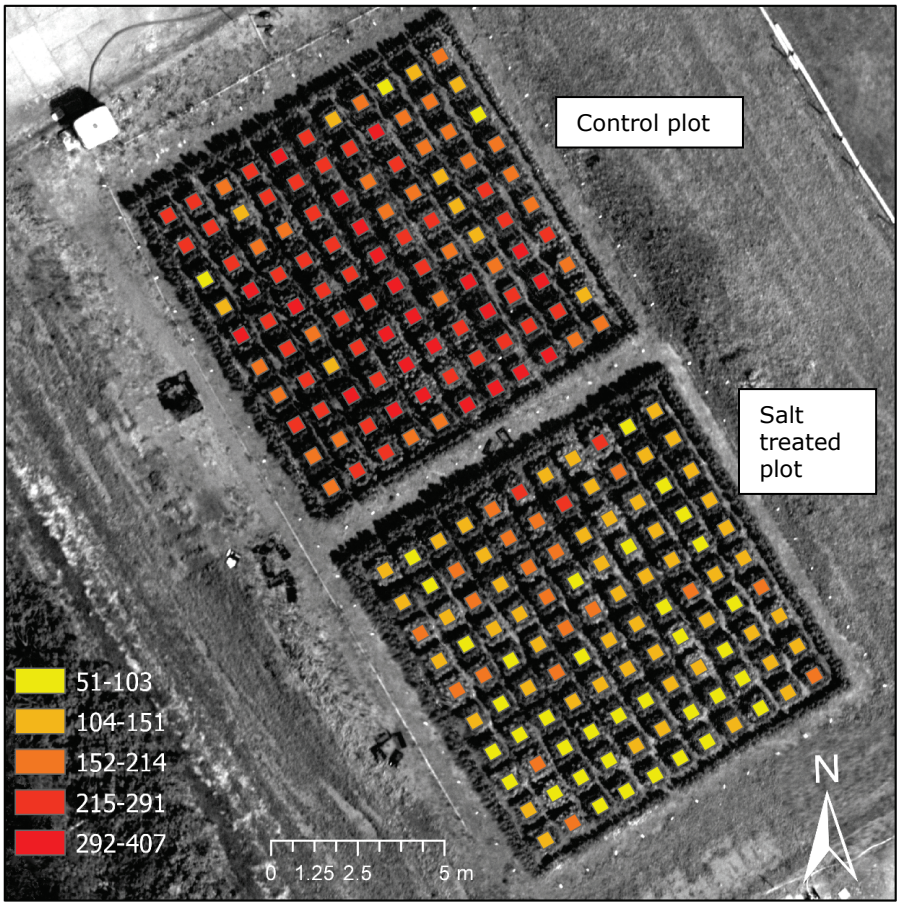

Figure 3.2. Stomatal conductance map showing the average stomatal conductance per planting unit. Units of stomatal conductance are mmol/m^2/s.

3.2.3 UAV data acquisition and processing

The UAV data used were acquired on 20th of June 2017. Two flights were made with an Altura AT8, one carrying the hyperspectral camera and the other one with the thermal camera on board. A third flight was conducted with the Riegl Ricopter system, carrying the Riegl VUX-SYS LiDAR system. The systems and data are described in more detail below.

3.2.3.1 Hyperspectral data system and processing

A light weight hyperspectral camera (Rikola Ltd., Oulu, Finland) based on a Fabry-Perot interferometer (FPI) (Honkavaara et al., 2013; Roosjen et al., 2017) has been used. The image produced has a resolution of 1010x1010 pixels. In total 16 bands were sampled in a range of 515-870 nm with full width at half maximum (FWHM) varying between 13 and 17 nm, as described in Table 3.2.

Table 3.2. Characterization of the spectral bands of the camera.

Spectral bands centre (nm)	515	530	550	570	630	670	680	690	700	710	720	740	760	780	800	870
FWHM (nm)	14	14	13	13	13	13	13	13	13	13	13	13	13	13	13	17

The area of the 2 plots was captured in 4 flight lines, parallel to the longest side of the area. The flight height was 20 meters above ground level and the flight speed was 2 meters/second. The overlap between flight lines was approximately 80%, within the flight line the overlap between images is approximately 60%. The images were acquired with a ground sampling distance of 0.015 m. The flight lines were constructed with the Unmanned Ground Control Software mission planning software (UGCS, 2017).

Due to intrinsic sensor characteristics, images corresponding to different wavelengths were not registered at the same time, since changes in the wavelengths measured depend on internal adjustment of the sensor system. The mismatch between images corresponding to different wavelengths was solved during photogrammetric processing of the images in Agisoft PhotoScan software (Agisoft LLC, 2017). This procedure depends on implementation of the Structure from Motion (SfM) algorithm, with feature matching, self-calibrating bundle adjustment and image-to-image registration based on overlapping imagery (Harwin et al., 2015). For that, image alignment and dense point cloud derivation were performed using the original resolution of the images (i.e., setting quality to 'high' and 'ultra-high' during these steps in the software processing chain, respectively).

Conversion of digital numbers (registered with 12-bit radiometric resolution) to radiance, in $mW*sr^{-1}*m^{-2}*nm^{-1}$, was performed based on dark current measurements, which were taken before the flight, using proprietary software provided with the camera (HyperspectralImager version 2.0). Radiance values were then converted into reflectance factor through the empirical line approach using images, also acquired before the flight, of a Spectralon reference panel with 50% reflectance (LabSphere Inc., North Sutton, NH, USA), under same general illumination conditions observed during the data acquisition.

3.2.3.2 Thermal data processing

The thermal camera used is a Workswell WIRIS 640 (Workswell s.r.o., Praha, Czech Republic). This thermal camera captures images with 640x512 pixels resolution, and has a temperature sensitivity of 0.05°C, with a spectral range of 7.5-13.5 μm. The default setting for emissivity of 0.95 was used. The thermal camera captures calibrated images which means that the actual temperature is recorded.

The area of the 2 plots was captured in 4 flight lines, parallel to the longest side of the area. The flight height was 20 meters above ground level and the flight speed was 2 meters/second. The overlap between flight lines was approximately 80%, within the flight line the overlap between images is approximately 60%. The images were acquired with a ground sampling distance of 0.025 m. The flight lines were constructed with the Unmanned Ground Control Software mission planning software (UGCS, 2017).

The calibrated images were processed with Agisoft PhotoScan software (Agisoft LLC, 2017) where a mosaic for the whole trial has been constructed. Unfortunately, the GPS malfunctioned during the acquisition, so no GPS coordinates were available for the imagery. Since the images were captured with sufficient overlap (70%), PhotoScan still can construct a mosaic applying the Structure from Motion (SfM) algorithm, but the result is without geo-reference. The geo-referencing was done manually in ArcMap (ESRI, 2016) by selecting recognizable locations on the thermal mosaic and a georeferenced hyperspectral image of the area.

3.2.3.3 Lidar height measurements and data processing

The RIEGL RiCOPTER with VUX®-1UAV (RIEGL Laser Measurement Systems GmbH, Horn, Austria) integrated UAV and sensor system has been used for LiDAR data acquisition. The RiCOPTER is a battery-driven octocopter with an empty weight (no batteries and equipment) of 9 kg that can carry a payload of up to 8 kg. Together with the VUX®-1UAV scanner (3.75 kg), the system controller (0.9 kg), the IMU (0.7 kg) and optional cameras the total system weights just under 25 kg. The batteries allow flight times of up to 30 min at 30 km/h maximum cruise speed. This allows flying multiple overlapping flight lines to increase target coverage (Brede et al., 2017).

The VUX®-1UAV is a survey-grade laser scanner that is mounted underneath the RiCOPTER. It uses a rotating mirror with a rotation axis in flight direction to direct the laser pulses and achieve an across-track Field Of View (FOV) of 330° perpendicular to the flight direction. This means that lateral flight line overlap is only restricted by the maximum operating range of the laser. An Applanix AP20 IMU attached to the VUX®-1UAV and Global Navigation Satellite System (GNSS) antennas on top of the RiCOPTER record flight orientation and GNSS data. The on-board instrument controller manages all sensors' data streams and includes a 220GB SSD storage, which is sufficient for several missions (Brede et al., 2017).

The area of the 2 plots was captured in 6 flight lines, 3 parallel to the longest side of the area, situated to the left, middle and right of the plots and 3 parallel to the shortest side of the area, also situated to the left, middle and right of the plots. This way, the quinoa plants are scanned from all sides. For each flight line a scan line is captured. The flight lines were constructed with the Unmanned Ground Control Software mission planning software (UGCS, 2017).

Pre-processing of the trajectory data (flight orientation and GNSS data) was performed with the POSPac Mobile Mapping Suite (Applanix, 2017) using base station data provided by 06-GPS (06-GPS, 2017). This makes it possible to achieve centimetre accuracy for the geo-location of the laser data.

Processing of the raw scanning data was done with the RIEGL RiPROCESS software which is the default software tool for processing data from the VUX®-1UAV scanner. With RiPROCESS, the raw data is converted to a geo-referenced point cloud using the pre-processed trajectory data for accurate geo-positioning. Internal co-registering of the different scan line data was carried out with the RiPRECISION tool. This tool finds matching control planes between scan lines and performs the co-registration. The resulting LiDAR point cloud data was exported as LAS files for further processing with the LAStools software (rapidlasso GmbH, 2017).

Classification of ground points and calculation of the plant height was done with the LAStools software suite. For ground point classification, the lasground_new tool was used with the wilderness option. This enables the detection of smaller features on the ground in high resolution LiDAR. The results were visually evaluated and the pattern of the ground classification was found accurate enough for further processing. Next, the height of all points above the ground was calculated with the lasheight tool. The result is still a point cloud with the Z value of each point is the relative height above the ground. The Z value for ground points is 0. This point cloud was rasterized into a raster file with the lasgrid tool using the highest option with a step size of 2.5 cm. This means that within a grid cell of 2.5 by 2.5 centimetres the highest Z value of LiDAR points that fall within this grid is assigned as value to the grid cell. The result is a raster file covering the whole plot area with the maximum height of the vegetation per 2.5 by 2.5 cm's. This file is used to derive statistical information about the plant height for each planting unit.

3.2.4 Vegetation indices calculation

Three vegetation indices were calculated for the research. The first one is well known and broadly used Normalised Difference Vegetation Index (NDVI):

$$NDVI = \frac{NIR - R}{NIR + R} \qquad (1)$$

The second one is Optimized Soil Adjusted Vegetation Index (OSAVI) (Rondeaux et al., 1996), calculated as:

$$OSAVI = \frac{NIR - R}{NIR + R + 0.16} \qquad (2)$$

In our calculation NIR is the reflectance at 870 nm and R is reflectance at 690 nm spectral band. The third index is PRI (Gamon et al., 1992), calculated as:

$$PRI = \frac{\mathrm{R531} - \mathrm{R570}}{\mathrm{R531} + \mathrm{R570}} \qquad (3)$$

where Rx is the reflectance on the corresponding wavelength in nm. PRI is known to be responsive to salinity stress in plants (Zinnert et al., 2012).

3.2.5 NDVI clustering

To filter out the influence of the total biomass on a UAV measured temperature we applied NDVI clustering. In this way we ensure that we compare the temperatures of the equal amount of a plant material per pixel. The clusters were created by sorting the plant units based on their average NDVI value and assigning them into groups of equal size. A total 5 clusters were established each containing 24 planting units, which means that 120 planting units were included into regression analysis. NDVI ranges for each class are indicated in Table 3.3.

3.2.6 Further geospatial and statistical analysis

Further geospatial analysis was implemented in ArcGIS Pro software package (ESRI, 2017). That analysis consisted of calculating average NDVI, PRI, OSAVI and temperature values for each planting unit using Zonal Statistic as Table tool. Then importing of the table into the readable form for IBM SPSS Statistics software (IBM Corp, 2015) for further statistical analysis and plotting. In SPSS correlation coefficients of Table 3.4 were calculated and boxplots were created. The Multiple Linear Regression model also has been calculated in SPSS software package. For that, functionality of Linear Regression tool has been applied, where canopy temperature, PRI and LiDAR measured plant height were chosen as independent variables. All statistical analysis has been implemented on a planting unit level, therefore average pixel values per planting units were used for producing boxplot graphs and calculating regression and correlation coefficients.

3.3 Results and discussion

3.3.1 Vegetation indices analysis

The multispectral indices did not show significant differences between control and salt treated plots, and to some extent even show an inverted correlation, where both NDVI and OSAVI showed slightly higher values for salt treated planting units (Figure 3.3). We connect this outcome with adaptation mechanisms of quinoa plants. Since quinoa is a well-known halophyte, it can increase its fresh weight under salinity stress and leaves show the highest increase in weight (Koyro et al., 2008). This means that multispectral vegetation indices that mainly relate to the greenness and green biomass will not be useful for salt tolerant plants like quinoa, where relationship of salt stress and biomass are not straightforward.

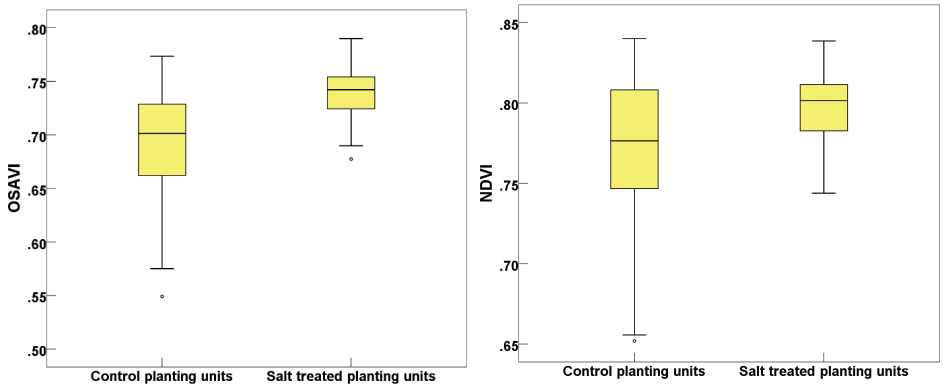

Figure 3.3. NDVI and OSAVI boxplots of control and salt treated quinoa plots.

Even though the total biomass of salt affected plants was slightly higher than for the control, the actual yield was lower (i.e. the harvest index was reduced by the salt treatment), which means that there are certain negative physiological responses even in such salt tolerant plants as quinoa. To detect these responses we have investigated Physiological Reflectance Index (PRI) values, which is known to be influenced by salinity stress (Zinnert et al., 2012). In this case results were more in line with previous studies and showed that PRI values of salt treated plants were lower than for the control (Figure 3.4). This confirms that actual photosynthetic

efficiency has decreased because of the salt stress. Visual assessment of the PRI map in Figure 3.6 shows these differences, with more reddish colours (higher PRI) on the control plot and more yellow (lower PRI) on salt treated plot. The map also shows that there are quite some inconsistencies and sometimes very low values in control plot and very high in the treated one. Because of this, the differences between two means reached only 0.005. Suspecting that these inconsistencies appear because of the differences in canopy cover per pixel and not because of actual performance of the plant at the moment of measurement, we applied NDVI clustering (ranges per cluster are in Table 3.3), as described in the Methods section. This allowed us to compare planting units with comparable canopy cover.

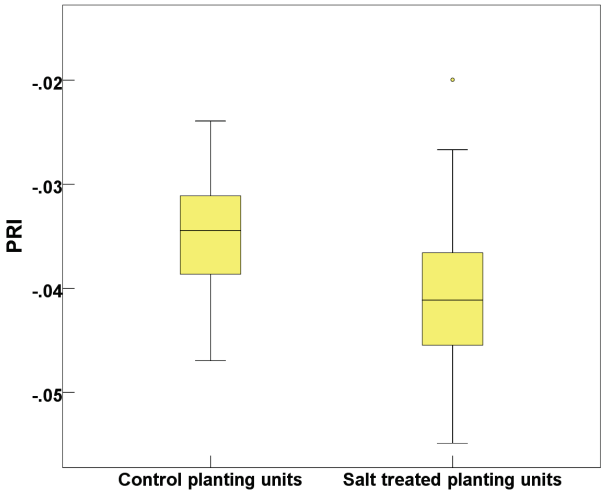

Figure 3.4. Physiological Reflectance Index (PRI) boxplot.

In Figure 3.5 it is visible that application of NDVI clustering increased the differences of means on average twofold, now reaching 0.01, which leads to a clearer distinction between control and salt treated plants. Therefore, NDVI clustering appears to be a useful step in the analysis for plants with non-common salinity stress responses, like quinoa.

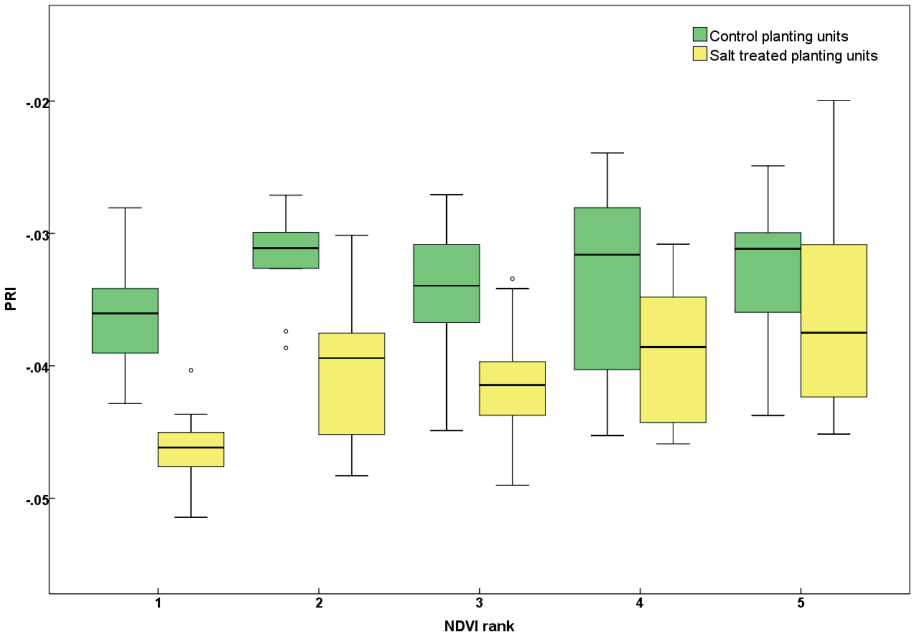

Figure 3.5. Physiological Reflectance Index (PRI) boxplot for different NDVI clusters

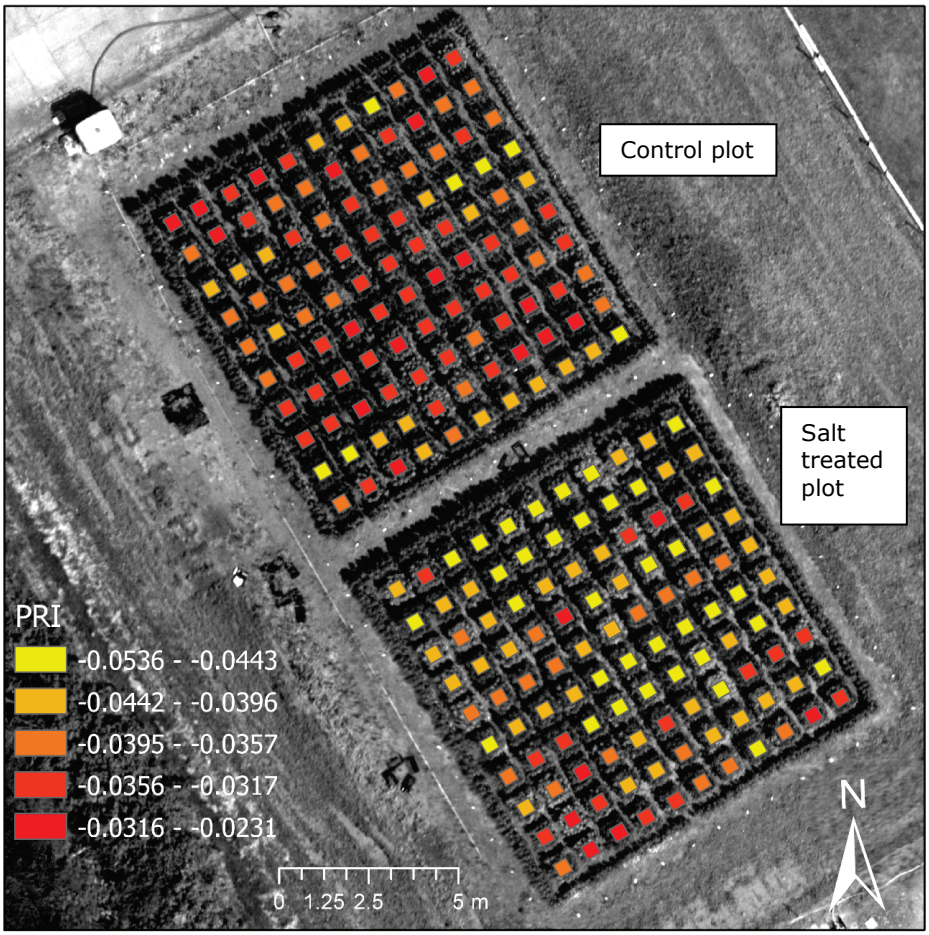

Figure 3.6. PRI map. The salt treated plot has visibly lower PRI values.

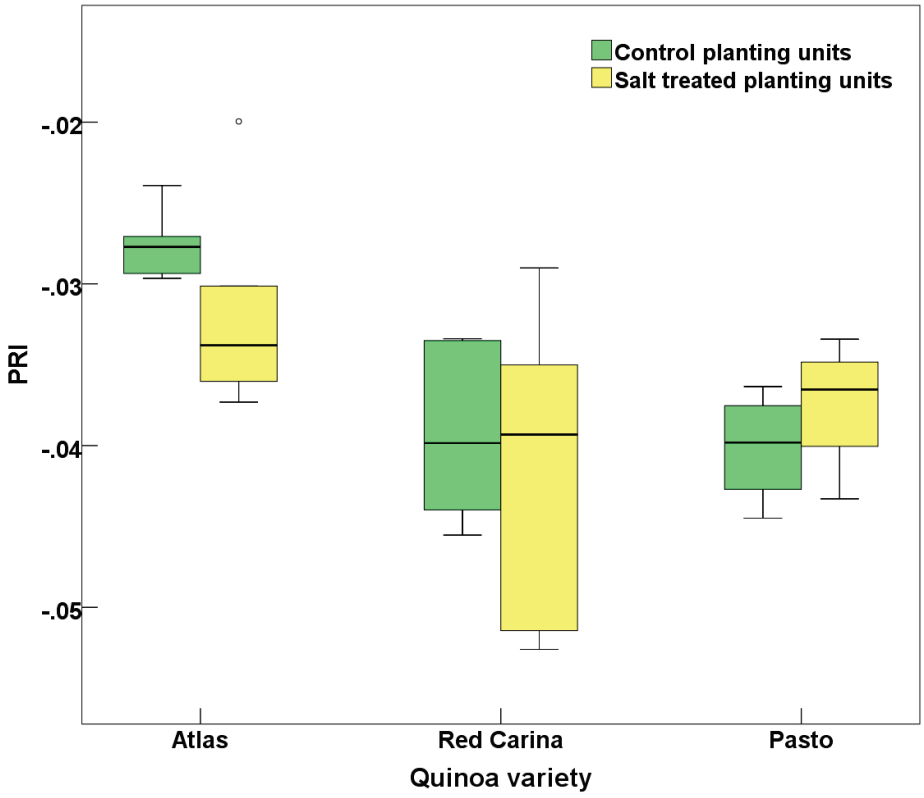

Figure 3.7. Physiological Reflectance Index (PRI) boxplot clustered by variety.

In addition to differences between control and salt treated plants, PRI was quite variable between different quinoa varieties (Figure 3.7). Pasto variety showed the most remarkable result because of the inverted relation – salt treated plant showed higher PRI values than control, which suggests that Pasto is the most salt tolerant variety among the three. These values correspond well with ground measured indicators of plant performance. Red Carina's mean PRI is also slightly higher on salt treated plot, but this difference is barely reaching 0.001 and the general boxplot distribution shows that the majority of the values are in the lower range, therefore PRI values in the case of Red Carina are not significantly different between control and salt affected plants. Atlas variety followed a general pattern of reduced PRI on salt treated plants compared to control.

3.3.2 Canopy temperature analysis

Analysis of canopy temperature differences between saline and non-saline plot are also much clearer when NDVI clustering is applied. Figure 3.8 shows that when temperature data are stratified only by soil salinity treatment, the temperature measurements are not significantly different. But in case of NDVI clustered analysis, depicted in Figure 3.9, in 4 out of 5 cases the average temperature of the plant is higher for salt affected plants. This suggests that the general principle of canopy temperature increase in response to salinity, which was previously observed with satellite sensors on landscape scale (Ivushkin et al., 2017; Ivushkin et al., 2018), is also present with aerial data acquired from a UAV on a plot scale.

Figure 3.8. Temperature boxplot for the unclustered dataset.

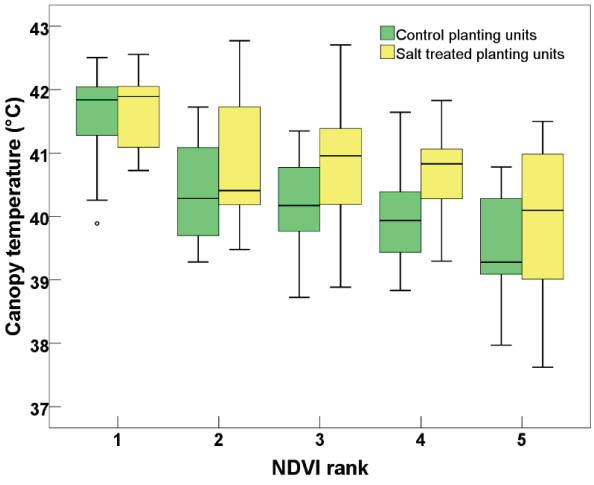

Figure 3.9. Temperature boxplot for different NDVI clusters.

The fact that a higher correlation is observed only after NDVI clustering, suggests that even though the canopy temperature is influenced by soil salinity, the amount of vegetation in each pixel is crucial for valid soil salinity assessment.

Moreover, this connection between canopy temperature and soil salinity can be observed in salt tolerant crop, which is a surprising finding, taking into account that salt tolerant and salt sensitive plants have different salt stress adaptation mechanisms (Shabala and Munns, 2012). In this trial this distinguishing was possible by applying additional step in the analysis – NDVI stratification. Therefore, canopy temperature increase in response to salinity stress can be observed in salt tolerant plants, though the effect is less pronounced compared to conventional crops (Ivushkin et al., 2017; Ivushkin et al., 2018).

Canopy temperature generally depends on stomatal conductance. Figure 3.10 and Table 3.3 show how they correspond in our case. When the dataset is analysed without any clustering the correlation between stomatal conductance and UAV recorded temperature was -0.188. This is quite surprising considering that stomatal conductance ground measurements have a clear spatial distribution (Figure 3.2) which shows significantly lower stomatal conductance on the salt affected plot. The reason for this is the different amount of vegetation signal per pixel and specifics of adaptation mechanism of quinoa, as described before. In this case, though stomatal conductance is decreased with a higher salinity level, the increase in total amount of vegetation per pixel (and, as a result total amount of stomata per pixel) leads to temperature compensation and there is no difference between control and salt affected plot observed in remote sensing data. But when the analysis was done on the NDVI clustered dataset the correlation coefficient reached -0.657 and 3 out of 5 coefficients are significant. However, the two marginal clusters (first and the last) showed low correlation coefficients. This suggests that plants with highest and lowest green biomass of the study area are less suitable for the thermal monitoring of salt induced stress.

Table 3.3. Correlation coefficients between stomatal conductance and UAV measured canopy temperature per NDVI cluster (correlation is significant at the *0.05 or **0.01 level).

NDVI rank	1	2	3	4	5	NDVI unclustered
NDVI range	<0.781	0.781-0.800	0.800-0.809	0.809-0.816	0.816-0.840	-
Correlation coefficient	-0.285	-0.445*	-0.406*	-0.657**	0.008	-0.188*

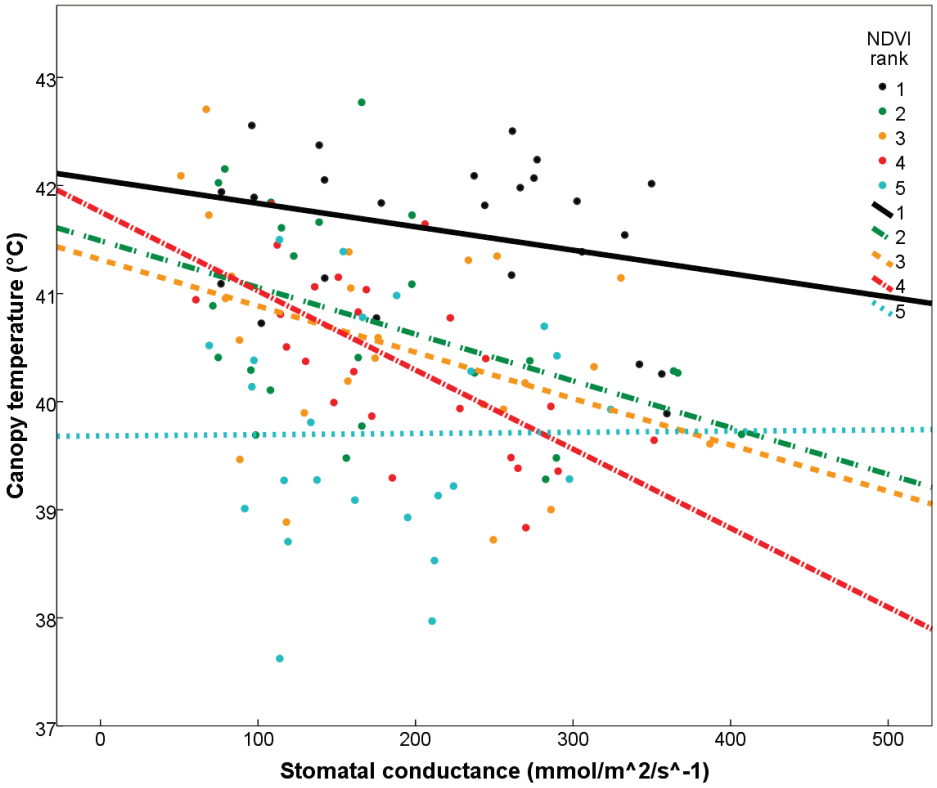

Figure 3.10. Stomatal conductance vs. canopy temperature scatterplot. Different colours represent different NDVI clusters. Lines are the best fit lines for each cluster.

3.3.3 LiDAR height measurements analysis

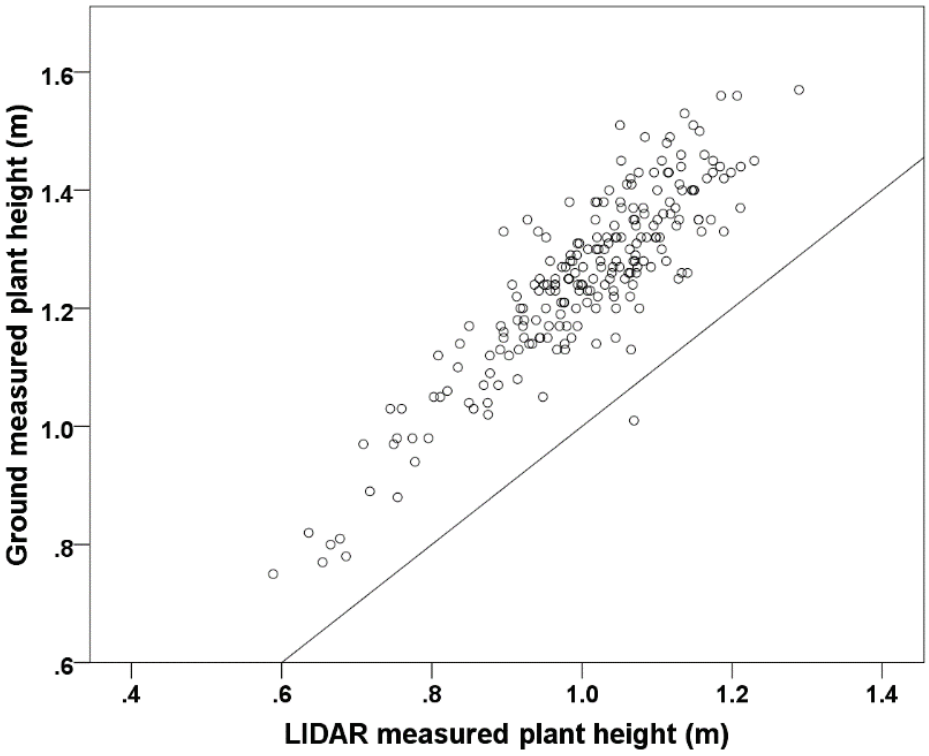

Figure 3.11. Scatterplot of plant height measured by Lidar and by hand 48 days later. The line is 1:1 line.

LiDAR measurements of plant height were compared with actual ground measurements. The results show that LiDAR can accurately predict plant height with the R^2 of 0.78. This is remarkably good as the height measurements of the LiDAR predict the height of the crop at the harvest 48 days later. That means that LiDAR data has a potential for plant height prediction at the time of harvest, which can further be used for yield prediction.

Moreover, the R^2 most likely has been decreased by the fact that not every single plant has been measured by ground measurements, but only the 90 % quantile of the plant height of 42 plants was determined, while LiDAR provided an average of every plant's height in each planting unit.

The plant height was significantly affected by salt treatment. The salt treated plants are on average 10 cm shorter than the control plants (Figure 3.12). However, this is not true for the Pasto variety, which showed a reversed correlation and salt affected plants are 5-10 cm higher than control. This can clearly be seen on the LiDAR height map, where Pasto can be identified by its difference in height compared to the neighbouring planting units of other varieties (Figure 3.13).

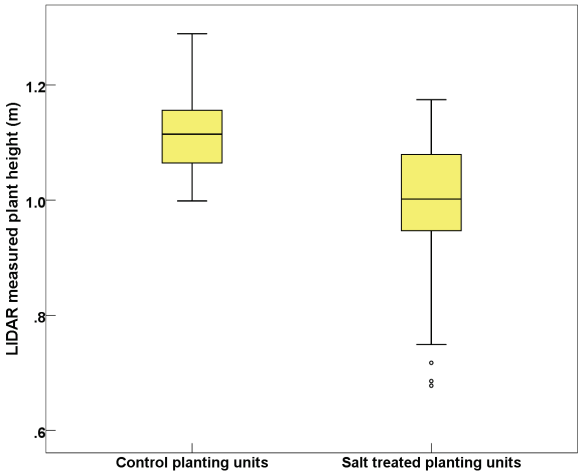

Figure 3.12. Lidar measured plant height.

Considering that plant height is usually affected by salt stress, LiDAR systems have an added value in soil salinity monitoring allowing to obtain plant height measurements over big areas in short period of time. Adding this data into multivariable analysis will increase the prediction power and accuracy of the results, which is demonstrated in the next subsection.

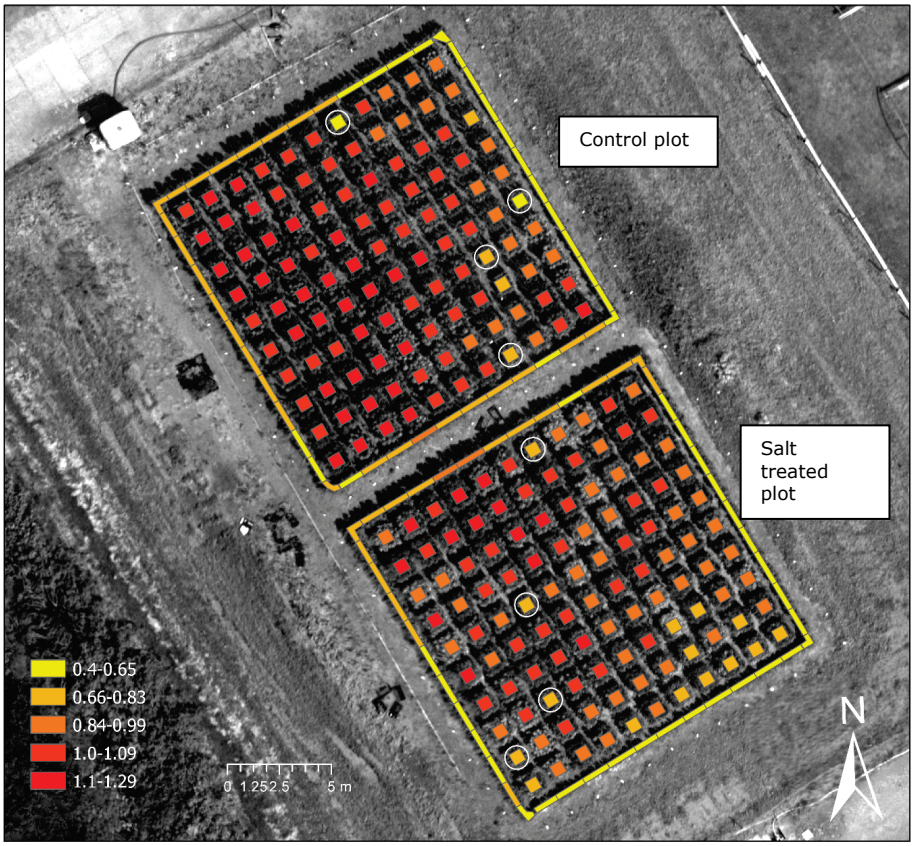

Figure 3.13. Lidar measured plant height (m) map (Pasto planting units are marked by the circles).

3.3.4 Multiple Linear Regression

Application of Multiple linear regression has showed higher regression coefficient compared to the cases when only a single predictor is used. When data from all three sensors were used (thermal, hyperspectral, LIDAR) the R^2 reached 0.64 (0.58 R^2 adjusted) for the fourth NDVI class (Table 3.4) and 0.46 for all classes combined (Figure 3.14). The predictors in this case were PRI, canopy temperature and LIDAR measured plant height. Though the average regression coefficient has been increased by application of multiple linear regression, the deviations of the

regression coefficients between different NDVI clusters are quite high and R^2 varies from 0.1 to 0.64 (Table 3.4) so there is a room for improvement on the consistency of the results.

Table 3.4. Determination coefficients (R^2) for different indicators vs. stomatal conductance (MLR combines PRI, canopy temperature and LIDAR measured plant height).

NDVI rank	1	2	3	4	5	NDVI unclustered
MLR	.590	.376	.410	.638	.104	.241
Canopy temperature	.081	.198	.165	.431	.000	.035
PRI	.434	.184	.200	.263	.043	.142
LIDAR measured plant height	.487	.218	.263	.417	.079	.213

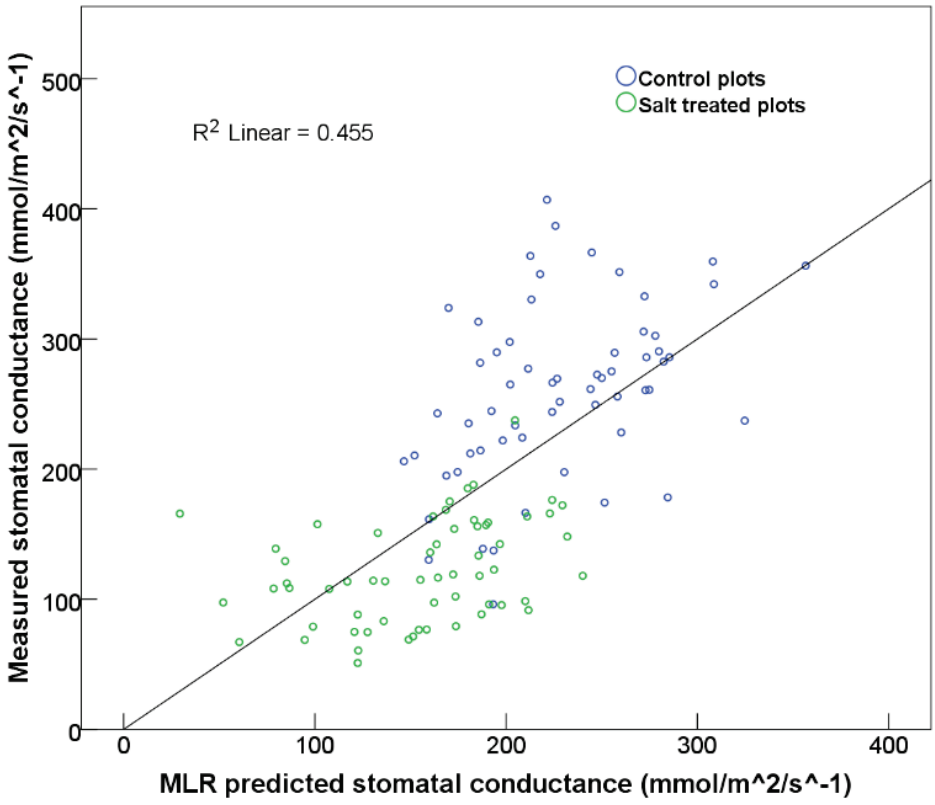

Figure 3.14. Scatterplot of MLR predicted vs measured stomatal conductance values. The line is 1:1 line.

It is fully conceivable that the remote sensing data could be more accurate than the actual stomatal conductance measurements, which were only done using measurements on four leaves and on two different days in a morning and afternoon part. The amount of work does not allow to finish this large number of stomatal conductance measurements on a larger number of leaves within a few hours. This might add bias and residual error in the stomatal conductance measurements. The remote sensing data have been collected in a much shorter period (less bias between different parts of the experiment) and on the whole planting unit instead of only on four leaves per planting unit.

In addition to salt stress, stomatal conductance can be used as an indicator of other stresses, like water stress. Its effective measurements using such cost and labour effective technique as UAV remote sensing can be useful as a component of a precision agriculture systems. In general, remote sensing measurements methods for different plant properties, might be a useful addition for modern agricultural management system, where UAVs are already playing an important role.

Among the directions for a future research we suggest investigating the application of the method to other crops. It is likely that other crops might have different degree of responses and with more sensitive crops the data analysis might be more efficient by skipping the NDVI stratification step. Though we are sure that the trend will be the same, since general physiological mechanisms are similar in most of the plants. Taking into account that salt treatments in this experiment correspond to highly and extremely affected lands we see an added value in conducting experiment with lesser concentrations, which will correspond to salinity conditions that are more widespread on cultivated lands.

3.4 Conclusions

This study investigated plot scale assessment of soil salinity using three different UAV mounted sensors: thermal camera, hyperspectral camera and LiDAR. The results showed that an increase of canopy temperature in response to salt stress is also happening in salt tolerant plants, like quinoa, though this increase is less

pronounced. The other variables investigated, namely Physiological Reflectance Index and LiDAR measured plant height, are also affected by soil salinity stress. Physiological Reflectance Index of quinoa plant is significantly decreased because of the increased soil salinity and seems to be a valuable indicator of salt stress, in opposite to multispectral indices like NDVI or OSAVI, which showed insignificant differences between control and salt treated plants, with even reverted correlations. LiDAR measured height of quinoa plant is significantly decreased because of the increased soil salinity. Stratification of an area by NDVI values ensures the equal amount of vegetation per pixel and, therefore, increases the correlation's strength between soil salinity level and remotely sensed physiological variables like PRI and canopy temperature. The combination of multiple remote sensing variables in Multiple Linear Regression model has improved regression coefficient and therefore we conclude that implementation of multiple measurement techniques bears a lot of potential for soil salinity monitoring of cropland by remote sensing.

Chapter 4

Soil salinity assessment through satellite thermography for different irrigated and rainfed crops

This chapter is based on:

Ivushkin, K., Bartholomeus, H., Bregt, A.K., Pulatov, A., Bui, E.N., Wilford, J., 2018. Soil salinity assessment through satellite thermography for different irrigated and rainfed crops. International Journal of Applied Earth Observation and Geoinformation 68, 230-237. 10.1016/j.jag.2018.02.004.

Abstract

The use of canopy thermography is an innovative approach for salinity stress detection in plants. But its applicability for landscape scale studies using satellite sensors is still not well investigated. The aim of this research is to test the satellite thermography soil salinity assessment approach on a study area with different crops, grown both in irrigated and rainfed conditions, to evaluate whether the approach has general applicability. Four study areas in four different states of Australia were selected to give broad representation of different crops cultivated under irrigated and rainfed conditions. The soil salinity map was prepared by the staff of Geoscience Australia and CSIRO Land and Water and it is based on thorough soil sampling together with environmental modelling. Remote sensing data was captured by the Landsat 5 TM satellite. In the analysis we used vegetation indices and brightness temperature as an indicator for canopy temperature. Applying analysis of variance and time series we have investigated the applicability of satellite remote sensing of canopy temperature as an approach of soil salinity assessment for different crops grown under irrigated and rainfed conditions. We concluded that in all cases average canopy temperatures were significantly correlated with soil salinity of the area. This relation is valid for all investigated crops, grown both irrigated and rainfed. Nevertheless, crop type does influence the strength of the relations. In our case cotton shows only minor temperature difference compared to other vegetation classes. The strongest relations between canopy temperature and soil salinity were observed at the moment of a maximum green biomass of the crops which is thus considered to be the best time for application of the approach.

4.1 Introduction

Soil salinity is one of the severe land degradation problems that affects 1 billion hectares in more than 100 countries (Squires and Glenn, 2004). Moreover, it will increase at a rate of 2 million hectares per year (Abbas et al., 2013) because of the continuing global warming, resulting in desertification and sea water intrusion (Dasgupta et al., 2014). The causes of soil salinity differ from place to place and can be both natural and anthropogenic. There are areas where soils naturally has an increased content of soluble salt because of the weathering process and areas where the main cause is secondary salinization of irrigated areas because of inefficient irrigation schemes and absence or malfunction of a drainage system (Ghassemi et al., 1995). The effect of soil salinity on agricultural crops are extremely negative as it leads to leaf necrosis, altered phenology and ultimately plant death (Volkmar et al., 1998)

Most often soil salinity is measured by the use of geophysical instruments that measure soil or soil water extract electrical conductivity. That is done either in the field or in the lab, if soil saturated paste extract should be prepared. With a proper calibration this is considered a standard measurement procedure in most of the countries that produce regular soil salinity surveys. The more classical chemical analysis of samples are still used sometimes, but less and less because of the high costs associated and the amount of time required. There is a rich body of literature on the topic of soil salinity assessment by field and laboratory analysis and main points are well summarised in FAO Irrigation and Drainage Paper #57 by Rhoades et al. (1999).

Nevertheless, even improved methods of assessment, like the use of geophysical instruments mentioned earlier, are labour and cost intensive and cannot be implemented several times per season or even early on a big scale. Given this situation, timely monitoring of the problem is crucial. Remote sensing is widely used for the monitoring of different environmental phenomena, including soil salinity (Metternicht and Zinck, 2009). Both the spectra of bare soils and vegetation have been used, the latter more widely. Assessment of bare soil salinity has been

implemented mainly as a two-step process where firstly soil samples are spectrally analysed in laboratory conditions and a predictive model is built to relate the laboratory measurements to satellite spectral data which is subsequently applied for landscape scale assessments (Aldabaa et al., 2015; Bai et al., 2016; Nawar et al., 2014; Sidike et al., 2014). The vegetation canopy has been studied mainly by calculating different vegetation indices, from which normalised difference vegetation index (NDVI), enhanced vegetation index (EVI) and soil-adjusted vegetation index (SAVI) are the most popular ones (Elhag and Bahrawi, 2017; Hamzeh et al., 2016; Muller and van Niekerk, 2016; Rahmati and Hamzehpour, 2017; Scudiero et al., 2015). But current methods using vegetation indices and bare soil reflectance are site specific and do not demonstrate good performance on different study areas (Allbed et al., 2014b).

The use of canopy thermography is an innovative approach for salinity stress detection in plants (Ishimwe et al., 2014; Urrestarazu, 2013). The mechanism of the temperature change is based on plant salt stress response. One of the first components of this response is stomatal closure, which leads to reduced transpiration of a plant and increase of its canopy temperature (Munns and Tester, 2008). The effectiveness of canopy thermography was proven in laboratory and small scale field trials for many plants, including wheat, cotton, barley, euonymus (Gómez-Bellot et al., 2015; Hackl et al., 2012; Howell et al., 1984; Peñuelas et al., 1997), but its applicability for landscape scale studies using satellite sensors is still not well investigated.

Ivushkin et al. (2017) demonstrated that there is a significant correlation between satellite-derived canopy temperature and soil salinity levels, using MODIS satellite thermal images together with NDVI and EVI vegetation indices and a soil salinity map. Using an NDVI threshold they selected only cropped areas and implemented an ANOVA analysis on series of images for the growing season of wheat and cotton (April-October) in Syrdarya province of Uzbekistan. That study showed that satellite thermography data is significantly correlated to soil salinity and has a potential application in soil salinity mapping. Moreover, the F-values were higher for the thermography data then for commonly used vegetation indices. Despite the

positive outcome, the research had some limitations. It was conducted on a homogeneous irrigated area with mainly two crops grown in one climatic zone. As a result, questions about the method's applicability in different arid and semi-arid regions of the world and on different crops remained.

Therefore, the aim of this research is to test the satellite thermography soil salinity assessment approach (Ivushkin et al., 2017) on a different study area with different crops, grown both in irrigated and rainfed conditions, to evaluate whether the approach has general applicability. Three research questions are addressed. Does the satellite thermography soil salinity assessment approach apply to study areas different from the one on which it was developed? Is it applicable for different crops? Does it apply to both irrigated and rainfed agriculture?

4.2 Methods and materials

4.2.1 Study area

Among many affected areas of the world we have chosen Australia as a test area. This continent has vast salt-affected areas and a thriving agriculture sector where different crops are grown, both under irrigated and rainfed conditions. Moreover, Australia has an extensive database of land cover and soil salinity data, which allows us to answer our research questions about applicability of the technique for different crops and different agricultural practices (rainfed and irrigated) together with the question about application on different study areas.

Four study areas in four different states were selected to give broad representation of different crops cultivated under irrigated and rainfed conditions (Figure 4.1 and Table 4.2).

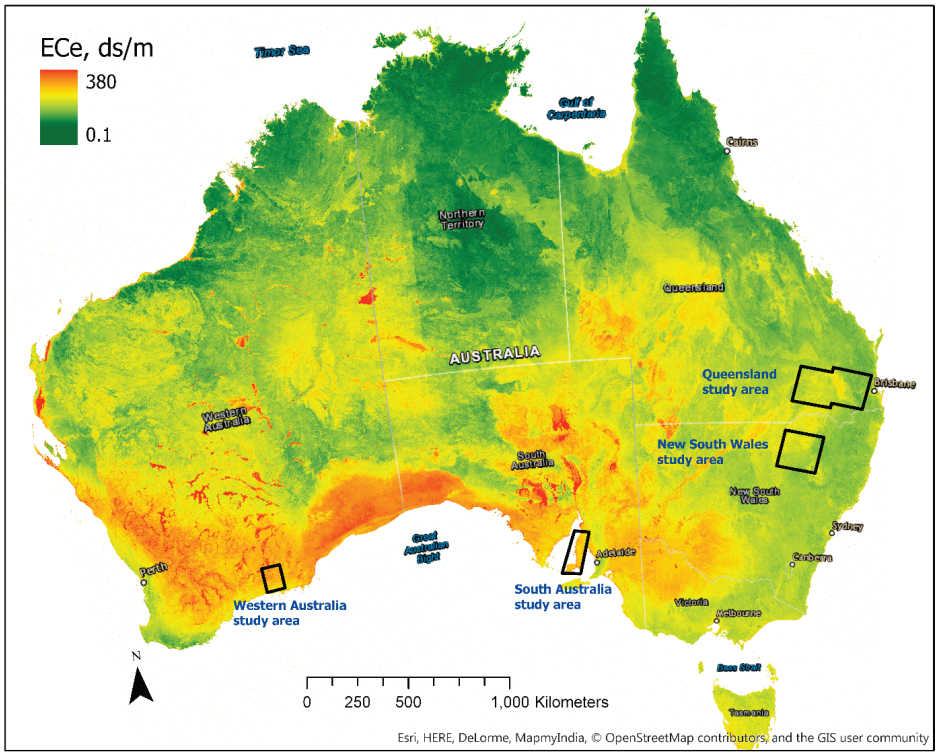

Figure 4.1. Study areas marked on soil salinity map of Australia (soil salinity data source: CSIRO Land and Water, Geoscience Australia).

The Western Australian study area is located to the North of Esperance and is the most arid area among the 4 selected locations (Table 4.1). Main crops grown here are wheat, barley and rapeseed. The main soil type is Sodosols. The other three study areas have comparable rainfall and temperature characteristics with mean annual rainfall of 500-600 mm. The South Australian study area is located on Yorke Peninsula, known as the barley capital of Australia. Main crops here are barley and wheat, with small part of areas for rapeseed. The most abundant soil type is Calcarasols with some areas covered by Rudosols, Tenosols and Sodosols. The New South Wales study area is located between Moree and Dubbo. Most of the cropped areas here are sown by wheat with small part for barley, irrigated and rainfed cotton. The area has diverse soil cover with an extensive cover of Vertosols and Sodosols and some areas of Kandosols, Ferrosols and Tenosols. The Queensland

study area is located to the west of Brisbane and sown mainly with sorghum and wheat, with small areas of irrigated and rainfed cotton. The most abundant soil types are Vertosols and Sodosols with smaller areas of Tenosols and Chromosols.

Table 4.1. Climatic characteristics of the study areas (Australian Bureau of Meteorology, 2017).

Study area state	Mean annual maximum temperature (°C)	Mean minimum temperature (°C)	Mean rainfall, mm	High rainfall months	Average soil salinity on the area investigated
Queensland	26.8	11.9	602	Dec, Jan, Feb	Slightly
New South Wales	26.7	11.6	646	Dec, Jan, Feb	Slightly
South Australia	21.7	11.3	506	May, Jun, Jul, Aug	Slightly to moderate
Western Australia	23.4	9.0	355	May, Jun, Jul, Aug	Moderately

4.2.2 Land use data

All land use data was accessed through the Australian Bureau of Agricultural and Resource Economics and Sciences website (ABARES, 2008a, b, 2009, 2012). Cotton was explicitly marked in the land use dataset and the class of (Irrigated) Cropping and Cereals were assumed to be either wheat or barley based on statistical data on agricultural lands areas from Australian Bureau of Statistics (2008). The data was collected in a period from 2006 to 2010. Based on the available land use classes we were able to analyse nine 'crop – study area' combinations (Table 4.2).

Table 4.2. Investigated 'crop - study area' combinations and their areas (ha).

	Irrigated cropping	Rainfed cropping	Rainfed cereals	Irrigated cotton	Rainfed cotton
Queensland	117877	1338606	-	62056	19742
South Australia	-	418656	406920	-	-
Western Australia	-	149037	-	-	-
New South Wales	89329	-	-	107145	-

4.2.3 Description of soil salinity data

The soil salinity data was prepared by the staff of Geoscience Australia and CSIRO Land and Water. The sampling campaign lasted from mid-2007 till the end of 2009, 1315 sites were sampled over Australia and EC values of 1:5 soil:water extract for

the 0-80 cm layer were measured (de Caritat and Cooper, 2011). Then log-transformed $EC_{1:5}$ for the whole continent were predicted using decision tree models that used climate variables, elevation and terrain attributes, soil and lithology classes, geophysics, and MODIS vegetation indices extracted at the same locations as the EC points. Values from 71 predictor variables in total were extracted from spatially co-registered 90-m grids. The machine learning software 'Cubist' (www.rulequest.com) was used as the inference engine for the modelling. Cubist builds piecewise linear regression trees. Models take the form: if [condition(s)], then [linear model], e.g., if [clim_etaaann > 259 and clim_rainsum <= 106.2 and soil_asc in (4, 6)], then log10 EC = [linear model]. A 90 : 10 training : test set data split was used to validate results, and 100 randomly sampled trees were built using the training data (Bui et al., 2017). The method is similar to the one used for mapping calcium carbonate across Australia, documented in Wilford et al. (2015). To use the currently most common classification of US Salinity Laboratory Staff (1954) $EC_{1:5}$ values were converted into ECe values by applying appropriate coefficients depending on soil texture. The final map we used is in a form of a raster grid with ≈90m resolution (Figure 4.1). Soil salinity classes used are based on FAO bulletin by Abrol et al. (1988) and described in Table 4.3.

Table 4.3. Soil salinity classes.

Soil salinity class	**ECe (dS/m)**	**Effect on crops**
Non saline	0 - 2	Salinity effects negligible
Slightly saline	2 - 4	Yields of sensitive crops may be restricted
Moderately saline	4 - 8	Yields of many crops are restricted
Highly saline	8 - 16	Only tolerant crops yield satisfactorily
Extremely saline	> 16	Only a few very tolerant crops yield satisfactorily

4.2.4 Description of Remote Sensing data

For analysis we used two kinds of satellite images products of Landsat 5 TM satellite. To mask out non-vegetated areas we used the NDVI product and to derive canopy temperature we used the Brightness Temperature product (USGS, 2017a). The NDVI product has a resolution of 30m and the Brightness Temperature has

120m resolution originally, but the system resamples it to 30m. To keep the data closer to its original resolution, both products has been ordered in 100m resolution and further analysis was implemented on a 100m grid. The Brightness temperature provided in kelvins with the accuracy up to one decimal place. All the products were downloaded through the 'On Demand Interface of Earth Science Processing Architecture', U.S. Geological Survey (USGS, 2017b). In total we analysed 118 images (38 for Queensland, 36 for New South Wales, 14 for South Australia and 30 for Western Australia) for the period from January 2007 to December 2009. These years were selected to have the best correspondence with the soil salinity map, which also was produced as a result of the sampling in the period from mid-2007 until the end of 2009.

4.2.5 Data analysis

First, images were clipped to the extent of the study area. After that, NDVI masks were applied to extract only vegetated areas for further analysis. The NDVI threshold we used is 0.3. This value was chosen after series of trials and ensures reasonable area coverage together with assurance that the area is vegetated. Further, all the images were clipped based on 'crop - study area' combinations (Table 4.1) to separately analyse different vegetation types. A special step was included for Western Australia because many small waterbodies were spread over the study area. To avoid their influence on canopy temperature data we buffered all waterbodies from the land use dataset by 200m and applied this buffer to the thermal data so only pixels farther then 200m from waterbody were used in the analysis. In the next stage all pixel values of all rasters (soil salinity, temperature, NDVI) were combined into database tables and relations between canopy temperature and salinity levels were statistically analysed by applying Analysis of Variance (ANOVA). The total amount of records analysed for each 'crop - study area' combination can be seen in Table 4.2, since the pixel size we used is equal to 1 ha.

All geodata was processed by means of a Python script in combination with ArcGIS software package through arcpy library (ESRI, 2016). Statistical analysis and data

visualisation was implemented with Python scripts and SPSS software (IBM Corp, 2015).

The analysis was implemented for different times during a growing season. That allowed us to investigate seasonality of the relationship between canopy temperature and soil salinity.

To enable a graphical comparison between different dates, study areas, and crops, we have plotted not the absolute temperature values but the deviation from the mean average temperature value for the scene under consideration (Figure 4.2). The schematic workflow is available in the Supplement material.

4.3 Results

Though we analysed the satellite images for three years, the data from 2007 demonstrated the most conclusive results and that is why here we show mainly results from that year. The data from 2008 and 2009 suffered from image quality issues, because of the intensive cloud cover, and being quite distant in time from the sampling dates, they were not included here.

There is a clear trend of temperature increase as soil salinity increases, as shown in the boxplots in Figure 4.2. The trend is more pronounced in the case of rainfed agriculture (Figure 4.2, South Australia and Queensland graphs), where differences between adjoining classes are usually more than 1°C. Irrigated vegetation on average shows less pronounced differences though the pattern is not significantly different from rainfed vegetation. Queensland graphs in Figure 4.2 demonstrate this as well, where the images for both areas (irrigated and rainfed) were captured on the same day. The irrigated and rainfed cotton boxplots also show identical patterns, but here the results are less conclusive, since we had only two salinity classes. Nevertheless, these results mean that the satellite thermography approach to assess soil salinity is applicable for both rainfed and irrigated agriculture.

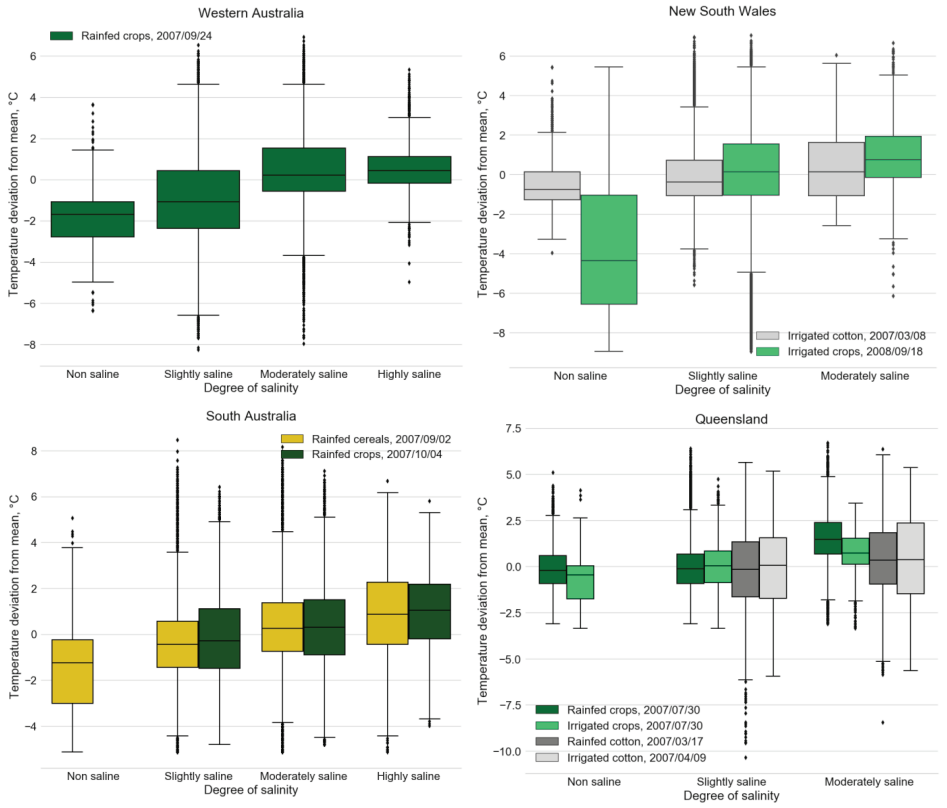

Figure 4.2. Canopy temperature boxplots for different study areas. All p-values < 0.01.

Between vegetation types there are also some differences. Under cotton, both rainfed and irrigated, there are lower mean temperature differences, which rarely reach 0.5 °C. This is an anticipated result and means that crop species under investigation should be taken into account and that less salt-tolerant crops will exhibit higher temperature differences.

Between study areas there are no significant differences, the trends are ascending in all 4 cases. This indicates that soil salinity leads to a general increase in canopy temperature independent of the crop type and presence or absence of irrigation.

The F-values, which are testing the relationship between canopy temperature and salinity level, and between canopy temperature and NDVI time series show that there is seasonality in the correlation (Figure 4.3). Highest F-values (the full ANOVA

tables are in the Supplement materials) are usually observed from August to October, which is a period of maximum green biomass for the main winter crops in Australia (wheat, barley, canola, rapeseed). On two study areas, where cotton is present, we detected a second peak of high correlations in March, when cotton is at its peak of green biomass. In most of the cases the peaks of NDVI and F-values coincide, which tells us that development stage of the crop is an important factor for the strength of the correlation.

In Figure 4.4 you can see and compare the soil salinity and canopy temperature map for the Yorke Peninsula. The general pattern is that high salinity values correspond quite well with high temperature values. For example, in the circles near the coast we can observe both high salinity and temperature values. In the map low salinity values corresponds overall also quite well with low temperature values. This is also clearly illustrated in the circle in the North-East part of the peninsula.

The Figure 4.5 also shows two maps of the soil salinity and canopy temperature for study areas in Queensland. The general pattern visible here is the difference between North and South parts. Highest temperatures are observed in the North part, the same as the highest salinity values. In the South there are less salt affected areas and also the lowest canopy temperature is observed.

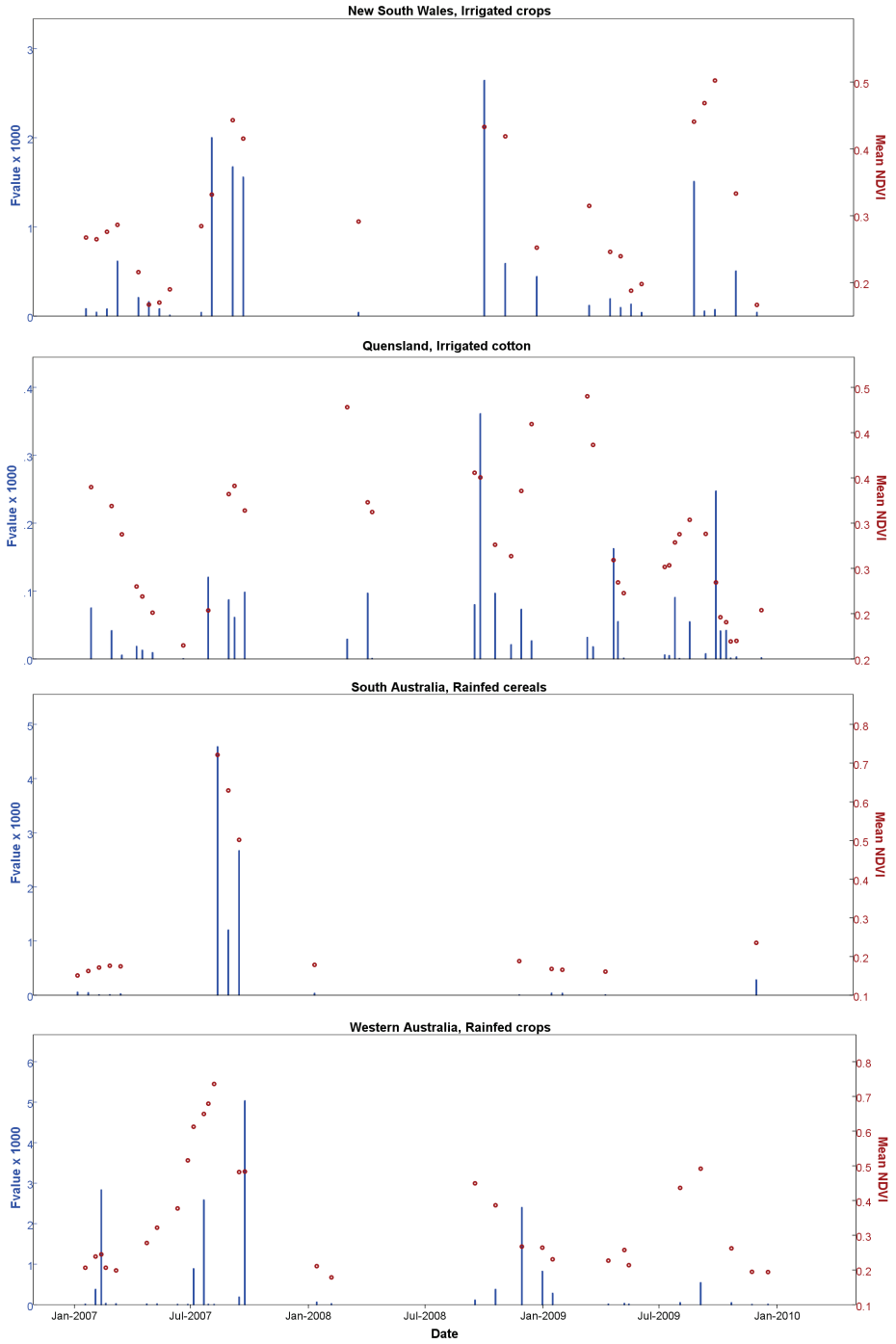

Figure 4.3. F-values and NDVI time series for different crops and areas.

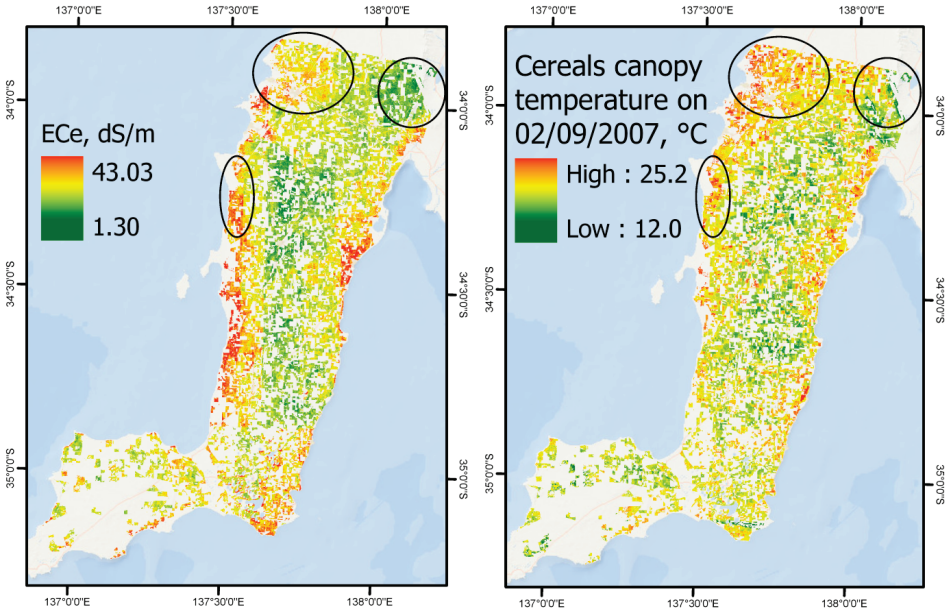

Figure 4.4. Maps of soil salinity and canopy temperature (South Australia, Yorke Peninsula).

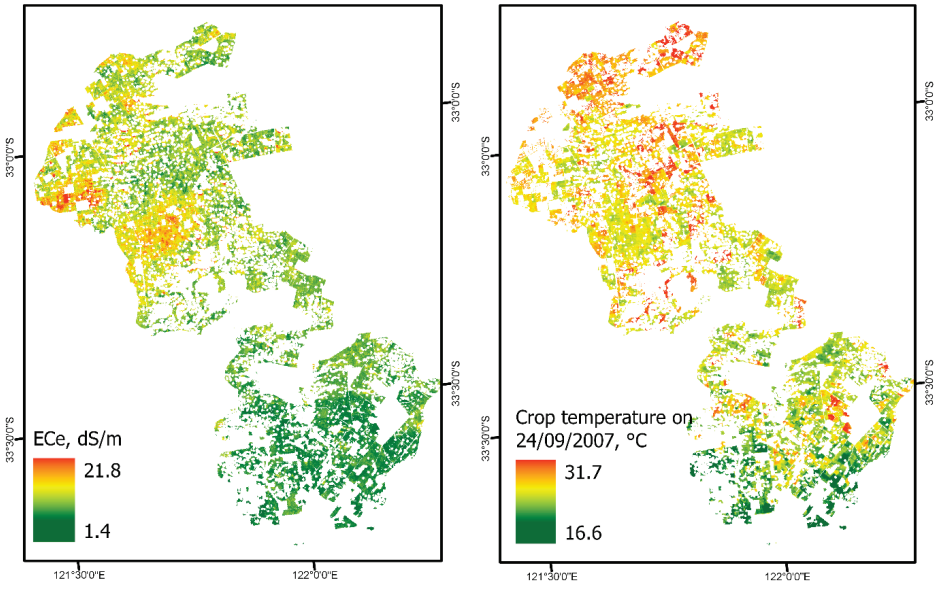

Figure 4.5. Maps of soil salinity and canopy temperature (Queensland, rainfed crop fields).

4.4 Discussion

The aim of the research was to test general applicability of satellite thermography to assess soil salinity on different areas. Australian study areas provided us with diverse set of environments in a range of arid and semi-arid climatic zones. Moreover, here we were able to investigate the method applicability for different crops including wheat, cotton, barley and rapeseed under different climatological and management conditions.

The temperature differences between salinity classes (Figure 4.2) are present in all study areas and for all crops, which suggests that soil salinity significantly influenced the crop temperature. These findings are in line with what was described in Ivushkin et al. (2017). However, in our current research cotton exhibited only a slight increase in canopy temperature as salinity increases while in Uzbekistan cotton was more sensitive to soil salinity compared to wheat. But that is explained by the leaching regime on the study area in Uzbekistan and its timing. In general, cotton is more salt tolerant than wheat and most other cereals (Ayers and Westcot, 1985). That is what we see in the Australian results, where cotton, both irrigated and rainfed, shows only a slight temperature increase, compared to other crops.

The investigation of seasonality suggests that the approach is not equally applicable all year round. Figure 4.3 shows that highest F-values in most of the cases corresponds with NDVI peaks, but there are some inconsistencies. To avoid them in the future we suggest to increase the NDVI threshold used from 0.3 to 0.5 on study areas with dense vegetation. We did not do it in the current study to be able to investigate seasonality patterns of the phenomena. But in operational application that will provide more clear results because then only highly developed vegetation at the peak of green biomass will be included into analysis.

The approach is universal in terms of thermal satellite images used. MODIS (Ivushkin et al., 2017) and now Landsat data show similar patterns and relationships between soil salinity and canopy temperature. Which means that both coarse resolution of MODIS (1km) and medium resolution of Landsat (120m) can

be effectively used. Though Landsat would be more applicable for farm and field scales, and MODIS for landscape scale, to characterise soil salinity in the whole province, for example.

Obviously, there might be other factors influencing canopy temperature, water bodies for example most likely will decrease canopy temperature in their vicinity. To mitigate this effect, we removed pixels adjacent to surface water bodies from the analysis in the Western Australia study area. Some other interfering factors like irrigation and irregular management may be irrelevant depending on scale. Irrigation schedule is unlikely to significantly influence temperatures on a regional scale, although definitely should be taken into account when farm or field scale assessment is implemented. The same is true for uniformity of land management.

Moreover, even when correct canopy temperature readings are obtained, there might be other stress factors that lead to canopy temperature increase. The most common of these factors is the water stress, which causes a response which is similar to salinity stress. Most of the work about canopy temperature which we referred to in the introduction are mentioning water stress as an important factor defining canopy temperature (Gómez-Bellot et al., 2015; Hackl et al., 2012). Mitigating this influence is possible by making sure that water stress is not present, or that its effect is negligible. That can be done by obtaining the water status of the investigated area. In case of irrigated agriculture this is less of a problem since most of the time crops will avoid water stress, and in case of rainfed agriculture the data on precipitation might be used. Moreover, water stress will change the measurements a lot in case of multitemporal or broad scale assessment, where multiple scenes will be used, but inside one scene plants' water status will be similar, even if stressed, and influence of water stress on the measurements will be nullified.

Of course, the ultimate goal of these kind of research would be an inversion model, which will allow conversion of temperature values into soil salinity values. Though additional factors of increased thermal energy dissipation, like macro and micronutrient deficiencies or metal toxicities should be accounted for (Morales et

al., 2014). The outcomes of the research suggest that inversion model could be done if auxiliary data is available. Preliminary data on the study area will be required. The extent to which an area is affected by salinity should be known to properly calibrate the model. Application without any prior knowledge and ground truth data will hardly lead to any meaningful assessment. Also, it is obvious that cropping pattern will matter, because of different salt tolerance of crops. The management practices data will also positively contribute to the model accuracy, temperature decrease caused by recent irrigation must be considered. That will especially matter in case of small scale assessment (several fields). In case of rainfed agriculture rainfall data will be of use. In general, we see potential for predictive models in case auxiliary data are available and contemporary computational capabilities, like machine learning, are applied.

4.5 Conclusions

The current study investigated the applicability of satellite remote sensing of canopy temperature as an approach of soil salinity assessment for different crops grown under irrigated and rainfed conditions. We concluded that in all cases average canopy temperatures were significantly correlated with soil salinity of the area (in the period of green biomass peak all p-values<0.01). It is valid for all investigated crops, grown both irrigated and rainfed. Nevertheless, crop type does influence the strength of the relations. In our case cotton, as salt tolerant plant, shows only minor temperature difference compared to other vegetation classes which suggests that less salt tolerant species will demonstrate higher temperature differences and will allow a more accurate assessment of soil salinity.

The approach is also flexible in terms of thermal imagery used. It has been applied using both MODIS and Landsat data and, in both cases, similar patterns and trends were present, despite the very different spatial resolution of these two sensors.

Up to now the method has been tested in two different parts of the world: Uzbekistan and Australia. In both cases soil salinity significantly defined canopy

temperature of the crops grown. That allows us to conclude that the method can be applied in other arid and semi-arid parts of the world.

Since the method is based on canopy temperature measurements, there is an obvious limitation for timing of the monitoring. The strongest relations between canopy temperature and soil salinity were observed at the moment of a maximum green biomass of the crops thus that is the best time for application of the approach.

Chapter 5

Global mapping of soil salinity change

This chapter is based on:

Ivushkin, K., Bartholomeus, H., Bregt, A.K., Pulatov, A., Kempen, B., de Sousa, L. Global mapping of soil salinity change. Submitted to Remote Sensing of Environment.

Abstract

Soil salinity increase is a serious global threat to agricultural production. The only database that currently provides soil salinity data with global coverage is the Harmonized World Soil Database, but it has several limitations when it comes to soil salinity assessment. Therefore, a new assessment is required. We hypothesized that combining soil properties maps with thermal infrared imagery and a large set of field observations within a machine learning framework will yield a global soil salinity map. The thermal infrared imagery acts as a dynamic variable and allows us to characterize the soil salinity change. For this purpose we used Google Earth Engine computational environment. The random forest classifier was trained using 7 soil properties maps, thermal infrared imagery and the ECe point data from the WoSIS database. In total, six maps were produced for 1986, 2000, 2002, 2005, 2009, 2016 respectively. The validation accuracy of the resulting maps was in the range of 67-70%. The total area of salt affected lands by our assessment is around 1 billion hectares, with a clear increasing trend. Comparison with 3 studies investigating local trends of soil salinity change showed that our assessment was in correspondence with 2 of these studies. The global map of soil salinity change between 1986 and 2016 was produced to characterize the spatial distribution of the change. We conclude that combining of soil properties maps and thermal infrared imagery allows mapping of soil salinity development in space and time on global scale.

5.1 Introduction

Soil salinity increase is a serious global threat to agricultural production. It affects an area of more than 1 billion hectares in more than 100 countries all over the world and these numbers are constantly growing (Abbas et al., 2013; FAO and ITPS, 2015; Squires and Glenn, 2004; Szabolcs, 1989). Besides this estimate of the global area affected by soil salinity, several others are available which differ in the extent of the affected area, sometimes quite dramatically (IAEA, 1995; Oldeman et al., 1991). Therefore, only a rough approximation of salt affected areas globally can be given. FAO (2018b) recognises this issue and stresses that the divergence of current estimations of the extent of salt affected areas are quite often the result of differences in methods for collecting and aggregating statistics. They specifically state that there is a need for data on the rate of change in areas affected by salinization at regional and global level (FAO, 2018b). Status of the World's Soil Resources report by FAO and ITPS (2015) also mentions that information on the extent and characteristics of salt-affected soils is very scattered.

The only database that currently provides soil salinity data with global coverage is the Harmonized World Soil Database. This database is an important source of soil data for global studies, but it has several limitations when it comes to the soil salinity assessment. First, the database consists of soil mapping units, rather than continuous grid with soil properties' values unique for each pixel. It has > 15,000 of such units and has only a single soil salinity value per unit, of which some are stretching for hundreds of kilometres. So, although the spatial resolution of the maps produced from this database is around 1 km, the actual spatial resolution in case of soil salinity is much coarser. Second, though the database was updated several times in the past (last time in 2012; version 1.2), most of it is based on the FAO/UNESCO Soil Map of the World created in 1970-1981, which can be considered outdated given the highly dynamic nature of soil salinity. Lack of spatial detail and outdated data illustrate the need for an updated global soil salinity map.

Having up to date information on spatial distribution and severity of soil salinity is crucial for agricultural management of affected areas, to take necessary measures

to reduce or even avoid economical losses and restore the productivity of the soil. Mapping dynamic soil properties like salinity has challenges compared with other, less dynamic properties. Soil salinity can rapidly change after irrigation or a rainfall event. Drought on the other hand might increase salinity in the course of several weeks. Therefore, monitoring by traditional methods will require sampling frequently in time, which can be cost-prohibitive. That is one of the reasons why remote sensing methods are now used more and more often for soil salinity monitoring and mapping (Allbed and Kumar, 2013).

Remote sensing is used for soil salinity mapping already for years (Metternicht and Zinck, 2009). Nevertheless, there are still no universally acceptable methods to derive soil salinity parameters from remote sensing data that can be used for different environments. On field and local scales many studies have been conducted that proposed conversion models from remote sensing variables to soil salinity levels on the ground. Nevertheless, these models usually do not demonstrate the same high accuracy in different parts of the world (Allbed et al., 2014a; Allbed et al., 2014b; Douaoui et al., 2006), which means that scaling up to global scale is problematic.

Recently, thermal infrared imagery was used to distinguish between different levels of soil salinity on agricultural lands (Ivushkin et al., 2017; Ivushkin et al., 2018). The principle behind this approach is that the canopy temperature of the plants grown on the affected area will be higher than of plants growing in a non-affected area. The approach has been tested on regional and local scales and showed its robustness in different climatic conditions and on areas covered with different crops. Therefore, it seems promising for use on a global scale.

We foresee, however, that scaling up to the global level will bring additional challenges like the issue of different climatic zones. The thermal approach has been previously applied to areas small enough to presume a constant air temperature per single satellite image acquisition scene, therefore there was no need to normalise the values. On the global scale this will be impossible because of the different climatic zones and extreme temperature differences between regions; and

use without normalisation will just lead to characterisation of a climate, rather than soil salinity. But even with some kind of normalisation using only the thermal data on the global scale will be insufficient because of other factors that will influence the temperature.

Here we propose to tackle that challenge by using auxiliary data. It is known that other soil properties are correlated with soil salinity. For example, Al-Busaidi and Cookson (2003) described the interrelations of pH and soil salinity, Setia et al. (2013a) studied the influence of soil salinity on the soil organic carbon content. A connection between cation exchange capacity and soil salinity has also been reported (Saidi, 2012). Moreover, bulk density and soil texture can have some auxiliary information for soil salinity monitoring. Often saline and alkaline soils are affected by compaction and lower water retention in sandy soils will make them less prone to salinity problems. Global maps of properties relevant for soil salinity mapping are available from the SoilGrids portal[2] (Hengl et al., 2017).

We hypothesize that combining these maps together with the thermal infrared imagery and a large set of field observations on soil salinity indicators, such as the electrical conductivity within a machine learning framework will yield a global soil salinity map. Moreover, since the SoilGrids data is static, using the thermal data from different time periods will enable us to assess soil salinity change in the area of interest over time. Therefore, the overall aim of this study is to investigate if combination of soil properties maps and thermal imagery will allow us to map the development of soil salinity in space and time on global scale and measure how accurate these estimates will be.

5.2 Methods and materials

Because our study was implemented at global scale, we decided to use Google Earth Engine (GEE) as freely available platform especially tailored for analysis and

[2] https://soilgrids.org

processing of geodata at global scale. Among GEE advantages are the extensive library of geospatial datasets, including the widely used satellite imagery, and computational power enough to process these data on the global scale. GEE has already been used for soil properties mapping. For example for soil moisture mapping (Sazib et al., 2018) or soil type and soil organic carbon mapping (Padarian et al., 2015). Therefore, it became our platform of choice for a further analysis.

5.2.1 Ground truth data

As ground truth we used the WoSIS Soil Profile Database (Ribeiro et al., 2015), which is maintained by ISRIC – World Soil Information and includes over 100,000 georeferenced soil profiles. For our study we selected soil profiles containing electrical conductivity (ECe) values for upper soil layer, which varied from 0-5 cm to 0-60 cm. In total, 15,188 data points were selected and used in further analysis. The spatial distribution of the data points is shown in Figure 5.1.

The ECe values were classified into Non saline (12,160 points), Slightly saline (2,106 points), Moderately saline (440 points) , Highly saline (232 points) and Extremely saline (250 points) classes according to the widely used classification of Abrol et al. (1988).

Table 5.1. Soil salinity classification used.

Salinity class	Non-saline	Slightly	Moderately	Highly	Extremely
ECe, ds/m	<2	2-4	4-8	8-16	>16

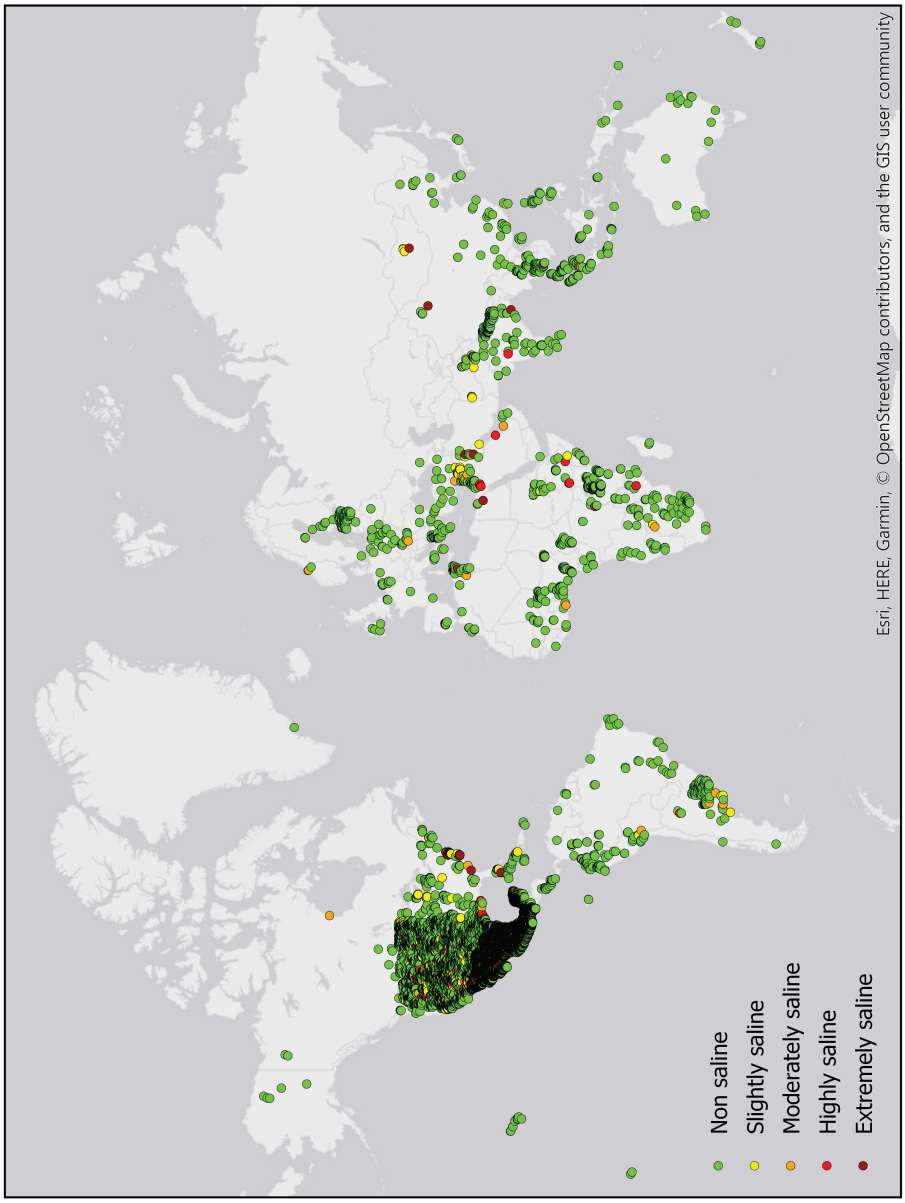

Figure 5.1. Distribution of ground truths sampling data.

5.2.2 Data processing and analysis

5.2.2.1 Thermal remote sensing data pre-processing

Two thermal datasets were used. The first one is the USGS Landsat 5 Surface Reflectance Tier 1 collection and second is the USGS Landsat 8 Surface Reflectance Tier 1 collection, both of which are available from the GEE data catalogue. Both collections provide orthorectified brightness temperature acquired in wavelength range from 10.4 to 12.5 micrometres. Landsat 8 data were used in this study for the year 2016, Landsat 5 data were used for 1986, 2000, 2002, 2005, 2009. In these years average mosaics from available cloud-free images in the period from March to September were calculated on per-pixel basis and used in further analysis. As an input variable for our modelling we chose to work with the temperature anomaly instead of the absolute temperature to harmonise the data for the global analysis. This means that for each pixel the recorded temperature value was subtracted from the long-term temperature average for this pixel. This was done for each global layer in our thermal time series. The long term average dataset have been constructed from the Landsat 5 GEE dataset mentioned before by calculating the average in the period from 1999 to 2012 from all available cloud-free images on per-pixel basis.

5.2.2.2 Data modelling

We used the temperature difference layers together with several SoilGrids layers. SoilGrids is a collection of global soil class and soil properties maps (Hengl et al., 2017). In our analysis we used seven grids that contain information indirectly connected with soil salinity: sand content, silt content, clay content, pH in H_2O, cation exchange capacity, bulk density, organic carbon content. These grids are available for seven depths up to two metres. Here we used the top layer (0 cm). The Landsat thermal images have been resampled during the processing to 250 m by a built-in functionality of GEE.

The random forest classifier was trained using the eight variables mentioned and the ECe data from the WoSIS database. The random forest algorithm constructs an ensemble of decision trees and lets them “vote” for the most probable class

(Breiman, 2001; Strobl et al., 2009). We set the number of trees parameter to 50 and mtry parameter (variablesPerSplit argument in GEE) to the square root of the number of variables. This number of trees was chosen after a set of trial runs during which we established that further increase in the number of trees does not bring any significant increase in the map validation accuracy.

In total six models were trained and six maps were produced. For each model we used thermal imagery from a different year. The maps have been produced for six time steps: 1986, 2000, 2002, 2005, 2009, 2016. These years have been selected to correspond with other studies describing temporal changes in soil salinity (Fan et al., 2012; Taghadosi and Hasanlou, 2017; Wang et al., 2008).

In the learning stage we used around 3500 points from the WoSIS database. They were selected by random stratified sampling, preserving the relative salinity class distribution in the ground-truth dataset. Meaning that the non saline class will be the most abundant and the highly and extremely saline classes will be less abundant in the training dataset. The final learning dataset consisted of 2,000 points of Non saline class, 1,000 of Slightly saline, 210 of Moderately saline, 105 of Highly saline and 110 of Extremely saline classes. The trained classifier was applied to the eight layers mentioned earlier to produce the final global map of soil salinity.

The map was validated by selecting randomly 100 points of each class from the WoSIS database. The 100 was selected as a maximum because of the limited amount of points in Highly and Extremely saline classes. A higher number would lead to significant overlap between learning and validation points in these classes. For the selection of validation points a different randomisation seed was used than for the learning stage. The equal amount of points for each class ensures that the final validation accuracy represents the accuracy throughout the entire range of salt affected areas. We expected that the Non-saline class will have the highest classification accuracy and using non-stratified selection of validation points will unjustly overestimate the accuracy. During the validation we compared the salinity class at the validation site with the mapped values. The same validation set has been used for maps of all years by using the same seed in random stratified sampling

function. The main accuracy metrics calculated are provided further in the results and these are confusion matrix, overall accuracy, user's accuracy and producer's accuracy.

We did not select more than 3500 points because attempts to increase the number of training points lead to critical errors in most runs, and for runs where the computation did finish the increase in validation accuracy was not significant. Therefore 3500 has been selected as a number of data points for all further runs.

The resolution of the final maps is 250 m, which is similar to the resolution of the SoilGrids input layers.

5.3 Results and discussion

5.3.1 Global distribution of soil salinity

Figure 5.2 shows a global map of soil salinity classes using the thermal image of 2016. It highlights main salt affected areas in North America, Central Asia, Middle East.

Global statistics of affected area for all six time steps are presented in Figure 5.3 and Table 5.2. Our analysis shows that the total area of salt affected lands increased with more than 100 Mha between 1986 and 2016, though some natural variation is present. The majority of the increase is the increase in slightly saline area. This suggests that more and more previously unaffected areas are starting to suffer from soil salinization. That is supported by the fact that the total area of affected lands is continuing to increase. The actual area of Moderately saline areas has decreased, while Highly and Extremely saline are more volatile in time.

Figure 5.2. Resulting global soil salinity map for 2016.

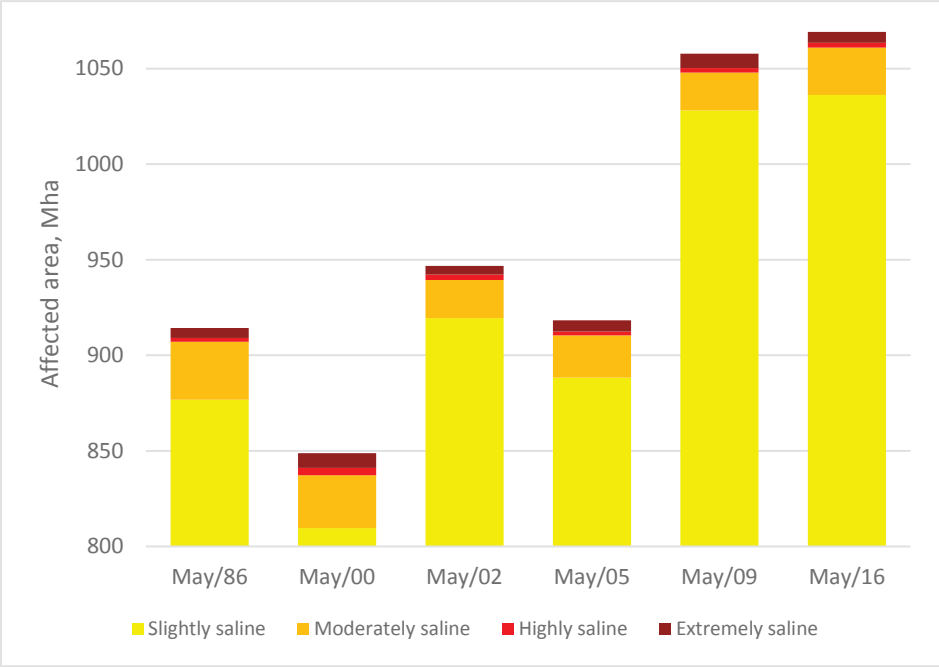

Figure 5.3. Salt affected lands composition in different years (y-axis uses offset).

Table 5.2. The world salt affected area as predicted from ground truth data, thermal satellite imagery and soil property maps for different years, Mha.

	Slightly saline	Moderately saline	Highly saline	Extremely saline	Total
May/86	877.9	30.3	2.1	5.2	915.5
May/00	809.6	27.7	3.8	7.7	848.8
May/02	919.5	20.0	2.7	4.5	946.7
May/05	888.3	22.2	2.0	5.8	918.3
May/09	1,028.2	19.8	2.3	7.4	1,057.7
May/16	1,036.2	24.8	2.5	5.8	1,069.3

We found two sources referring to a global distribution of salt affected lands. Szabolcs (1989) assessed the total area of salt affected lands globally to be around 955 Mha, which is not far from our assessment of 914 Mha in 1986. The second source is the review by Squires and Glenn (2004) where the salt affected area approximately covers 1 billion hectare. We consider correspondence of other

studies with our assessment quite encouraging, since 68% validation accuracy (Table 5.3) and unequal distribution of training and validation data might suggest bigger discrepancy with other assessments that were based more on field studies.

Another interesting observation from the global map in Figure 5.2 is that affected areas in Central Asia have been captured. We had almost no training points in that area (Figure 5.1), but the region is known to be one of the most severely affected by soil salinization. In our opinion, this finding is supporting the principal validity of the method. However, we acknowledge that comparison with ground truth data from this area is required to further assess how well the maps produced here represent the spatial soil salinity patterns in Central Asia.

The map generally captures known hotspots in salinity-affected regions, which we further discuss towards the end of this section, but also shows overestimation of salt-affected areas. For example, the map shows that Mexico is almost completely salt affected, which is an overestimation. Szabolcs (1989) states that 1.65 Mha is the area of salt affected lands in Mexico. This number would increase to this time, but still would be far from the total area of the country. We supposed that one of the reasons for this overestimation is an underrepresentation of Non saline class data points in the samples collected in Mexico. But after scrutinizing the sample dataset this appeared not to be the case. A vast majority of these samples (77%) belong to the Non saline class, which is comparable with the distribution in the dataset for the whole world. Moreover, trial maps produced with different seed numbers still had the same overestimation for Mexico. Therefore, it is not the result of a sampling bias, but probably the specific combination of values in soil properties maps we used for prediction that lead to this overestimation. In global affected area assessments this overestimation was probably negated by some cases of underestimation, like in Australia, where only few patches of salt affected lands are shown.

The validation accuracy of this map is 68%. For different time steps classification is in a range of 67-70%, depending on the date of thermal images used. In general,

highest accuracy of 70% has been achieved when thermal images of 2000-2002 were used.

Most of the classification errors appear in highly and extremely saline classes (Table 5.3). Those are the less common classes globally and they represented only a small fraction of WoSIS database, therefore we presume that using a larger number of highly and extremely saline training points might increase the accuracy. The influence of the amount of training points is especially visible if you compare the accuracy of two classes. The highly saline class is even less abundant in WoSIS database than Extremely saline. Therefore, less training points for the Highly saline class have been used and accuracy for it is less than for Extremely saline, though in reality Highly saline areas are more widespread than Extremely saline ones.

The important result is that when a point is misclassified, in most cases this point is still in a saline class, though maybe of different degree, and only rarely is assigned to the Non saline class. When only two classes are considered (saline and non saline) producer's accuracy raises up to 89%. That suggests that the approach is quite useful in distinguishing between salt affected and non affected lands, and only the definition of the degree of salinity remains challenging.

Table 5.3. Confusion matrix and accuracy statistics of 2016 map.

		Predicted						
	Salinity class	Non saline	Slightly saline	Moderately saline	Highly saline	Extremely saline	Total	Producer's accuracy, %
Observed	Non saline	**90**	10	0	0	0	100	90
	Slightly saline	10	**88**	1	0	1	100	88
	Moderately saline	11	28	**61**	0	0	100	61
	Highly saline	15	34	4	**47**	0	100	47
	Extremely saline	18	29	1	0	**52**	100	52
	Total	144	189	67	47	53	500	
	User's accuracy, %	62.5	46.6	91	100	98.1		

Together with random forest algorithm we checked two other classifiers available in GEE that are based on machine learning principles. The Support Vector Machine did not produce any meaningful results in our case. Almost the whole map has been classified as non-saline area. Classification and Regression Trees (CART) algorithm showed some better results, but still worse than the Random Forest algorithm. The

accuracy was around 50% and the map unrealistically overestimated highly and extremely saline areas.

As we mentioned previously in this section, the global maps captured known soil salinization hotspots. One of them is Grand Forks county on the border of North Dakota and Minnesota in the United States. It is a known salt affected area (Seelig, 2000) and it has been depicted on the map we produced (Figure 5.4). In Seelig (2000) this area is marked as an area of frequent inclusion in productive land, which correspond to areas marked as Moderately saline in Figure 5.4.

One of a few countries in Europe affected by inland soil salinity problem is Hungary. Our map of the area in Figure 5.5 shows some slightly affected areas, which is correct for the area where ECe values are just slightly higher than 2 ds/m (Kovács et al., 2006). Though some areas have been correctly identified, the big areas in the east of Hungary have been missed. The probable cause is that most of the areas with higher salinity are grasslands and croplands with more tolerant species, therefore our method, which includes crop canopy temperature metric, did not capture those areas.

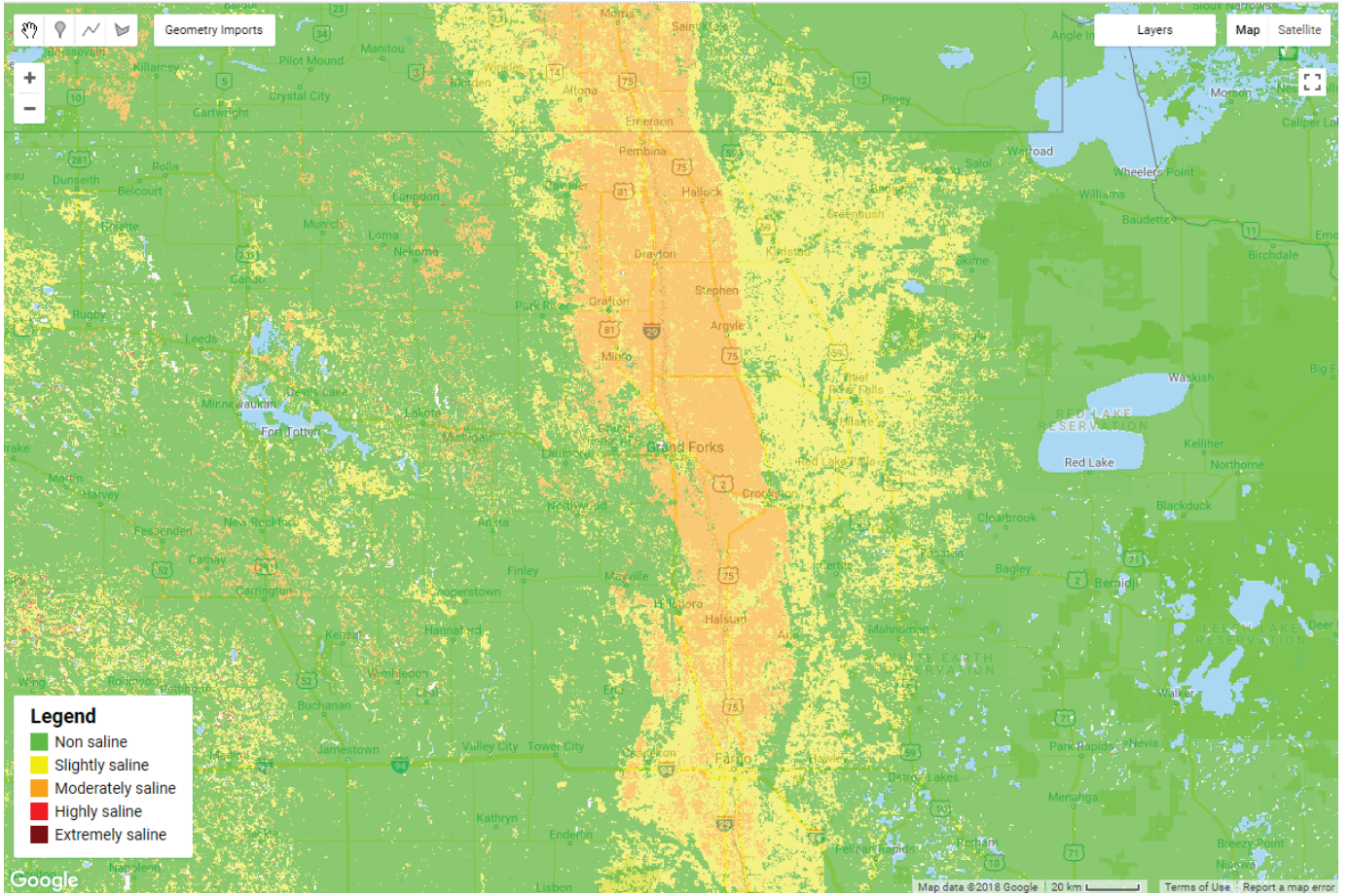

Figure 5.4. Soil salinity map of Grand Forks county and surroundings (2016).

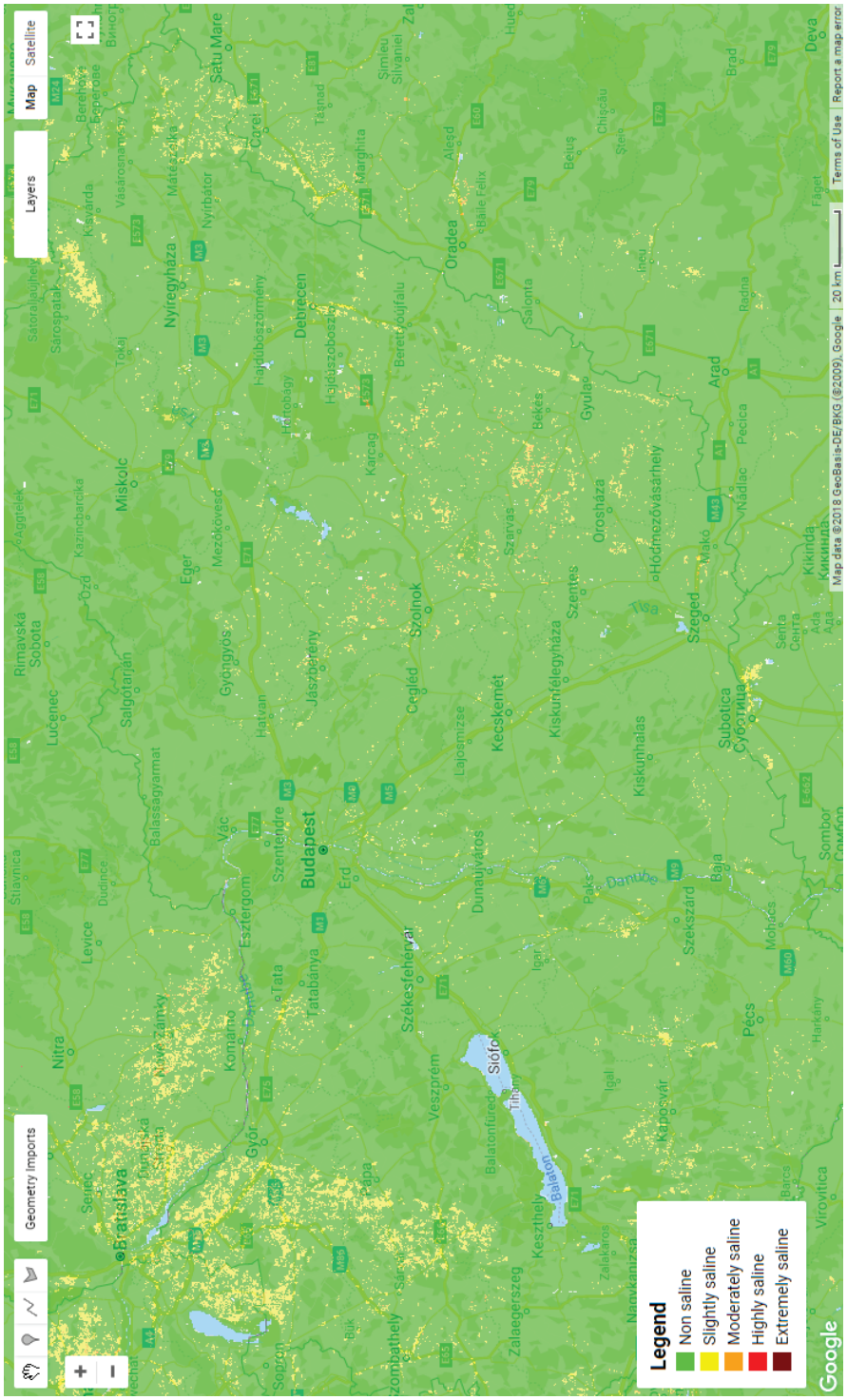

Figure 5.5. Hungary map of soil salinity (2016).

5.3.2 Local soil salinity change

To verify our hypothesis that integration of thermal infrared imagery from different periods of time will allow us to asses temporal change in soil salinity, we compared our maps with outcomes of several studies where such change is assessed for certain areas.

Figure 5.6 shows the soil salinity map for study area in Xinjiang Province, China. According to Wang et al. (2008) this area in a period from 1983 to 2005 suffered an increase in soil salinity due to irrigation and a rise in the shallow water table. A similar increase is shown by the maps.

Another area of interest we found data on is the Bakhtegan Salt Lake region in Iran. According to Taghadosi and Hasanlou (2017) more that 76% of vegetated areas of this region experienced increase in soil salinity from 2000 to 2016. This is in accordance with the maps shown in Figure 5.7, where the map from 2016 shows significantly more salt affected areas compared with the map from 2000.

The next area we investigated is the Yellow river delta in China. Fan et al. (2012) have researched the dynamics of the soil salinization in the region for the period from 1985 to 2006. Their results show that while in 1985 salt affected areas were mostly located in the immediate vicinity of the river, in 2006 the majority of salt affected areas have been mapped around the coast. In general, during those two decades the area suffered rapid increase in soil salinity.

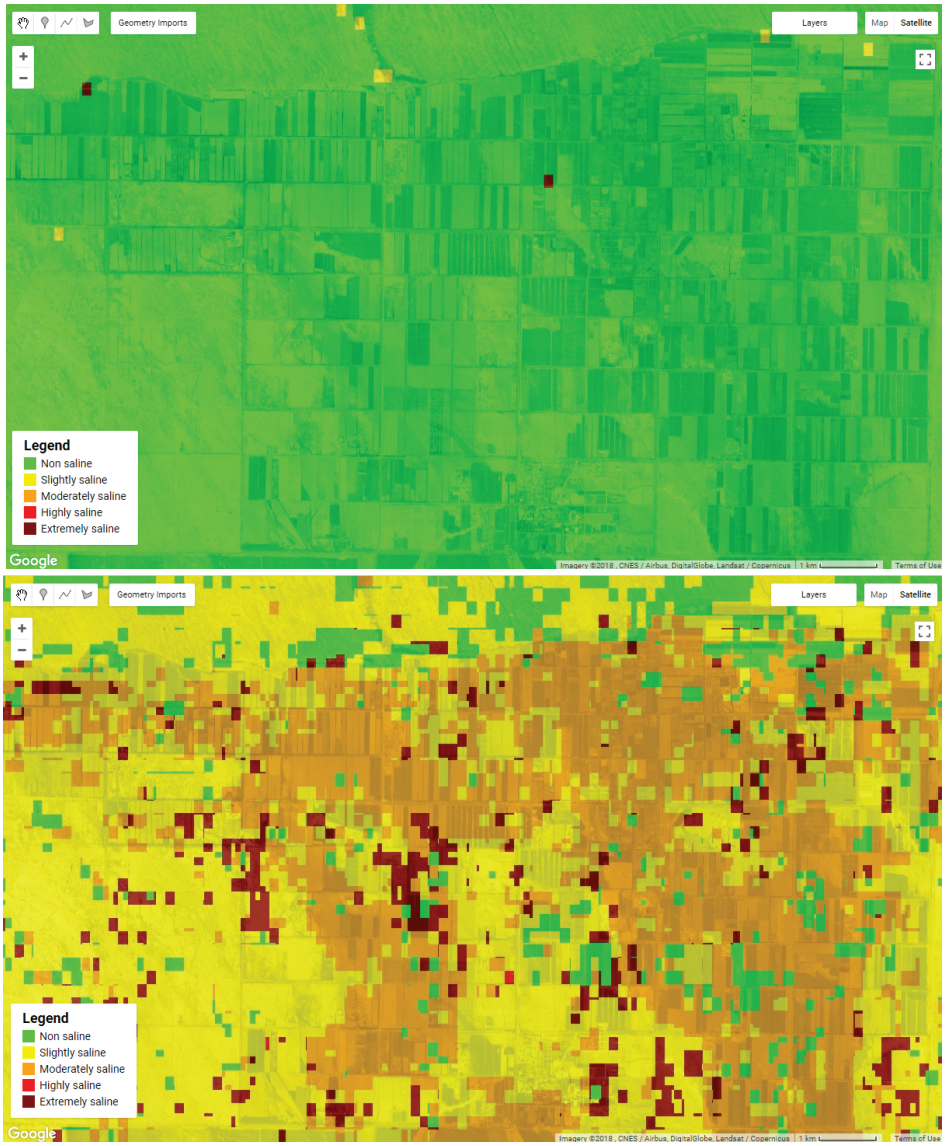

Figure 5.6. Soil salinity maps (upper from 1986 and lower from 2005) of the Fubei region of Xinjiang Province, China. According to Wang et al. (2008) soil salinity increased in this area.

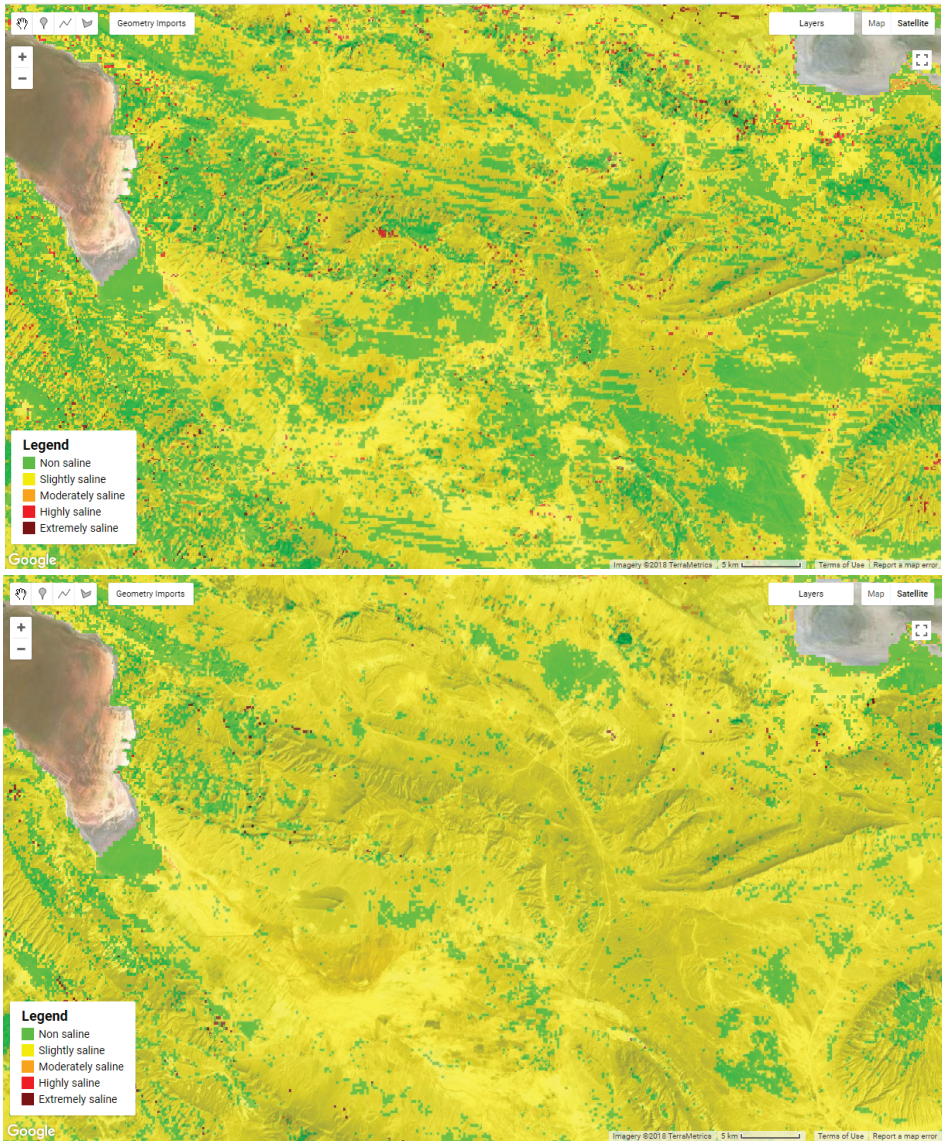

Figure 5.7. Soil salinity maps (upper from 2000 and lower from 2016) of the Bakhtegan Salt Lake region in Iran. According to Taghadosi and Hasanlou (2017) soil salinity increased in this area.

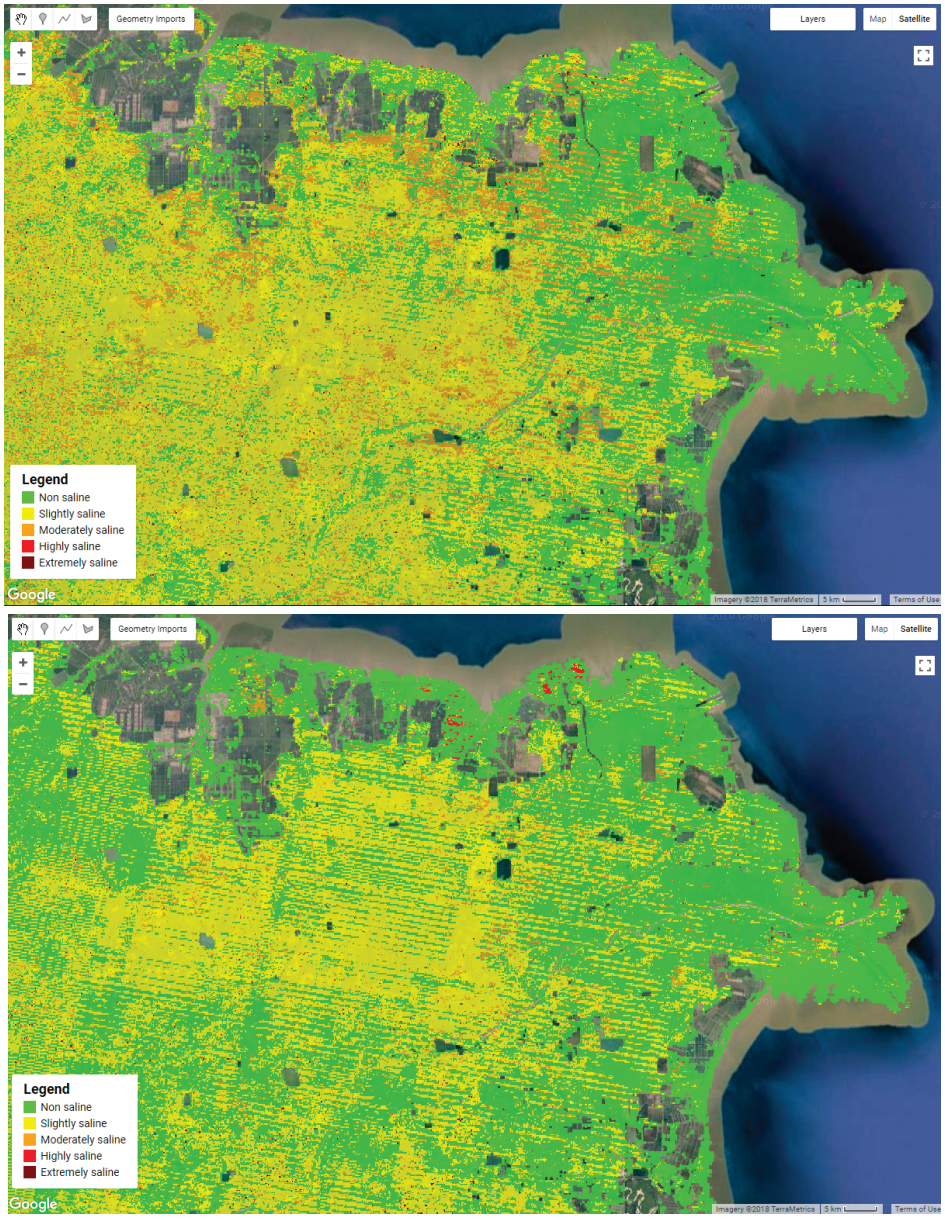

Figure 5.8. Soil salinity maps (upper from 1986 and lower from 2005) of the Yellow River Delta, China. According to Fan et al. (2012) the soil salinity increased in this area.

On contrary to the cases described previously, our map of the Yellow River Delta is not in complete accordance with the reference. In Figure 5.8 the map from 1986 shows visibly more salt affected areas compared with the map from 2005. Nevertheless, some of the changes seem to be captured. For example, from 1986 to 2005 salt affected areas in immediate vicinity of the Yellow river have decreased. Moreover, some highly affected spots appeared on the coastal area in the north of the 2005 map. Both of which is in accordance with the results of Fan et al. (2012).

The probable reason of the discrepancy in this result is the specifics of soil salinity development in this area. Here the main reason is the seawater intrusion, while in previous cases we looked into the problem of inland, dryland salinity. Moreover, close proximity of the sea could also influence the thermal data results.

5.3.3 Global changes map

To understand the spatial distribution of soil salinity change we produced a soil salinity change map (Figure 5.9). That is a difference map between 1986 and 2016 maps. In accordance with the statistics presented earlier (Table 5.2, Figure 5.3) the map shows mainly an increase in soil salinity. Yellow colours, representing the increase, are prevalent, while only few areas of the decrease can be seen. The majority of the salt affected areas experienced a change to a neighbouring class (i.e. from Non saline to Slightly saline or from Extremely saline to Highly saline) that is why only two colours are shown in the map. However, there are some areas of interest where more dramatic changes appeared. Those are marked by circles on the map. The area in Kazakhstan experienced an increase in soil salinity severity of up to 3 classes up and areas in the North of the US have experienced a decrease of up to two classes.

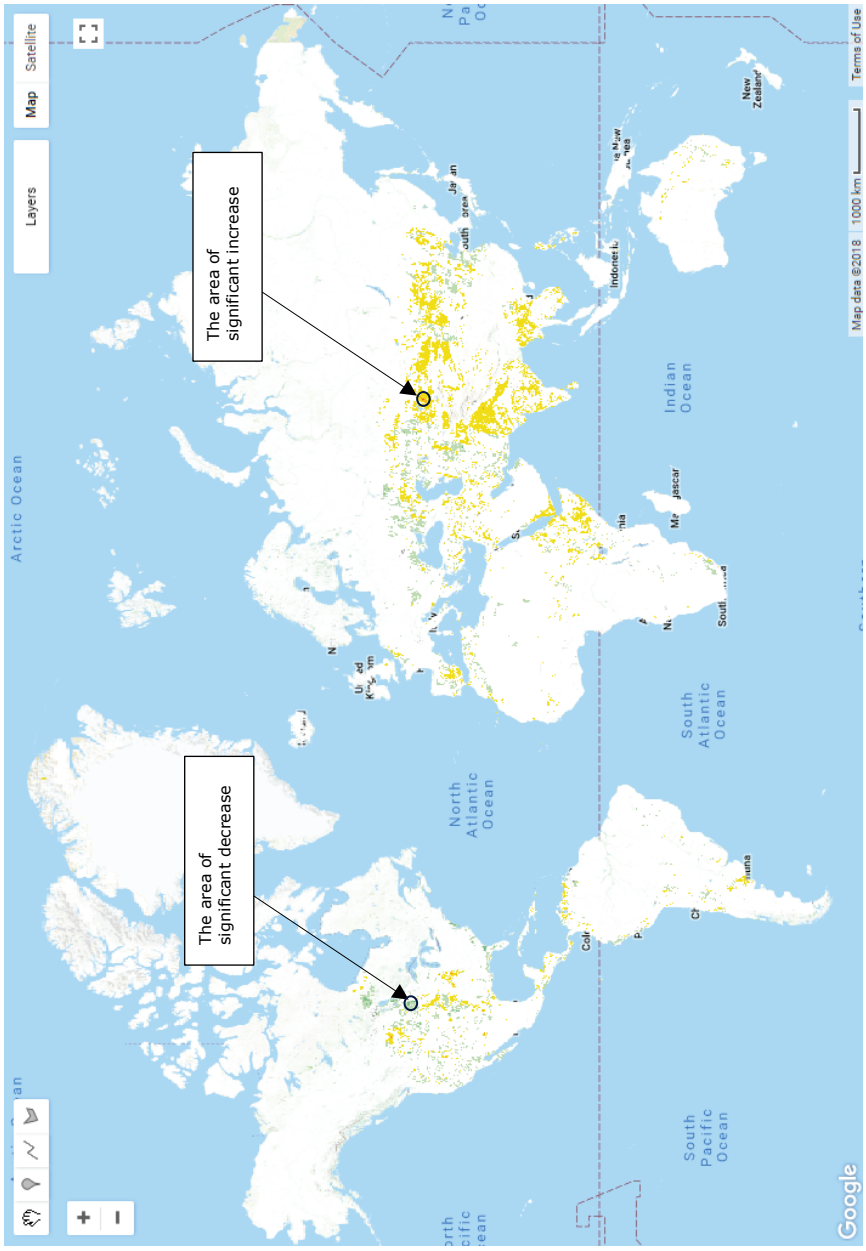

Figure 5.9. Global soil salinity changes map from 1986 to 2016 (yellow shades show soil salinity increase and green shades show soil salinity decrease).

5.3.4 Discussion of the method and implications

The trend in soil salinity increase over time we showed was in most of the cases in accordance with other studies (Taghadosi and Hasanlou, 2017; Wang et al., 2008). However, a comparison with studies that describe soil salinity decrease over time would provide better validity of the method. Though areas where soil salinity decreased in time might exist, they definitely would not be widespread. Overall consensus among experts is that soil salinization is expanding on global scale, probably at a rate of 2 Mha per year (Abbas et al., 2013). As a result, we could not find a study describing soil salinity decrease through time. Without it, the trend might also represent general trend of global warming. Interestingly enough, even if so, our change maps still might be valid. Climate change is promoting soil salinization through more frequent drought events, seawater intrusion in coastal areas and general increase in temperature (Dasgupta et al., 2015; Várallyay, 1994). Therefore, we can assume that many areas suffering from climate change would be prone to soil salinization.

The basis of thermal infrared imagery approach we used is described in Ivushkin et al. (2017); Ivushkin et al. (2018); Ivushkin et al. (2019). In those studies certain pre-processing has been done to assure that the thermal infrared data used in the analysis were coming from cropped areas vegetated above a certain threshold of vegetation cover. Therefore, that thermal infrared data could be related to canopy temperature. In our case we did not do such a pre-processing because of issues that are the consequence of a global scale study, like vegetation season spanning all year round. Nevertheless, since increase in canopy temperature is a universal response to salt stress for a vast majority of plants (Munns, 1993, 2002), we assume that it will hold for other vegetation covers. In case of extremely saline areas where no vegetation is present, the surface temperature will be affected anyway, because open soil at a day time will have higher temperature than vegetated areas.

One of the limitations of the WoSIS dataset we used is the quite unequal sample distribution spatially. That might be one of the reasons why the amount of salt affected lands in Mexico is overestimated. On the other hand, our approach was able

to map salt affected areas in regions where training data were absent, like Central Asia. Therefore, we conclude that the unequal spatial distribution of training points did influence the results, but did not influence them significantly.

Though Google Earth Engine is a powerful tool that provides access to the biggest library of open earth observation data and computational power to process it, the scientific community is quite cautious in adopting it. The main reason is that exact implementation of different functions, including random forest we used, is not always known. Moreover, these implementations can be changed at any moment, leading to different results even if you use the same functions to compute these results later. We recognise this issue. Nevertheless, its free of charge access and rich earth observation data archive makes GEE a useful tool for global assessments of different kinds.

As we mentioned before, assessments of salt affected soils on global scale are quite limited and approximate. Though the knowledge about the total affected area and its change would be an important information to improve global food security. The economic costs of soil salinity are also impressive. For example, just 2 million hectares of salt affected lands are costing Uzbekistan about US $1 billion annually (UNDP, 2009; World Bank, 2007). On global scale the economic losses are just tremendous. A proper inventory of the affected lands would allow proper mitigation measures to be applied and cut the losses to the minimum. We hope that our study will contribute to this cause.

5.4 Conclusions

The results show that GEE random forest classifier is a useful tool for the global assessment of soils salinity. The resulting global soil salinity maps have a validation accuracy of up to 70% with several known hotspots captured by the maps. The assessment of global area affected is comparable with the assessments of other authors. The addition of thermal infrared imagery into the analysis can act as a dynamic variable that allow to capture the trend of soil salinity change. That was confirmed in 2 out of 3 investigated cases. The one case where our results were

different from the referred study had soil salinity of different origin and we suspect that this might be the reason why the method did not perform well in this case. The method we applied allowed to predict affected areas even in the areas where training data were unavailable. Therefore, we conclude that a combination of soil properties maps and thermal infrared imagery can allow mapping of soil salinity development in space and time on global scale.

The code and data used to produce the global soil salinity maps can be accessed by registered Google Earth Engine users at https://code.earthengine.google.com/d43e5a92ae1deed32a0929f57b572756.

Chapter 6

Synthesis

6.1 Main results

The overall objective of this thesis is to investigate the potential of thermal imagery analysis as an approach to soil salinity assessment in cropped areas at different scales. To achieve this objective, four research questions have been formulated and researched. Following are the main findings for each question.

6.1.1 Can remotely sensed canopy temperature be used as an indicator of soil salinity in cropped areas?

The majority of the previous studies investigated canopy temperature mainly on a small scale and using ground thermal cameras. Only few of them are focused on soil salinity specifically and no studies on landscape scale are described.

In Chapter 2 I explored the potential of canopy temperature as an indicator of soil salinity at landscape scale and compared its performance with more traditionally used indicators like Normalised Difference Vegetation Index, Enhanced Vegetation Index, and elevation. To do this, I investigated the relationship between a high accuracy soil salinity map and thermal data on a salt affected agricultural area in Uzbekistan, where 51% of irrigated land is affected by some degree of soil salinity. The Syrdarya province of Uzbekistan, which was selected as a study area, is an agricultural province with large irrigated fields, where mainly two crops (wheat and cotton) are grown under uniform management. I considered this province as an appropriate area for a proof-of-concept study of the thermography approach.

From the results of this study, I conclude that satellite thermography data is significantly correlated to soil salinity. Statistical analysis showed that satellite thermography data clearly distinguished between salinity classes, producing F-values higher than those for NDVI and EVI. Moreover, visual examination of maps showed that actual salinity patterns were more similar to the canopy temperature map than to the map produced using vegetation indices. Overall, the first step in this thesis confirmed that the satellite thermography approach has substantial potential for salinity monitoring on cropped areas.

Another finding of this study was that the timing of the assessment is important. Thermal images taken in September produced the highest F-values, meaning they have the greatest predictive power. Nevertheless, for the whole vegetation period from end July to mid-September, F-values were steady and showed significant relations, indicating considerable potential for use in monitoring. In the study area the highest F-values corresponded with the period of maximum crop development at the end of the dry season. Maximum F-values for vegetation indices were observed a bit earlier in the season, in July and August, when cotton's green biomass was close to its maximum. Therefore, I conclude that the point of maximum vegetation development after the dry season can be considered the best time for application of the thermography approach.

Summarizing all above, I can answer the question of this section with yes; remotely sensed canopy temperature can be used as an indicator of soil salinity in cropped areas.

So, I confirmed that satellite based thermography is indeed useful in soil salinity monitoring, but other sensor platforms are also used in agriculture. A platform that becomes more and more popular is the Unmanned Aerial Vehicle (UAV).

6.1.2 Do UAV based observations show comparable result to satellite based observations?

The UAV becomes more and more popular in the fields like surveying, media industry, and agriculture. Therefore, investigating if the thermography approach is applicable to UAV based sensors is of vital importance for the operationalisation of the approach.

For this I implemented plot scale assessment of soil salinity using UAV based thermal camera (Chapter 3). The study set up included two test plots, one control and one salt treated plot, where quinoa plants were grown. The plots' areas were 0.1 ha, which made them quite suitable for multiple UAV surveys. A remarkable feature of this experimental setup is that quinoa plant is very salt tolerant, and testing if the thermography approach is applicable to salt tolerant plants became

an additional goal. This is important because more and more halophyte varieties are proposed as a viable alternative for cultivation on salt affected lands, where conventional crops are no longer economically feasible.

The results showed that an increase of canopy temperature in response to salt stress is also detectable using UAV based thermal camera. Moreover, in this study I also confirmed that it is happening in salt tolerant plants, like quinoa, though this increase is less pronounced. The detection of this increase required an additional step in the analysis – NDVI clustering – which ensures that the temperatures of the equal amount of a plant material per pixel are compared. In addition to thermal data the Physiological Reflectance Index and LiDAR measured plant height were investigated, which were also affected by soil salinity stress.

The Physiological Reflectance Index of quinoa plants was significantly decreased because of the increased soil salinity and seems to be a valuable indicator of salt stress, in opposite to multispectral indices like NDVI or OSAVI, which showed insignificant differences between control and salt treated plants, with even reverted correlations. LiDAR measured height of quinoa plant was significantly decreased because of the increased soil salinity.

The UAV is a universal platform, which allows mounting of different sensors in short period of time, so integration of different kind of data is possible. In case of this study the combination of multiple remote sensing variables in a Multiple Linear Regression model has improved R^2 values and therefore I concluded that implementation of multiple measurement techniques bears a lot of potential for soil salinity monitoring of cropland by remote sensing.

All aspects considered, I can say that UAV based thermal observations show comparable results to satellite based observations and have the same usability in soil salinity assessment.

In this section I described that the thermography approach is working in the case of a single crop grown in small plot under controlled, irrigated conditions. But a robustness test is required, where several different crops are grown under both irrigated and rainfed conditions.

6.1.3 How robust is the thermography approach when applied on study areas with different crops grown in both rainfed and irrigated conditions?

While answering previous questions the selected study areas had irrigated cultivation. Irrigation schedule and water stress in plants may influence the thermal measurements. Therefore, understanding how applicable the thermography approach is in case of rainfed agriculture is important. Moreover, the crop species would also influence the results. Testing the thermography approach on as many different crop species as possible would strengthen my argument.

In Chapter 4 I investigated the robustness of the thermography approach. It has been done by applying the approach on a regional scale for different crops grown under irrigated and rainfed conditions in 4 Australian states. The main crops grown there are wheat, barley, rapeseed and cotton. For most of them, I was able to make a comparison between irrigated and rainfed cultivation. The results showed that in all cases average canopy temperatures were significantly correlated with soil salinity of the area. In the period of green biomass peak all p-values were <0.01. These findings are valid for all investigated crops, grown both irrigated and rainfed. Nevertheless, crop type does influence the strength of the relations. Cotton, as a relatively salt tolerant plant, shows only minor temperature difference compared to other vegetation classes which suggests that less salt tolerant species will demonstrate higher temperature differences and will allow a more accurate assessment of soil salinity.

During this study in Australia it is demonstrated that the thermography approach is also flexible in terms of satellite sensors used. It has been applied using both MODIS and Landsat data and, in both cases, similar patterns and trends were present, despite very different spatial resolution of these two sensors.

The results from Chapter 4 allow me to conclude that the thermography approach is robust in relation to different study areas and different crops in both rainfed and irrigated conditions.

In the questions answered up to now the scale of the application consistently decreased. Therefore, the last question deals with the ultimate scale for earth observation sciences – global scale.

6.1.4 Can a combination of soil properties maps and thermal imagery allow us to track the development of soil salinity in space and time on global scale?

Having tested the thermography approach on different scales while answering the three previous questions I dared to implement a global assessment. It was clear that too many influencing factors on global scale would make the use of thermal data alone insufficient. Therefore, in this study the main role of thermal data is to introduce a dynamic component into the analysis and allow us to track the evolution of soil salinity in time.

The main base in the analysis were maps of soil properties correlated with soil salinity. These maps together with global thermal mosaics of different time periods, were processed in Google Earth Engine environment to produce global soil salinity maps for different periods in time. The results showed that Google Earth Engine random forest classifier is a useful tool for the global assessment of soils salinity. The resulting global soil salinity maps have a validation accuracy of up to 70% with several known hotspots captured on them. The assessment of global area affected was comparable with the assessment of other authors and summed up to 1 billion hectares.

The addition of thermal imagery into the analysis can act as a dynamic variable that allows to capture the trend of soil salinity change. That was confirmed in 2 out of 3 investigated cases. The one case where my results were inconsistent with the referred study had soil salinity of different origin and I suspect this is the reason of the disagreement in the results. The approach applied, allowed us to predict affected areas even in the regions where training data were unavailable. Therefore, I can conclude that a combination of soil properties maps and thermal imagery allows mapping of soil salinity development in space and time on global scale.

6.2 Reflection and outlook

The increasing demand on food production and non-food agricultural products will lead to a greater pressure on agricultural ecosystems (FAO, 2018a). Majority of this pressure will result in a more intensive use of already cultivated lands, rather than in cultivation of new lands. In this case, problems that are often the consequence of wrong intensification practices, like soil salinization, will exacerbate.

To prevent this, first the severity and spatial extent of the problem should be known. Considering the dynamic nature of soil salinity, remote sensing assessment techniques will play an increasingly important role (Metternicht and Zinck, 2003). The traditional methods of soil survey are much more labour and cost intensive compared to remote sensing. Therefore, they are barely done on a required temporal and spatial resolution for soil salinity, which can differ dramatically at the beginning and end of a vegetation season.

Nevertheless, remote sensing approaches have their limitations and can in the current stage of development hardly be applied without using ground truth data of more traditional soil surveys. One of the reasons for this is that current remote sensing methods for soil properties are quite site specific. Therefore, this thesis is about developing a remote sensing approach that can be more universal, producing a comparable soil salinity assessment in different parts of the world.

6.2.1 Is the overall objective achieved?

The overall objective of this thesis was to investigate the potential of thermal imagery analysis as an approach to soil salinity assessment in cropped areas at different scales. This objective was achieved by developing and applying the thermography approach where the relationship between satellite/UAV-borne thermal images and soil salinity of the area were investigated. The investigation was done on local, regional and global scales and on study areas located in Uzbekistan, the Netherlands and Australia. The results confirmed that remotely sensed canopy temperature of plants is significantly correlated with soil salinity of

the soil they are grown on. That was observed on local and global scales on study areas in different parts of the world, where different crops were cultivated under rainfed and irrigated conditions. On the global scale the thermography approach was adjusted, therefore direct comparison is not possible. The added value of thermal imagery on global scale was characterization of temporal soil salinity change.

One of the important characteristics for a successful assessment approach is universality of application in different environments. Lack of it is the main drawback of the existing assessment approaches. Therefore, universality of the approach was an important criterion of success. The proposed thermography approach has this universality trait. This is shown by application on different crops, including the case of salt tolerant crop described in Chapter 3, where the advantage of the proposed approach over traditional vegetation indices is especially clear.

All in all, I can say that thermography approach has a significant potential for soil salinity assessment and worth further development to the stage of operationalisation.

6.2.2 On operationalisation of the thermography approach

One of the concerns I often hear as a response to the proposed approach of using remote sensing in soil salinity assessment is the difficulty of operationalisation and the associated cost. It is true that currently the thermography approach proposed in the previous parts of this book will require certain skills in remote sensing data analysis and software for this analysis. This expertise is mainly provided by private companies as a ready to use product (like eLEAF or AgroCares in the Netherlands). The problem I see here is that only a few of these companies are operational in developing countries, where the majority of salt affected areas are located. Among developed countries, where earth observation services are more developed, only a few of them are dealing with soil salinity (FAO and ITPS, 2015), therefore operationalisation of soil salinity assessment by remote sensing is not among their priorities.

Nevertheless, I think that in a few years time, growth of precision agriculture will increase the demand for spatially and temporally precise monitoring of soil properties. This monitoring will include a strong remote sensing component, be it satellite or UAV based remote sensing. In the areas affected by soil salinization, soil salinity assessment will be an important part of this monitoring. Therefore, I see the most probable model for operationalisation of soil salinity remote sensing as a part of a more complex monitoring approach that will characterise an area in question by general usability for cropping. This kind of product would be more attractive for farmers.

But farmers would be not the only potential users. Local and national governments might be also interested in the assessment of the extent and severity of soil salinization on their area. The expected economic losses in case of salinization might reach billions of dollars (UNDP, 2009; World Bank, 2007). Therefore, there is a clear incentive for governments to steer water management and guide investments to fight soil salinization.

International organisations and agencies might be more interested in global assessment. And on this scale operationalisation might be not so straightforward, as I encountered issues myself while upscaling the thermography approach to global scale.

6.2.3 Global scale issues

The information on the extent of salt affected lands is very scattered and existing assessments are mainly rough approximation (FAO, 2018b; FAO and ITPS, 2015). Therefore, the need exists for accurate and up to date assessment, which I attempt to provide in Chapter 5.

The assessment is based on the same principle of canopy temperature increase under salt stress (Gómez-Bellot et al., 2015; Hackl et al., 2012). When I applied the thermography approach on local and regional scales, I ensured that I measure canopy temperature by using thermal data only from pixels that are above a certain NDVI threshold. But implementation of the same technique on global scale proved

to be unfeasible. The vegetation season on global scale stretched through the whole year, therefore the application of the same technique with NDVI thresholds would lead to a global thermal mosaic with radically different temperatures collected with the difference in time of up to one year. Though being quite a cumbersome task, such a mosaic could have been produced, but another global scale issue would render it irrelevant.

The canopy temperature is firstly controlled by the ambient air temperature, and only secondly by other factors like stress responses of a plant. Therefore, absolute canopy temperature does not tell us anything about soil salinity and only difference in canopy temperature inside one scene, where air temperature is stable, will indicate salt affected areas. On local and regional scales, I assumed stable air temperature per scene and analysis was quite straightforward. But on global scale this is clearly impossible, so normalisation was required. To achieve this, it was decided to use the temperature difference from the long-term average for each pixel. That removed the influence of climate and allowed to focus more on spatial differences and anomalies in the year(s) of interest.

Therefore, on the global scale thermal data acted as a dynamic variable that allowed tracking of the soil salinity change in space and time, while basic information on soil salinity was modelled using soil properties maps, as described in Chapter 5.

6.2.4 Bare soil vs. vegetation as a proxy approach

The two principally different approaches used in monitoring of soil salinity are the use of soil remote sensing signal or vegetation remote sensing signal as a proxy. I see more potential in the latter.

My affinity with vegetation as a proxy approach stems from the applicability in specific conditions of cropped areas. Though naturally saline areas have their importance, the more pressing issues of soil salinity are in the agricultural sector. The focus of this thesis is on cropped areas because of the societal and economic importance of the problem in this setting.

Use of bare soil assessment is useful when soil salinization progressed to the extreme degree, which means that saline crusts are formed on the surface of the soil (Aldabaa et al., 2015; Bai et al., 2016; Nawar et al., 2014). In this situation no crops can be grown and land is lost for agriculture. But when the situation is still manageable, bare soil remote sensing can hardly provide any useful information to characterise soil salinization of the area.

When land is still suitable for cropping to some degree, the use of the plant signal as a proxy is a better choice (Elhag and Bahrawi, 2017; Hamzeh et al., 2016; Scudiero et al., 2015). Firstly, if we are talking about cultivated land, most of the time the soil surface will be covered by a crop. Therefore, using the plant signal will allow more time for assessment, while only a short window of opportunity will be available in case of bare soil monitoring. Secondly, the plant signal will reveal soil conditions in the whole root zone (0-30 cm), which is the most valuable information in agriculture. Bare soil remote sensing will only characterise the surface of the soil, which can be misleading, since soil salinity on the surface can be quite different than soil salinity 10 cm below. Thirdly, many factors influence the spectral signature of a soil. This might be environmental factors, like soil moisture or ploughing, and intrinsic properties of soil, like texture or colour (Dwivedi, 2017).

All in all, I propose to use vegetation as a proxy for soil salinity assessment.

6.2.5 Discussion of methods and materials used

To a large extent the methods described in this thesis are newly proposed and have not been tested previously. This introduced certain specificities to it:

1. For example, the proposed thermography approach can be applied only on vegetated, preferably cropped, areas. What are the challenges when it is applied on different land cover types?

2. Another specificity is the timing of the monitoring. The results show that the best moment of application is close to the end of a vegetation season. That limits the frequency of assessment to once or twice per year. This would be sufficient in most cases, but on areas where special measures are

in progress to reduce soil salinization more frequent assessment might be required.

3. One of the key questions about the methods used in the global scale research (Chapter 5) is the question of climate. Namely, are we measuring the change in soil salinity or a change in climate? Since consensus is that soil salinity is increasing on global scale, the same is air temperature, it is hard to distinguish between these two phenomena. Comparison with a study describing soil salinity decrease in time would help to distinguish between these two phenomena, but no such studies were found at the moment of this thesis publication. However, on local and regional scales the thermal differences are clearly driven by differences in soil salinity.

Next to the specificities mentioned above, there were some consequences of satellite sensors systems currently used. In remote sensing a trade-off between temporal and spatial resolution is always present. It is even more so with infrared thermography, because of the lower energy of the wavelengths used (Rodríguez-Galiano et al., 2011). Therefore, the global assessment using current sensors would always be spread in time (Landsat), or low resolution (MODIS). In Chapter 5 the choice was made in favour of resolution, since 1km soil salinity map would have limited use because of the patchy character of soil salinization in general. Nevertheless, it meant that images with acquisition dates differences of up to 6 months were combined in one mosaic and used in one model. That might lead to blurring of the resulting map and loss of details, especially on smaller scales. Therefore, a sensor platform combining spatial resolution of Landsat and temporal resolution of MODIS would be more optimal and would provide more detailed assessment of global soil salinity change.

6.3 Further research

From the outcomes of this thesis I suggest the directions for a further research:

1. The global assessment chapter of this thesis has several questions left that require further research. The global soil salinity map proposed in that chapter had cases of local overestimation and underestimation, which probably were the consequence of the training dataset used. I used probably the fullest dataset on soil salinity currently available, nevertheless it has almost no points in Central Asia, which is one of the most severely affected regions of the world, and only few points in Australia. Moreover, the question of extracting canopy temperature from surface temperature on global scale will require further research for operationalisation of the thermography approach.

2. In this thesis I did not focus on the socio-economic side of soil salinity assessment, which will be required for operationalisation of the thermography approach. Therefore, questions like economic benefits from having up-to date information on soil salinity and its influence on the effectiveness of mitigation measures should be investigated. I expect that timely information on soil salinity situation will allow application of mitigation measures in a more spatially targeted manner. That will reduce expenditure on those measures. Or, it will even lead to a decision to plant more salt tolerant crop or variety in coming season, which again will help to reduce losses. All these measures would positively influence the wellbeing of farming communities living on affected areas. In developing countries it can even prevent migration from the affected areas, which often happens when soil salinization degrade lands to an extreme degree.

3. Despite all the efforts to stop its progression, soil salinization still continues and more and more lands are affected. Therefore, adaptation measures also should be taken. One of the most effective among them is biosaline agriculture, which is a cultivation of salt tolerant species and salt tolerant varieties of traditional crops (Abdelly et al., 2008; Öztürk et al., 2006). Further research in this direction will help to mitigate soil salinization impact and adapt farmers communities of affected regions to a new way of practicing agriculture on salinized lands.

References

06-GPS, 2017. 06-GPS, Sliedrecht, The Netherlands.

ABARES, 2008a. Land Use in Western Australia, v7 (2008) (ESRI Shapefile). Accessed through http://www.agriculture.gov.au/abares/aclump/land-use/data-download on March 2017.

ABARES, 2008b. Land Use South Australia 2008(ESRI File Geodatabase). Accessed through http://www.agriculture.gov.au/abares/aclump/land-use/data-download on March 2017.

ABARES, 2009. Land Use: New South Wales 2009 (ESRI Personal Geodatabase). Accessed through http://www.agriculture.gov.au/abares/aclump/land-use/data-download on March 2017.

ABARES, 2012. Land use mapping – Queensland current (ESRI File Geodatabase). Accessed through http://www.agriculture.gov.au/abares/aclump/land-use/data-download on March 2017.

Abbas, A., Khan, S., Hussain, N., Hanjra, M.A., Akbar, S., 2013. Characterizing soil salinity in irrigated agriculture using a remote sensing approach. Physics and Chemistry of the Earth, Parts A/B/C 55-57, 43-52. 10.1016/j.pce.2010.12.004.

Abdelly, C., Öztürk, M., Ashraf, M., Grignon, C., 2008. Biosaline agriculture and high salinity tolerance. Birkhäuser; Springer [distributor], Basel, London.

Abrol, I.P., Yadav, J.S.P., Massoud, F.I., 1988. Salt-Affected Soils and their Management. FAO.

Agisoft LLC, 2017. Agisoft PhotoScan Professional 1.3.2, 1.3.2 ed. Agisoft LLC, St. Petersburg, Russia.

Akramkhanov, A., 2005. The spatial distribution of soil salinity: detection and prediction. Cuvillier, Göttingen, p. 120.

Akramova, I., 2008. Mapping spatial distribution of soil salinity using Remote Sensing and GIS, Laboratory of Geo-Information Science and remote sensing. Wageningen University and Research Centre, Wageningen, The Netherlands, p. 62.

Al-Busaidi, A.S., Cookson, P., 2003. Salinity–pH Relationships in Calcareous Soils. Journal of Agricultural and Marine Sciences 8, 6. 10.24200/jams.vol8iss1pp41-46.

Al-Khaier, F., 2003. Soil salinity detection using satellite remote sensing. International institute for Geo-Information science and Earth observation, Enschede, The Netherlands, p. 61.

Aldabaa, A.A.A., Weindorf, D.C., Chakraborty, S., Sharma, A., Li, B., 2015. Combination of proximal and remote sensing methods for rapid soil salinity quantification. Geoderma 239-240, 34-46. 10.1016/j.geoderma.2014.09.011.

Aldakheel, Y.Y., Elprince, A.M., Aatti, M.A., 2006. Mapping vegetation and saline soil using ndvi in arid irrigated lands, ASPRS 2006 Annual Conference, Reno, Nevada.

Allbed, A., Kumar, L., 2013. Soil Salinity Mapping and Monitoring in Arid and Semi-Arid Regions Using Remote Sensing Technology: A Review. Advances in Remote Sensing 02, 373-385. 10.4236/ars.2013.24040.

Allbed, A., Kumar, L., Aldakheel, Y.Y., 2014a. Assessing soil salinity using soil salinity and vegetation indices derived from IKONOS high-spatial resolution imageries: Applications in a date palm dominated region. Geoderma 230-231, 1-8. 10.1016/j.geoderma.2014.03.025.

Allbed, A., Kumar, L., Sinha, P., 2014b. Mapping and Modelling Spatial Variation in Soil Salinity in the Al Hassa Oasis Based on Remote Sensing Indicators and Regression Techniques. Remote Sensing 6, 1137-1157. 10.3390/rs6021137.

Álvarez, S., Sánchez-Blanco, M.J., 2014. Long-term effect of salinity on plant quality, water relations, photosynthetic parameters and ion distribution in Callistemon citrinus. Plant Biology 16, 757-764. 10.1111/plb.12106.

Applanix, 2017. POSPac MMS 7.2. Applanix, Ontario, Canada.

Australian Bureau of Meteorology, 2017. Climate statistics. Accessed through http://www.bom.gov.au/climate/data/ on May 2017.

Australian Bureau of Statistics, 2008. Agricultural Commodities: Small Area Data, Australia, 2006-07. data cube: Excel spreadsheet, cat. no. 7125.0, viewed March 2017, http://www.abs.gov.au/AUSSTATS/abs@.nsf/Lookup/7125.0Main+Features12006-07?OpenDocument.

Ayers, R.S., Westcot, D.W., 1985. Water quality for agriculture. FAO.

Bai, L., Wang, C., Zang, S., Zhang, Y., Hao, Q., Wu, Y., 2016. Remote Sensing of Soil Alkalinity and Salinity in the Wuyu'er-Shuangyang River Basin, Northeast China. Remote Sensing 8, 163.

Bannari, A., Guedon, A.M., El-harti, A., Cherkaoui, F.Z., El-ghmari, A., Saquaque, A., 2007. Slight and moderate saline and sodic soils characterization in irrigated agricultural land using multispectral remote sensing. The International Archives of the Photogrammetry, Remote Sensing and Spatial Information Sciences 34, Part XXX.

Biber, P.D., 2006. Measuring the effects of salinity stress in the red mangrove, Rhizophora mangle L. African Journal of Agricultural Research 1, 1-4.

Brede, B., Lau, A., Bartholomeus, H.M., Kooistra, L., 2017. Comparing RIEGL RiCOPTER UAV LiDAR Derived Canopy Height and DBH with Terrestrial LiDAR. Sensors (Basel) 17. 10.3390/s17102371.

Breiman, L., 2001. Random Forests. Machine Learning 45, 5-32. 10.1023/a:1010933404324.

Brunner, P., Li, H.T., Kinzelbach, W., Li, W.P., 2007. Generating soil electrical conductivity maps at regional level by integrating measurements on the ground and remote sensing data. International Journal of Remote Sensing 28, 3341-3361. 10.1080/01431160600928641.

Bucknall, J., Klytchnikova, I., Lampietti, J., Lundell, M., Scatasta, M., Thurman, M., 2003. Irrigation in Central Asia. Social, economic and environmental considerations. World Bank, p. 104.

Bui, E., Wilford, J., de Caritat, P., 2017. Predictive spatial modelling for mapping soil salinity at continental scale, EGU General Assembly, Vienna, Austria. 10.13140/RG.2.2.25552.20483.

Dasgupta, S., Hossain, M.M., Huq, M., Wheeler, D., 2014. Climate change, soil salinity, and the economics of high-yield rice production in coastal Bangladesh. The World Bank.

Dasgupta, S., Hossain, M.M., Huq, M., Wheeler, D., 2015. Climate change and soil salinity: The case of coastal Bangladesh. Ambio 44, 815-826. 10.1007/s13280-015-0681-5.

de Caritat, P., Cooper, M., 2011. National Geochemical Survey of Australia: The Geochemical Atlas of Australia. Geoscience Australia, Record 2011/20.

Dehni, A., Lounis, M., 2012. Remote sensing techniques for salt affected soil mapping: Application to the Oran Region of Algeria. Procedia Engineering 33, 188-198. 10.1016/j.proeng.2012.01.1193.

Ding, J.L., Wu, M.C., Tiyip, T., 2011. Study on soil salinization information in arid region using remote rensing technique. Agricultural Sciences in China 10, 404-411. 10.1016/s1671-2927(11)60019-9.

Domingues Franceschini, M.H., Bartholomeus, H., van Apeldoorn, D., Suomalainen, J., Kooistra, L., 2017. Intercomparison of Unmanned Aerial Vehicle and Ground-Based Narrow Band Spectrometers Applied to Crop Trait Monitoring in Organic Potato Production. Sensors (Basel) 17. 10.3390/s17061428.

Don, K.K.G., Xia, Y.P., Zhu, Z., Le, C., Wijeratne, A.W., 2010. Some deleterious effects of long-term salt stress on growth, nutrition, and physiology of gerbera (Gerbera jamesonii l.) and potential indicators of its salt tolerance. Journal of Plant Nutrition 33, 2010-2027. 10.1080/01904167.2010.512058.

Douaoui, A.E.K., Nicolas, H., Walter, C., 2006. Detecting salinity hazards within a semiarid context by means of combining soil and remote-sensing data. Geoderma 134, 217-230. 10.1016/j.geoderma.2005.10.009.

Dwivedi, R.S., 2017. Remote sensing of soils. Springer, Berlin. 10.1007/978-3-662-53740-4.

Elhaddad, A., Garcia, L.A., 2009. Remote sensing application in agriculture. Using remote sensing to estimate soil salinity and evapotranspiration. VDM Publishing House Ltd.

Elhag, M., Bahrawi, J.A., 2017. Soil salinity mapping and hydrological drought indices assessment in arid environments based on remote sensing techniques. Geosci. Instrum. Method. Data Syst. 6, 149-158. 10.5194/gi-6-149-2017.

ESRI, 2016. ArcGIS Desktop 10.5, 10.5 ed. Environmental Systems Research Institute, Redlands, CA.

ESRI, 2017. ArcGIS Pro 2.0.1. Environmental Systems Research Institute, Redlands, CA.

Fan, X., Pedroli, B., Liu, G., Liu, Q., Liu, H., Shu, L., 2012. Soil salinity development in the yellow river delta in relation to groundwater dynamics. Land Degradation and Development 23, 175-189. 10.1002/ldr.1071.

FAO, 2003. World agriculture : Towards 2015/2030 an FAO perspective. FAO, London, p. 432.

FAO, 2018a. The future of food and agriculture – Alternative pathways to 2050. FAO,, Rome, p. 224.

FAO 2018b. Salt-affected soils. Accessed on 04-10-2018. http://www.fao.org/soils-portal/soil-management/management-of-some-problem-soils/salt-affected-soils/more-information-on-salt-affected-soils/en/.

FAO and ITPS, 2015. Status of the World's Soil Resources (SWSR) – Main Report. Food and Agriculture Organization of the United Nations and Intergovernmental Technical Panel on Soils, Rome, Italy.

Farifteh, J., van der Meer, F., van der Meijde, M., Atzberger, C., 2008. Spectral characteristics of salt-affected soils: A laboratory experiment. Geoderma 145, 196-206. 10.1016/j.geoderma.2008.03.011.

Farooq, M., Hussain, M., Wakeel, A., Siddique, K.H.M., 2015. Salt stress in maize: effects, resistance mechanisms, and management. A review. Agronomy for Sustainable Development 35, 461-481. 10.1007/s13593-015-0287-0.

Fernández-Buces, N., Siebe, C., Cram, S., Palacio, J.L., 2006. Mapping soil salinity using a combined spectral response index for bare soil and vegetation: A case study in the former lake Texcoco, Mexico. Journal of Arid Environments 65, 644-667. 10.1016/j.jaridenv.2005.08.005.

Gama, P.B.S., Tanaka, K., Eneji, A.E., Eltayeb, A.E., Siddig, K.E., 2009. Salt-Induced Stress Effects on Biomass, Photosynthetic Rate, and Reactive Oxygen Species-Scavenging Enzyme Accumulation in Common Bean. Journal of Plant Nutrition 32, 837-854. 10.1080/01904160902787925.

Gamon, J.A., Peñuelas, J., Field, C.B., 1992. A narrow-waveband spectral index that tracks diurnal changes in photosynthetic efficiency. Remote Sensing of Environment 41, 35-44. https://doi.org/10.1016/0034-4257(92)90059-S.

Ghassemi, F., Jakeman, A., Nix, H., 1995. Salinization of land and water resources: human causes, extent, management and case studies, Canberra, Australia. CAB International, Wallingford, Oxon, UK.

Gómez-Acata, E.S., Valencia-Becerril, I., Valenzuela-Encinas, C., Velásquez-Rodríguez, A.S., Navarro-Noya, Y.E., Montoya-Ciriaco, N., Suárez-Arriaga, M.C., Rojas-Valdez, A., Reyes-Reyes, B.G., Luna-Guido, M., Dendooven, L., 2016. Deforestation and Cultivation with Maize (Zea mays L.) has a Profound Effect on the Bacterial Community Structure in Soil. Land Degradation & Development 27, 1122-1130. 10.1002/ldr.2328.

Gómez-Bellot, M.J., Nortes, P.A., Sánchez-Blanco, M.J., Ortuño, M.F., 2015. Sensitivity of thermal imaging and infrared thermometry to detect water status changes in Euonymus japonica plants irrigated with saline reclaimed water. Biosystems Engineering 133, 21-32. 10.1016/j.biosystemseng.2015.02.014.

Goskomgeodezkadastr, 2010. Atlas of soil cover of Republic of Uzbekistan (In Russian), Tashkent, Uzbekistan.

Grant, O.M., Tronina, Ł., Jones, H.G., Chaves, M.M., 2007. Exploring thermal imaging variables for the detection of stress responses in grapevine under different irrigation regimes. Journal of experimental botany 58, 815-825. 10.1093/jxb/erl153.

Hack-ten Broeke, M.J.D., Kroes, J.G., Bartholomeus, R.P., van Dam, J.C., de Wit, A.J.W., Supit, I., Walvoort, D.J.J., van Bakel, P.J.T., Ruijtenberg, R., 2016. Quantification of the impact of hydrology on agricultural production as a result of too dry, too wet or too saline conditions. SOIL 2, 391-402. 10.5194/soil-2-391-2016.

Hackl, H., Baresel, J.P., Mistele, B., Hu, Y., Schmidhalter, U., 2012. A comparison of plant temperatures as measured by thermal imaging and infrared thermometry. Journal of Agronomy and Crop Science 198, 415-429. 10.1111/j.1439-037X.2012.00512.x.

Hamzeh, S., Naseri, A.A., AlaviPanah, S.K., Bartholomeus, H., Herold, M., 2016. Assessing the accuracy of hyperspectral and multispectral satellite imagery for categorical and Quantitative mapping of salinity stress in sugarcane fields. International Journal of Applied Earth Observation and Geoinformation 52, 412-421. 10.1016/j.jag.2016.06.024.

Hamzeh, S., Naseri, A.A., AlaviPanah, S.K., Mojaradi, B., Bartholomeus, H.M., Clevers, J.G.P.W., Behzad, M., 2013. Estimating salinity stress in sugarcane fields with spaceborne hyperspectral vegetation indices. International Journal of Applied Earth Observation and Geoinformation 21, 282-290. 10.1016/j.jag.2012.07.002.

Harwin, S., Lucieer, A., Osborn, J., 2015. The Impact of the Calibration Method on the Accuracy of Point Clouds Derived Using Unmanned Aerial Vehicle Multi-View Stereopsis. Remote Sensing 7, 11933.

Hengl, T., Mendes de Jesus, J., Heuvelink, G.B.M., Ruiperez Gonzalez, M., Kilibarda, M., Blagotić, A., Shangguan, W., Wright, M.N., Geng, X., Bauer-Marschallinger, B., Guevara, M.A., Vargas, R., MacMillan, R.A., Batjes, N.H., Leenaars, J.G.B., Ribeiro, E., Wheeler, I., Mantel, S., Kempen, B., 2017. SoilGrids250m: Global gridded soil information based on machine learning. PLOS ONE 12, e0169748. 10.1371/journal.pone.0169748.

Hester, M.W., Mendelssohn, I.A., McKee, K.L., 2001. Species and population variation to salinity stress in Panicum hemitomon, Spartina patens, and Spartina alterniflora: morphological and physiological constraints. Environmental and Experimental Botany 46, 277-297. 10.1016/s0098-8472(01)00100-9.

Hillel, D., Feinerman, E., 2000. Salinity management for sustainable irrigation : integrating science, environment, and economics. World Bank, Washington, DC.

Honkavaara, E., Saari, H., Kaivosoja, J., Pölönen, I., Hakala, T., Litkey, P., Mäkynen, J., Pesonen, L., 2013. Processing and Assessment of Spectrometric, Stereoscopic Imagery Collected Using a Lightweight UAV Spectral Camera for Precision Agriculture. Remote Sensing 5, 5006.

Howari, F.M., 2003. The use of remote sensing data to extract information from agricultural land with emphasis on soil salinity. Australian Journal of Soil Research 41, 1243-1253. 10.1071/SR03033

Howell, T.A., Hatfield, J.L., Yamada, H., Davis, K.R., 1984. Evaluation of cotton canopy temperature to detect crop water stress. Transactions of the American Society of Agricultural Engineers 27, 84-88.

Hussain, S., Luro, F., Costantino, G., Ollitrault, P., Morillon, R., 2012. Physiological analysis of salt stress behaviour of citrus species and genera: Low chloride accumulation as an indicator of salt tolerance. South African Journal of Botany 81, 103-112. 10.1016/j.sajb.2012.06.004.

IAEA, 1995. Management strategies to utilize salt affected soils : isotopic and conventional research methods. IAEA, Vienna.

IBM Corp, 2015. IBM SPSS Statistics 23.0 for Windows, 22.0 ed. IBM Corp., Armonk, NY.

Ishimwe, R., Abutaleb, K., Ahmed, F., 2014. Applications of Thermal Imaging in Agriculture—A Review. Advances in Remote Sensing 03, 128-140. 10.4236/ars.2014.33011.

Ivushkin, K., Bartholomeus, H., Bregt, A.K., Pulatov, A., 2017. Satellite Thermography for Soil Salinity Assessment of Cropped Areas in Uzbekistan. Land Degradation & Development 28, 870-877. 10.1002/ldr.2670.

Ivushkin, K., Bartholomeus, H., Bregt, A.K., Pulatov, A., Bui, E.N., Wilford, J., 2018. Soil salinity assessment through satellite thermography for different irrigated and rainfed crops. International Journal of Applied Earth Observation and Geoinformation 68, 230-237. 10.1016/j.jag.2018.02.004.

Ivushkin, K., Bartholomeus, H., Bregt, A.K., Pulatov, A., Franceschini, M.H.D., Kramer, H., van Loo, E.N., Jaramillo Roman, V., Finkers, R., 2019. UAV based soil salinity assessment of cropland. Geoderma 338, 502-512. https://doi.org/10.1016/j.geoderma.2018.09.046.

James, R.A., Rivelli, A.R., Munns, R., Caemmerer, S.v., 2002. Factors affecting CO2 assimilation, leaf injury and growth in salt-stressed durum wheat. Functional Plant Biology 29, 1393-1403. 10.1071/FP02069.

Jimenez, M.S., Gonzalez-Rodriguez, A.M., Morales, D., Cid, M.C., Socorro, A.R., Caballero, M., 1997. Evaluation of cholorophyll fluorescence as a tool for salt stress detection in roses. Photosynthetica 33, 291-301. 10.1023/A:1022176700857.

Judkins, G., Myint, S., 2012. Spatial variation of soil salinity in the Mexicali Valley, Mexico: Application of a practical method for agricultural monitoring. Environmental management 50, 478-489. 10.1007/s00267-012-9889-3.

Karavanova, E.I., Shrestha, D.P., Orlov, D.S., 2001. Application of remote sensing techniques for the study of soil salinity in semi-arid Uzbekistan, in: Bridges, E.M., Hannam, I.D., Oldeman, L.R., Penning de Vries, F.W.T., Scherr, S.J., Sombatpanit, S. (Eds.), Response to Land Degradation. Oxford & IBH Publishing Co. Pvt. Ltd., New Delhi, India, pp. 261-273.

Kluitenberg, G.J., Biggar, J.W., 1992. Canopy temperature as a measure of salinity stress on sorghum. Irrigation Science 13, 115-121. 10.1007/bf00191053.

Kovács, D., Tóth, T., Marth, P., 2006. Soil Salinity between 1992 and 2000 in Hungary. AGROKÉMIA ÉS TALAJTAN 55, 89-98.

Koyro, H.-W., Lieth, H., Eisa, S.S., 2008. Salt Tolerance of Chenopodium quinoa Willd., Grains of the Andes: Influence of Salinity on Biomass Production, Yield, Composition of Reserves in the Seeds, Water and Solute Relations, in: Lieth, H., Sucre, M.G., Herzog, B. (Eds.), Mangroves and Halophytes: Restoration and Utilisation. Springer Netherlands, Dordrecht, pp. 133-145. 10.1007/978-1-4020-6720-4_13.

Läuchli, A., Grattan, S.R., 2012. Plant responses to saline and sodic conditions, in: Wallender, W.W., Tanji, P.E., Tanji, K.K. (Eds.), Agricultural salinity assessment manual and management. American Society of Civil Engineers, Reston.

Li, G., Wan, S., Zhou, J., Yang, Z., Qin, P., 2010. Leaf chlorophyll fluorescence, hyperspectral reflectance, pigments content, malondialdehyde and proline accumulation responses of castor bean (Ricinus communis L.) seedlings to salt stress levels. Industrial Crops and Products 31, 13-19. 10.1016/j.indcrop.2009.07.015.

Maas, E.V., Grattan, S.R., 1999. Crop Yields as Affected by Salinity, in: Skaggs, R.W., van Schilfgaarde, J. (Eds.), Agricultural Drainage. American Society of Agronomy, Crop Science Society of America, Soil Science Society of America, Madison, WI, pp. 55-108. 10.2134/agronmonogr38.c3.

Manaa, A., Ben Ahmed, H., Smiti, S., Faurobert, M., 2011. Salt-Stress Induced Physiological and Proteomic Changes in Tomato (Solanum lycopersicum) Seedlings. Omics-a Journal of Integrative Biology 15, 801-809. 10.1089/omi.2011.0045.

Mashimbye, Z.E., Cho, M.A., Nell, J.P., De Clercq, W.P., Van Niekerk, A., Turner, D.P., 2012. Model-based integrated methods for quantitative estimation of soil salinity from hyperspectral remote sensing data: A case study of selected South African soils. Pedosphere 22, 640-649. 10.1016/s1002-0160(12)60049-6.

Melendez-Pastor, I., Navarro-Pedreño, J., Koch, M., Gómez, I., 2010. Applying imaging spectroscopy techniques to map saline soils with ASTER images. Geoderma 158, 55-65. 10.1016/j.geoderma.2010.02.015.

Metternicht, G., Zinck, J.A., 2009. Remote sensing of soil salinization impact on land management. CRC Press, Boca Raton, FL.

Metternicht, G.I., Zinck, J.A., 2003. Remote sensing of soil salinity: potentials and constraints. Remote Sensing of Environment 85, 1-20. 10.1016/s0034-4257(02)00188-8.

Morales, F., Abadía, J., Abadía, A., 2014. Thermal Energy Dissipation in Plants Under Unfavorable Soil Conditions, in: Demmig-Adams, B., Garab, G., Adams Iii, W., Govindjee (Eds.), Non-Photochemical Quenching and Energy Dissipation in Plants, Algae and Cyanobacteria. Springer Netherlands, Dordrecht, pp. 605-630. 10.1007/978-94-017-9032-1_27.

Muller, S.J., van Niekerk, A., 2016. An evaluation of supervised classifiers for indirectly detecting salt-affected areas at irrigation scheme level. International Journal of Applied Earth Observation and Geoinformation 49, 138-150. https://doi.org/10.1016/j.jag.2016.02.005.

Munns, R., 1993. Physiological processes limiting plant growth in saline soils: some dogmas and hypotheses. Plant, Cell & Environment 16, 15-24. 10.1111/j.1365-3040.1993.tb00840.x.

Munns, R., 2002. Comparative physiology of salt and water stress. Plant, Cell & Environment 25, 239-250. 10.1046/j.0016-8025.2001.00808.x.

Munns, R., 2005. Genes and salt tolerance: bringing them together. New Phytologist 167, 645-663. 10.1111/j.1469-8137.2005.01487.x.

Munns, R., Tester, M., 2008. Mechanisms of salinity tolerance. Annual Review of Plant Biology 59, 651-681. 10.1146/annurev.arplant.59.032607.092911.

Nawar, S., Buddenbaum, H., Hill, J., Kozak, J., 2014. Modeling and Mapping of Soil Salinity with Reflectance Spectroscopy and Landsat Data Using Two Quantitative Methods (PLSR and MARS). Remote Sensing 6, 10813-10834. 10.3390/rs61110813.

Noroozi, A.A., Homaee, M., Farshad, A., 2012. Integrated application of remote sensing and spatial statistical models to the identification of soil salinity: A case study from Garmsar Plain, Iran. Environmental Sciences 9 (1), 59-74.

Novara, A., Rühl, J., La Mantia, T., Gristina, L., La Bella, S., Tuttolomondo, T., 2015. Litter contribution to soil organic carbon in the processes of agriculture abandon. Solid Earth 6, 425-432. 10.5194/se-6-425-2015.

Oldeman, L.R., Hakkeling, R.T.A., Sombroek, W.G., 1991. World map of the status of human-induced soil degradation: an explanatory note, 2nd. rev. ed. ISRIC, UNEP, Wageningen [etc.].

Oleire-Oltmanns, S., Marzolff, I., Peter, K., Ries, J., 2012. Unmanned Aerial Vehicle (UAV) for Monitoring Soil Erosion in Morocco. Remote Sensing 4, 3390.

Oo, A.N., Iwai, C.B., Saenjan, P., 2015. Soil Properties and Maize Growth in Saline and Nonsaline Soils using Cassava-Industrial Waste Compost and Vermicompost with or Without Earthworms. Land Degradation & Development 26, 300-310. 10.1002/ldr.2208.

Öztürk, M.n., Waisel, Y., Khan, M.A., Gork, G., 2006. Biosaline agriculture and salinity tolerance in plants. Birkhäuser, Basel ;.

Padarian, J., Minasny, B., McBratney, A.B., 2015. Using Google's cloud-based platform for digital soil mapping. Computers & Geosciences 83, 80-88. 10.1016/j.cageo.2015.06.023.

Panagea, I.S., Daliakopoulos, I.N., Tsanis, I.K., Schwilch, G., 2016. Evaluation of promising technologies for soil salinity amelioration in Timpaki (Crete): a participatory approach. Solid Earth 7, 177-190. 10.5194/se-7-177-2016.

Peñuelas, J., Isla, R., Filella, I., Araus, J.L., 1997. Visible and Near-Infrared Reflectance Assessment of Salinity Effects on Barley. Crop Science 37. 10.2135/cropsci1997.0011183X003700010033x.

Percival, G.C., 2005. Identification of foliar salt tolerance of woody perennials using chlorophyll fluorescence. Hortscience 40, 1892-1897.

Platonov, A., Noble, A., Kuziev, R., 2013. Soil salinity mapping using multi-temporal satellite images in agricultural fields of Syrdarya province of Uzbekistan, in: Shahid, S.A., Abdelfattah, M.A., Taha, F.K. (Eds.), Developments in soil salinity assessment and reclamation: Innovative thinking and use of marginal soil and water resources in irrigated agriculture. Springer Science+Business Media Dordrecht, pp. 87-98. 10.1007/978-94-007-5684-7_5.

Quebrajo, L., Perez-Ruiz, M., Pérez-Urrestarazu, L., Martínez, G., Egea, G., 2018. Linking thermal imaging and soil remote sensing to enhance irrigation management of sugar beet. Biosystems Engineering 165, 77-87. 10.1016/j.biosystemseng.2017.08.013.

Rahmati, M., Hamzehpour, N., 2017. Quantitative remote sensing of soil electrical conductivity using ETM+ and ground measured data. International Journal of Remote Sensing 38, 123-140. 10.1080/01431161.2016.1259681.

Rahnama, A., James, R.A., Poustini, K., Munns, R., 2010. Stomatal conductance as a screen for osmotic stress tolerance in durum wheat growing in saline soil. Functional Plant Biology 37, 255-263. 10.1071/fp09148.

rapidlasso GmbH, 2017. LAStools 141017, academic. rapidlasso GmbH, Gilching, Germany.

Rhoades, J.D., F, C., Lesch, S., Smith, M., 1999. Soil salinity assessment: methods and interpretations of electrical conductivity measurements. FAO, Rome.

Ribeiro, E., Batjes, N.H., Leenaars, J.G.B., van Oostrum, A.J.M., Mendes de Jesus, J., 2015. Towards the standardization and harmonization of world soil data: Procedures manual ISRIC World Soil Information Service (WoSIS version 2.0). Report 2015/03. ISRIC - World Soil Information, Wageningen, p. 100.

Rodríguez-Galiano, V.F., Pardo-Igúzquiza, E., Chica-Olmo, M., Rigol-Sánchez, J.P., 2011. Increasing the spatial resolution of thermal infrared images using cokriging. Procedia Environmental Sciences 3, 117-122. 10.1016/j.proenv.2011.02.021.

Romero-Trigueros, C., Nortes, P.A., Alarcón, J.J., Hunink, J.E., Parra, M., Contreras, S., Droogers, P., Nicolás, E., 2017. Effects of saline reclaimed waters and deficit irrigation on Citrus physiology assessed by UAV remote sensing. Agricultural Water Management 183, 60-69. 10.1016/j.agwat.2016.09.014.

Rondeaux, G., Steven, M., Baret, F., 1996. Optimization of soil-adjusted vegetation indices. Remote Sensing of Environment 55, 95-107. https://doi.org/10.1016/0034-4257(95)00186-7.

Roosjen, P., Suomalainen, J., Bartholomeus, H., Kooistra, L., Clevers, J., 2017. Mapping Reflectance Anisotropy of a Potato Canopy Using Aerial Images Acquired with an Unmanned Aerial Vehicle. Remote Sensing 9, 417.

Roosjen, P.P.J., Brede, B., Suomalainen, J.M., Bartholomeus, H.M., Kooistra, L., Clevers, J.G.P.W., 2018. Improved estimation of leaf area index and leaf chlorophyll content of a potato crop using multi-angle spectral data – potential of unmanned aerial vehicle imagery. International Journal of Applied Earth Observation and Geoinformation 66, 14-26. 10.1016/j.jag.2017.10.012.

Saidi, D., 2012. Importance and Role of Cation Exchange Capacity on the Physicals Properties of the Cheliff Saline Soils (Algeria). Procedia Engineering 33, 435-449. https://doi.org/10.1016/j.proeng.2012.01.1223.

Sazib, N., Mladenova, I., Bolten, J., 2018. Leveraging the Google Earth Engine for Drought Assessment Using Global Soil Moisture Data. Remote Sensing 10, 1265.

Scudiero, E., Skaggs, T.H., Corwin, D.L., 2015. Regional-scale soil salinity assessment using Landsat ETM+ canopy reflectance. Remote Sensing of Environment 169, 335-343. 10.1016/j.rse.2015.08.026.

Seelig, B.D., 2000. Salinity and Sodicity in North Dakota Soils. NDSU Extension Service, North Dakota State University of Agriculture and Applied Science, Fargo, ND, p. 16.

Setia, R., Gottschalk, P., Smith, P., Marschner, P., Baldock, J., Setia, D., Smith, J., 2013a. Soil salinity decreases global soil organic carbon stocks. Science of The Total Environment 465, 267-272. https://doi.org/10.1016/j.scitotenv.2012.08.028.

Setia, R., Lewis, M., Marschner, P., Raja Segaran, R., Summers, D., Chittleborough, D., 2013b. Severity of salinity accurately detected and classified on a paddock scale with high resolution multispectral satellite imagery. Land Degradation & Development 24, 375-384. 10.1002/ldr.1134.

Seutloali, K.E., Beckedahl, H.R., 2015. Understanding the factors influencing rill erosion on roadcuts in the south eastern region of South Africa. Solid Earth 6, 633-641. 10.5194/se-6-633-2015.

Shabala, S., Munns, R., 2012. Salinity stress: Physiological constraints and adaptive mechanisms, in: Shabala, S. (Ed.), Plant Stress Physiology. CABI Publishing, pp. 59-93.

Shirokova, Y., Forkutsa, I., Sharafutdinova, N., 2000. Use of electrical conductivity instead of soluble salts for soil salinity monitoring in Central Asia. Irrigation and Drainage Systems 14, 199-205. 10.1023/A:1026560204665.

Sidike, A., Zhao, S., Wen, Y., 2014. Estimating soil salinity in Pingluo County of China using QuickBird data and soil reflectance spectra. International Journal of Applied Earth Observation and Geoinformation 26, 156-175. 10.1016/j.jag.2013.06.002.

Sona, G., Passoni, D., Pinto, L., Pagliari, D., Masseroni, D., Ortuani, B., Facchi, A., 2016. Uav Multispectral Survey to Map Soil and Crop for Precision Farming Applications. ISPRS - International Archives of the Photogrammetry, Remote Sensing and Spatial Information Sciences XLI-B1, 1023-1029. 10.5194/isprsarchives-XLI-B1-1023-2016.

Squires, V.R., Glenn, E.P., 2004. Salination, desertification, and soil erosion, in: Squires, V.R. (Ed.), The role of food, agriculture, forestry and fisheries in human nutrition. UNESCO, EOLSS Publishers, Oxford ,UK.

State Research Institute of Soil Science and Agrochemistry, S., 2005. Arable soils of Syrdarya and Jizzakh (In Uzbek). Fan, Tashkent, Uzbekistan.

Strobl, C., Malley, J., Tutz, G., 2009. An introduction to recursive partitioning: rationale, application, and characteristics of classification and regression trees, bagging, and random forests. Psychological methods 14, 323-348. 10.1037/a0016973.

Szabolcs, I., 1989. Salt-affected soils. CRC Press, Boca Raton, Fla.

Taghadosi, M.M., Hasanlou, M., 2017. Trend analysis of soil salinity in different land cover types using Landsat Time Series Data (Case Study Bakhtegan salt lake). Int. Arch. Photogramm. Remote Sens. Spatial Inf. Sci. XLII-4/W4, 251-257. 10.5194/isprs-archives-XLII-4-W4-251-2017.

UGCS, 2017. UgCS 2.10,. UGCS, Riga, Latvia.

UNDP, 2009. National irrigated land reclamation fund capacity development, project document, p. 54.

Urrestarazu, M., 2013. Infrared thermography used to diagnose the effects of salinity in a soilless culture. Quantitative InfraRed Thermography Journal 10, 1-8. 10.1080/17686733.2013.763471.

US Salinity Laboratory Staff, 1954. Diagnosis and improvement of saline and alkaline soils (Agriculture handbook No. 60). Government Printing Office, Washington, DC.

USGS, 2017a. Earth Resources Observation and Science (EROS) center Science Processing Architecture (ESPA) on demand interface. User Guide, p. 36.

USGS 2017b. LSDS Science Research and Development (LSRD). Accessed on August-November. https://espa.cr.usgs.gov/index/.

V.V. Dokuchaev Soil Science Institute, 1970. Methodological guidelines on melioration of solonetz and accounting of salt affectes soils (In Russian). Kolos, Moscow.

van der Meij, B., Kooistra, L., Suomalainen, J., Barel, J.M., De Deyn, G.B., 2017. Remote sensing of plant trait responses to field-based plant–soil feedback using UAV-based optical sensors. Biogeosciences 14, 733-749. 10.5194/bg-14-733-2017.

Várallyay, G., 1994. Climate Change, Soil Salinity and Alkalinity. Springer Berlin Heidelberg, Berlin, Heidelberg, pp. 39-54.

Volkmar, K.M., Hu, Y., Steppuhn, H., 1998. Physiological responses of plants to salinity: A review. Canadian Journal of Plant Science 78, 19-27. 10.4141/P97-020.

Wang, F., Chen, X., Luo, G., Ding, J., Chen, X., 2013. Detecting soil salinity with arid fraction integrated index and salinity index in feature space using Landsat TM imagery. Journal of Arid Land 5, 340-353. 10.1007/s40333-013-0183-x.

Wang, Q., Li, P., Chen, X., 2012. Modeling salinity effects on soil reflectance under various moisture conditions and its inverse application: A laboratory experiment. Geoderma 170, 103-111. 10.1016/j.geoderma.2011.10.015.

Wang, Y., Xiao, D., Li, Y., Li, X., 2008. Soil salinity evolution and its relationship with dynamics of groundwater in the oasis of inland river basins: case study from the Fubei region of Xinjiang Province, China. Environmental monitoring and assessment 140, 291-302. 10.1007/s10661-007-9867-z.

Wankhade, S.D., Cornejo, M.J., Mateu-Andrés, I., Sanz, A., 2013. Morpho-physiological variations in response to NaCl stress during vegetative and reproductive development of rice. Acta Physiologiae Plantarum 35, 323-333. 10.1007/s11738-012-1075-y.

Wilford, J., de Caritat, P., Bui, E., 2015. Modelling the abundance of soil calcium carbonate across Australia using geochemical survey data and environmental predictors. Geoderma 259–260, 81-92. http://doi.org/10.1016/j.geoderma.2015.05.003.

World Bank, 2007. Integrating environment into agriculture and forestry. Progress and prospects in Eastern Europe and Central Asia. Uzbekistan, p. 12.

Young, J., Udeigwe, T.K., Weindorf, D.C., Kandakji, T., Gautam, P., Mahmoud, M.A., 2015. Evaluating management-induced soil salinization in golf courses in semi-arid landscapes. Solid Earth 6, 393-402. 10.5194/se-6-393-2015.

Yu, R., Liu, T., Xu, Y., Zhu, C., Zhang, Q., Qu, Z., Liu, X., Li, C., 2010. Analysis of salinization dynamics by remote sensing in Hetao Irrigation District of North China. Agricultural Water Management 97, 1952-1960. 10.1016/j.agwat.2010.03.009.

Zhang, F., Tiyip, T., Ding, J., Kung, H., Johnson, V.C., Sawut, M., Tashpolat, N., Gui, D., 2012. Studies on the reflectance spectral features of saline soil along the middle reaches of Tarim River: a case study in Xinjiang Autonomous Region, China. Environmental Earth Sciences 69, 2743-2761. 10.1007/s12665-012-2096-y.

Zhang, T.-T., Qi, J.-G., Gao, Y., Ouyang, Z.-T., Zeng, S.-L., Zhao, B., 2015. Detecting soil salinity with MODIS time series VI data. Ecological Indicators 52, 480-489. 10.1016/j.ecolind.2015.01.004.

Zinnert, J.C., Nelson, J.D., Hoffman, A.M., 2012. Effects of salinity on physiological responses and the photochemical reflectance index in two co-occurring coastal shrubs. Plant and Soil 354, 45-55. 10.1007/s11104-011-0955-z.

Zribi, M., Baghdadi, N., Nolin, M., 2011. Remote Sensing of Soil. Applied and Environmental Soil Science 2011, 1-2. 10.1155/2011/904561.

Summary

Increased soil salinity is a significant agricultural problem that decreases yields for common crops. It is quite dynamic in time, which makes timely soil salinity data a crucial point in agricultural management. Remote sensing can provide the necessary spatial and temporal resolution, but widely accepted methods and techniques for soil salinity monitoring using remote sensing are not present yet.

Canopy temperature change is one of the stress indicators in plants. Its behaviour in response to salt stress on individual plant level is well studied, but its potential for field or landscape scale studies is not investigated yet. In this study, potential of satellite and UAV thermography for plot, regional and global scale soil salinity assessment was investigated.

Chapter 1 is the introductory chapter where main terms and definitions are given and the extent of the problem is described. Moreover, the line of reasoning that lead to the selection of canopy temperature as a potential indicator of soil salinity is provided. Fundamental reasons of why canopy temperature is affected by salt stress are described and thermography approach is proposed.

In Chapter 2 a proof-of-concept study is described, where first application of the thermography approach is made. This study was done in the Syrdarya province of Uzbekistan, which consists of salt affected irrigated croplands of mainly cotton and wheat. Moderate-resolution imaging spectroradiometer (MODIS) satellite images were used for canopy temperature measurements and the provincial soil salinity map as a ground truth dataset. Analysis of variance (ANOVA) was used to analyse relations between the soil salinity map and canopy temperature, normalised difference vegetation index (NDVI), enhanced vegetation index (EVI), and digital elevation model (DEM). The results showed significant relation between soil salinity and canopy temperature, but the strength of this relation varied over the year. The strongest relation between soil salinity and canopy temperature was observed for cotton in September. The calculated F-values were higher for canopy temperature than for all other compared indicators. Satellite thermography

appeared to be a valuable approach for detecting soil salinity under agricultural crops at landscape scale.

Chapter 3 is devoted to the application of the thermography approach on the plot scale and the use of Unmanned Aerial Vehicles for this. Three different UAV sensors were used: a WIRIS thermal camera, a Rikola hyperspectral camera and a Riegl VUX-SYS Light Detection and Ranging (LiDAR) scanner. Canopy temperature, several vegetation indices and LiDAR measured plant height were derived from the remote sensing data and their relations with ground measured parameters like salt treatment, stomatal conductance and actual plant height were analysed. The results showed that widely used multispectral vegetation indices are not efficient in discriminating between salt affected and control quinoa plants. The hyperspectral Physiological Reflectance Index (PRI) performed better and showed a clear distinction between salt affected and control plants. This distinction is also visible for LiDAR measured plant height, where salt treated plants were on average 10 centimetres shorter than control plants. Canopy temperature was significantly affected, though detection of this required an additional step in the analysis – Normalised Difference Vegetation Index (NDVI) clustering. This step assured temperature comparison for equally vegetated pixels. Data combination of all three sensors in a multiple linear regression model increased the prediction power and for the whole dataset R^2 reached 0.46, with some subgroups reaching an R^2 of 0.64. The UAV borne remote sensing proved to be useful for measuring salt stress in plants and a combination of multiple measurement techniques is advised to increase the accuracy.

In chapter 4 the thermography approach is applied on regional scale and its robustness was tested. Four study areas in four different states of Australia were selected to give a broad representation of different crops cultivated under irrigated and rainfed conditions. In the analysis vegetation indices and brightness temperature were used as an indicator for canopy temperature. Applying analysis of variance and time series analysis I investigated the applicability of satellite remote sensing of canopy temperature as an approach of soil salinity assessment for different crops grown under irrigated and rainfed conditions. In all cases

average canopy temperature was significantly correlated with soil salinity of the area. This relation is valid for all investigated crops, grown both irrigated and rainfed. Nevertheless, crop type did influence the strength of the relations. Cotton showed only minor temperature difference compared to other vegetation classes. The strongest relations between canopy temperature and soil salinity were observed at the moment of a maximum green biomass of the crops, which is thus considered to be the best time for application of the thermography approach.

In chapter 5 global scale assessment is presented. The only database that currently provides soil salinity information with global coverage is the Harmonized World Soil Database, but it has several limitations when it comes to soil salinity assessment. Therefore, a new assessment is required. I hypothesized that combining soil properties maps together with the thermal infrared imagery and a large set of field observations within a machine learning framework will yield a global soil salinity map. The thermal infrared imagery would act as a dynamic variable that will characterize the change. For this purpose, Google Earth Engine computational environment was used. The random forest classifier was trained using 7 soil properties maps, thermal infrared imagery and the ECe point data from the WoSIS database. In total six maps were produced for 1986, 2000, 2002, 2005, 2009, 2016. The validation accuracy of the resulting maps was in the range of 67-70%. The total area of salt affected lands by the presented assessment is around 1 billion hectares, with a clear increasing trend. Comparison with 3 studies investigating local trends of soil salinity change showed that presented assessment was in correspondence with 2 of these studies. The global map of soil salinity change between 1986 and 2016 was produced to characterize the spatial distribution of the change. I conclude that the combination of soil properties maps and thermal infrared imagery can allow mapping of soil salinity development in space and time on a global scale.

Chapter 6 synthesises the findings from all previous chapters, puts them into a broader perspective and reflects on implications, methods and data used. Moreover, suggestions for further research are given.

Краткое содержание

Засоленность почвы является серьезной сельскохозяйственной проблемой, которая снижает урожайность многих культур. Феномен довольно динамичен во времени, что делает своевременные данные о засолении почвы важным фактором в управлении сельским хозяйством. Дистанционное зондирование может обеспечить необходимое пространственное и временное разрешение, но общепринятые методы для мониторинга засоленности почвы с использованием дистанционного зондирования сегодня отсутствуют.

Изменение температуры надземной части растения является одним из показателей стресса. Особенности этой реакции на солевой стресс на уровне отдельных растений хорошо изучены, но потенциал для применения в масштабах целого поля или ландшафта еще не исследован. В работе изучен потенциал спутниковой термографии и термографии с использованием беспилотного летательного аппарата (БПЛА) для оценки засоленности почв в региональном и глобальном масштабе.

Глава 1 является вводной главой, в которой приведены основные термины и определения, а также описаны масштабы проблемы. Более того, описан ход рассуждений, которые привели к выбору температуры растения как потенциального индикатора засоленности почвы. Перечислены фундаментальные причины того, почему температура растения зависит от солевого стресса, и предложен термографический подход.

В Главе 2 описывается исследование для проверки концепции, в котором впервые применяется термографический подход. Это исследование было проведено в Сырдарьинской области Узбекистана, большая часть которой состоит из засоленных пахотных земель, где основными культурами является хлопок и пшеница. Снимки со спутника MODIS были использованы для измерения температуры растительного покрова и анализировались вместе с картами засоленности почвы, произведенных традиционными методами. Дисперсионный анализ (ANOVA) использован для выявления

связей между картами засоленности почвы и температурой растительного покрова, нормированным разностным индексом растительности (NDVI), улучшенным индексом растительности (EVI) и цифровой моделью рельефа (DEM). Результаты показали значительную зависимость температуры растительного покрова от степени засоления почвы, но эта зависимость менялась в течение года. Наиболее выраженной она была в сентябре в случае с хлопком. Рассчитанные F-значения были выше для температуры, чем для всех других сравниваемых индикаторов. Спутниковая термография оказалась многообещающим подходом для определения засоленности почвы под сельскохозяйственными культурами в региональном масштабе.

Глава 3 посвящена применению термографического подхода в масштабе одного поля и использованию для этого БПЛА. Использовались три разных сенсора, монтированных на БПЛА: тепловизионная камера WIRIS, гиперспектральная камера Rikola и лазерный сканер Riegl VUX-SYS Light Detection and Ranging (LiDAR). Температура растительного покрова, несколько индексов растительности и LiDAR-измеренная высота растительного покрова были рассчитаны на основе данных дистанционного зондирования, и были проанализированы их связи с такими полевыми данными, как уровень засолённости, устьичная проводимость и фактическая высота растения. Результаты показали, что широко используемые мультиспектральные индексы растительности не эффективны для различения пораженных солью и контрольных растений киноа. Индекс физиологической отражательной способности (PRI) показал лучшие результаты и различие в значениях между пораженными солью и контрольными растениями. Это различие также заметно и в измерениях высоты растений, полученных при помощи LiDAR, где обработанные солью растения были в среднем на 10 сантиметров короче контрольных. Значительные изменения претерпела и температура растительного покрова, хотя обнаружение этого потребовало дополнительного этапа анализа - кластеризации NDVI. Этот шаг гарантировал сравнение температуры между пикселями с аналогичной площадью растительного покрова. Комбинация

данных всех трех сенсоров в модели множественной линейной регрессии повысила эффективность прогнозирования и для всего набора наблюдений регрессионный коэффициент R^2 достиг 0,46, в некоторых подгруппах R^2 достиг 0,64. Дистанционное зондирование с помощью БПЛА оказалось полезным подходом для измерения солевого стресса растений. Для повышения точности рекомендуется сочетание нескольких методов измерения.

В главе 4 термографический подход применяется в масштабе нескольких регионов. Четыре региона в четырех различных штатах Австралии были выбраны для того, чтобы в исследовании были представлены различные культуры, выращиваемые как в богарных условиях, так и в условиях орошаемого земледелия. В анализе комбинация индексов растительности и термальных спутниковых снимков использовалась в качестве индикатора температуры растительного покрова. Используя дисперсионный анализ и анализ временных рядов, исследована применимость спутниковой термографии для оценки засоленности почвы под различными культурами, выращиваемых как в богарных условиях, так и в условиях орошаемого земледелия. Во всех случаях, средняя температура растительного покрова достоверно коррелировала с засоленностью почвы в этом районе. Эта взаимосвязь справедлива для всех исследованных культур, выращенных как на орошаемых, так и на богарных участках. Тем не менее, вид культуры влиял на степень этой взаимосвязи. Хлопок показал лишь незначительную разницу температур по сравнению с другими культурами. Наиболее сильные зависимости между температурой растительного покрова и засолением почвы наблюдались в момент пика зеленой биомассы растений. Таким образом этот период может считается оптимальным для применения описываемого термографического подхода.

В главе 5 представлена оценка в глобальном масштабе. Единственная база данных, которая в настоящее время предоставляет информацию о засоленности почв с глобальным охватом это Гармонизированная Мировая Почвенная База Данных, но она имеет несколько ограничений в случае

оценки засоленности почв. В связи с этим, необходима обновленная оценка. Я предположил, что объединение карт свойств почвы вместе с тепловыми инфракрасными снимками и большим набором полевых наблюдений в рамках алгоритма машинного обучения, позволит получить глобальную карту засоленности почвы. Тепловые инфракрасные снимки будут действовать как динамическая переменная, которая будет характеризовать изменения во времени. Для этой цели использовалась вычислительная среда Google Earth Engine. Классификатор случайных лесов был обучен с использованием 7 карт свойств почвы, тепловых инфракрасных снимков и значений электропроводимости почвы (ECe) из базы данных WoSIS. Всего было подготовлено шесть карт за 1986, 2000, 2002, 2005, 2009 и 2016 годы. Точность валидации полученных карт находилась в диапазоне 67-70%. Общая площадь засоленных земель, по представленной оценке, составляет около 1 млрд. Га, с явной тенденцией к увеличению. Сравнение с 3 исследованиями, изучающими локальные изменения засоленности почвы, показало, что представленная оценка соответствовала двум из этих исследований. Была составлена глобальная карта изменений засоленности почв в период с 1986 по 2016 гг. Из полученных результатов можно сделать вывод, что комбинация карт свойств почвы и тепловых инфракрасных снимков может позволить картировать процессы развития засоления почвы в пространстве и времени в глобальном масштабе.

В главе 6 обобщены результаты всех предыдущих глав, они рассмотрены в более широкой перспективе. Представлено критическое обсуждение методов и использованных данных. Более того, даются предложения по дальнейшим исследованиям.

Acknowledgements

This thesis is a result of a four-year journey on which I was accompanied by many great people. First, I would like to thank my promotor Arnold Bregt, whose guidance helped me to reach the endpoint of this journey. Arnold, your open and optimistic attitude was always transmitted to me and made my PhD journey much more enjoyable than it would have been otherwise.

My deepest gratitude is to my co-promotors – Harm Bartholomeus and Alim Pulatov. Harm, you were able to show me ways out of many difficult methodological and other kind of dead ends of my research, which is definitely a factor in my timely graduation. I always could come to your office for short discussions that solved long-standing issues. Alim Salimovich, thank you for opening to me the world of scientific research and a constant reminder that I am capable of more and have unrealised potential. I do not know whether I realised it now completely, but I certainly realised it to a bigger extent than before.

Another special thanks I would like to express to Ewa Wietsma, Marthy Boudewijn and whole team of Erasmus Mundus TIMUR project, that financed bigger part of my PhD stay in Wageningen. Without you this research would not be possible.

Doing a scientific research all by yourself these days hardly possible, therefore I am thankful to my collaborators: Elisabeth Bui, John Wilford, Marston Franceschini, Henk Kramer, Robert van Loo, Viviana Jaramillo Roman, Richard Finkers, Bas Kempen, Luis de Sousa. Your contribution greatly improved the depth and breadth of my research.

I'm very grateful to my colleagues for friendly and fun working atmosphere. For that I would like to thank Agnieszka, Aldo, Andrei, Anne, Antoinette, Arend, Arun, Astrid, Ben B, Beni, Ben DV, Brice, Corne, Dainius, Danaë, Daniela, Devis, Diego, Eliakim, Eskender, Erika S, Giulia, Jalal, Jan C, Jan V, Joao, Johannes B, Johannes R, John, Jose, Juha, Kalkidan, Lala, Lammert, Loïc, Lucasz, Marcello, Maria, Marian, Martin, Mathieu, Michi, Nandika, Niki, Patric, Peter, Richard, Ron, Rosa Maria, Sabina, Samantha, Shivangi, Simon, Sylvain, Sytze, Truus, Tsoefiet, Willy, Ximena,

Yang. I am especially grateful to my office mates Qijun, Erika and Panpan. Chats with you made the working days enjoyable.

No matter how good the office days were, I would hardly be able to spend them effectively without relaxing out of the office. For this I would like to thank my friends: Alex R, Alex S, Adil, Anna, Fernando, Islambek, Marina, Mirzokhid, Mumin and Tatiana.

Great thanks are to my family, mom, dad, and sister. Ваша безусловная любовь и поддержка во всех моих начинаниях — это то, что позволяет мне двигаться вперёд. Мои поездки домой на новогодние праздники заряжали меня на весь следующий год. Словами я могу выразить лишь толику моей благодарности и любви к вам.

I met too many people to mention who helped me one way or another through these years and I would like to thank them all.

List of publications

Ivushkin, K., Bartholomeus, H., Bregt, A.K., Pulatov, A., 2017. Satellite Thermography for Soil Salinity Assessment of Cropped Areas in Uzbekistan. Land Degradation & Development 28, 870-877. 10.1002/ldr.2670.

Ivushkin, K., Bartholomeus, H., Bregt, A.K., Pulatov, A., Bui, E.N., Wilford, J., 2018. Soil salinity assessment through satellite thermography for different irrigated and rainfed crops. International Journal of Applied Earth Observation and Geoinformation 68, 230-237. 10.1016/j.jag.2018.02.004.

Ivushkin, K., Bartholomeus, H., Bregt, A.K., Pulatov, A., Franceschini, M.H.D., Kramer, H., van Loo, E.N., Jaramillo Roman, V., Finkers, R., 2019. UAV based soil salinity assessment of cropland. Geoderma 338, 502-512. https://doi.org/10.1016/j.geoderma.2018.09.046.

Other scientific contributions

Ivushkin, K., Bartholomeus, H., Bregt, A.K., Pulatov, A., Bui, E.N., Wilford, J., van Loo, E.N., 2018. Satellite and UAV thermography for soil salinity assessment. Netherlands Center for Geodesy and Geo-informatics Symposium, Delft, the Netherlands.

Ivushkin, K., Bartholomeus, H., Bregt, A.K., Pulatov, A., Bui, E.N., Wilford, J., 2017. Soil salinity assessment through novel application of satellite thermography. Pedometrics Conference, Wageningen, the Netherlands.

Ivushkin, K., Bartholomeus, H., Bregt, A.K., Pulatov, A., Bui, E.N., Wilford, J., 2017. Infrared thermal remote sensing for soil salinity assessment on landscape scale. European Geosciences Union General Assembly, Vienna, Austria.

Ivushkin, K., Bartholomeus, H., Bregt, A.K., Pulatov, A., 2016. Soil salinity assessment using satellite thermal images. 37th Asian Conference on Remote Sensing, Colombo, Sri Lanka.

About the author

Konstantin Ivushkin was born in 1989 in Tashkent, Soviet Union (currently Uzbekistan). There he studied in school #195 with in-depth math teaching. Probably this in-depth teaching of math was the reason why after school he chose to study life sciences, in comparison with majority of his classmates who pursued technical and IT studies. All the more so since chemistry and biology was always interesting and easy to follow for him. Therefore, in 2006 he started his bachelor's degree in Ecology and Nature Management at National University of Uzbekistan in Tashkent. After graduating in 2010 he started working in local NGO Ecological Movement of Uzbekistan, where he was responsible for organisation of awareness rising events and functioning of a hotline on environmental issues. Always aiming to continue his education until master's degree at least, in 2011 he decides to apply for a Double Degree program between Tashkent Institute of Irrigation and Melioration and Wageningen University, of which he was informed by his colleague. In a frame of this program Konstantin completed the thesis related to soil salinization detection using Remote Sensing techniques. After successfully finalising the program in 2014, he was advised by one of his supervisors to apply for a PhD grant with Erasmus Mundus TIMUR project to continue his research. The grant was awarded and in 2015 he started his doctorate research, which culminated in 2019 in this thesis.

PE&RC Training and Education Statement

With the training and education activities listed below the PhD candidate has complied with the requirements set by the C.T. de Wit Graduate School for Production Ecology and Resource Conservation (PE&RC) which comprises of a minimum total of 32 ECTS (= 22 weeks of activities)

Review of literature (6 ECTS)

- Soil salinity assessment and mapping using remote sensing and GIS

Writing of project proposal (6 ECTS)

- Spatiotemporal assessment of soil salinity impact on crop production in arid and semi-arid zones

Post-graduate courses (5.5 ECTS)

- Spatial sampling for mapping; PE&RC, SENSE (2015)
- Land dynamics, getting to the bottom of Mount Kenya; PE&RC, WASS, SENSE (2015)
- Global soil information facilities; ISRIC (2015)

Invited review of (unpublished) journal manuscript (2 ECTS)

- Land Degradation & Development: soil salinity mitigation policies (2018)
- Journal of Selected Topics in Applied Earth Observations and Remote Sensing: soil salinity monitoring using remote sensing (2018)

Competence strengthening / skills courses (2.1 ECTS)

- PhD Competence assessment; WGS (2015)
- Brain Training; WGS (2016)
- Career orientation; WGS (2018)

PE&RC Annual meetings, seminars and the PE&RC weekend (1.2 ECTS)

- PE&RC Weekend (2015)
- PhD Workshop carousel (2015)

Discussion groups / local seminars / other scientific meetings (6. ECTS)

- National PhD day (2015)
- Nederlands Centrum voor Geodesie en Geo-informatica symposium (2016)
- Landscape Dynamics discussion group (2016)
- AgroFood Robotics discussion group (2016)
- Nederlands Centrum voor Geodesie en Geo-informatica symposium (2017)
- Remote Sensing discussion group (2018)

International symposia, workshops and conferences (10.6 ECTS)

- 37th Asian Conference on Remote Sensing; Colombo, Sri Lanka (2016)
- EGU General Assembly; Vienna, Austria (2017)
- Pedometrics; Wageningen, the Netherlands (2017)
- 21st World Congress of Soil Science; Rio de Janeiro, Brazil (2018)

The author's research for the most of his PhD was supported by the project ERASMUS MUNDUS ACTION 2 PARTNERSHIPS STRAND I "Training of Individuals through Mobility to EU from Uzbek Republic - TIMUR" Grant Agreement Number: 2013 - 2723.

Financial support from Wageningen University for printing this thesis is gratefully acknowledged.

Cover design by Adil Yakubov

Printed by DigiForce || ProefschriftMaken